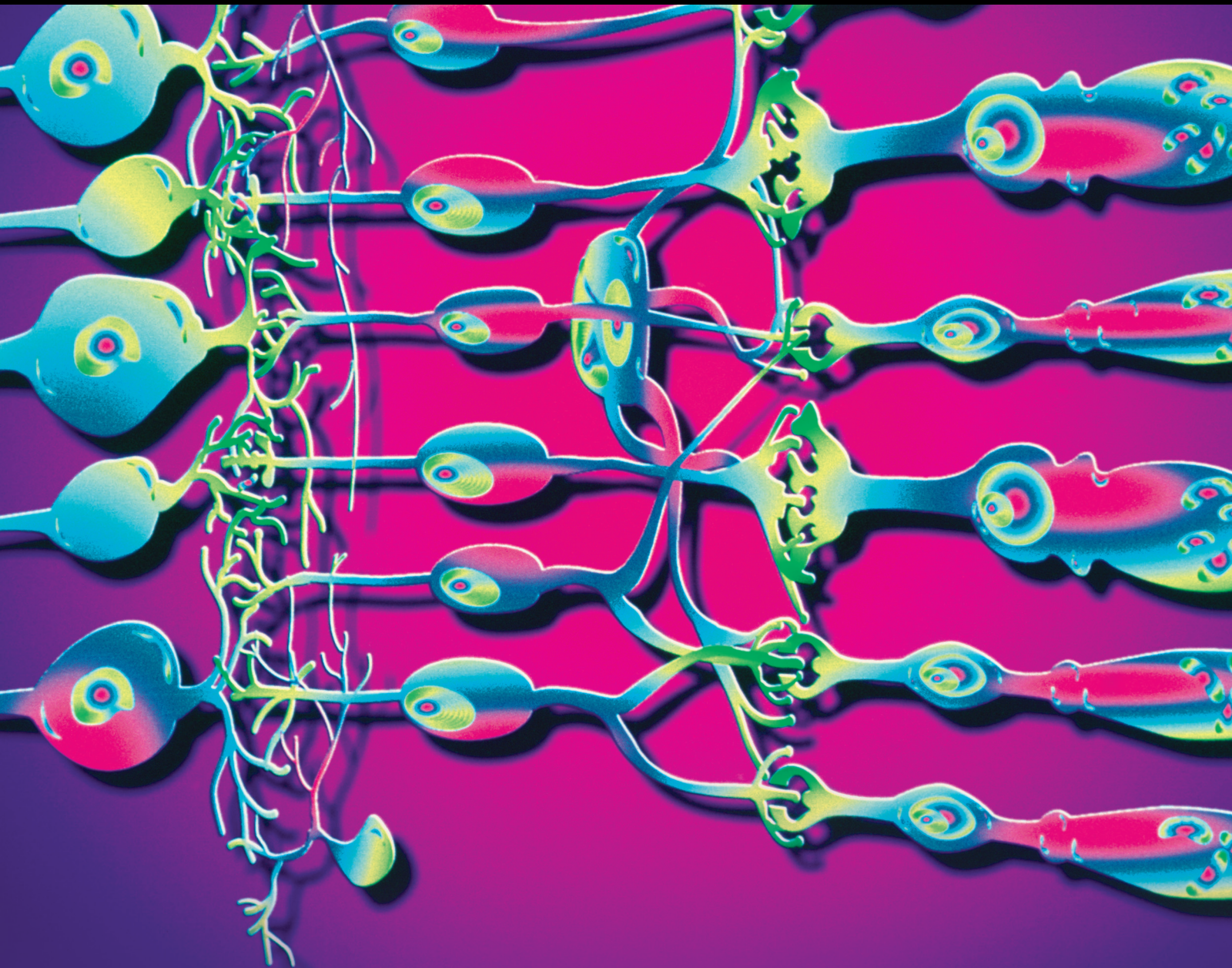# Optical Coherence Tomography Biomarkers and Where to Find Them

Lead Guest Editor: Carlo Lavia
Guest Editors: Marco Nassisi, Isabelle Audo, and Alain Gaudric

Optical Coherence Tomography Biomarkers and Where to Find Them

Optical Coherence Tomography Biomarkers and Where to Find Them

Lead Guest Editor: Carlo Lavia
Guest Editors: Marco Nassisi, Isabelle Audo, and Alain Gaudric

Shivalingappa K. Swamynathan (iD), USA
Nóra Szentmáry, Hungary
Masaru Takeuchi (iD), Japan
Suphi Taneri (iD), Germany
Miguel Teus (iD), Spain
Biju B. Thomas (iD), USA
Oren Tomkins-Netzer (iD), United Kingdom
Lisa Toto (iD), Italy
Maurizio Uva (iD), Italy
Manuel Vidal-Sanz, Spain
Paolo Vinciguerra (iD), Italy
Nilufer Yesilirmak (iD), Turkey
Vicente Zanon-Moreno (iD), Spain
Yedi Zhou (iD), China

Contents

Review Article

Optical Coherence Tomography Imaging of the Lamina Cribrosa: Structural Biomarkers in Nonglaucomatous Diseases

Alice Paulo,[1] Pedro G. Vaz [ID],[1] Danilo Andrade De Jesus [ID],[2] Luisa Sánchez Brea [ID],[2] Jan Van Eijgen [ID],[3,4] João Cardoso [ID],[1] Theo van Walsum [ID],[2] Stefan Klein [ID],[2] Ingeborg Stalmans [ID],[3,4] and João Barbosa Breda [ID][3,5,6]

[1]*Laboratory for Instrumentation, Biomedical Engineering and Radiation Physics (LIBPhys-UC), Department of Physics, University of Coimbra, Coimbra, Portugal*
[2]*Biomedical Imaging Group Rotterdam, Department of Radiology & Nuclear Medicine, Erasmus MC, Rotterdam, Netherlands*
[3]*Research Group Ophthalmology, Department of Neurosciences, KU Leuven, Leuven, Belgium*
[4]*Department of Ophthalmology, University Hospitals UZ Leuven, Leuven, Belgium*
[5]*Cardiovascular R&D Center, Faculty of Medicine of the University of Porto, Porto, Portugal*
[6]*Ophthalmology Department, Centro Hospitalar e Universitário São João, Porto, Portugal*

Correspondence should be addressed to Danilo Andrade De Jesus; d.andradedejesus@erasmusmc.nl

The lamina cribrosa (LC) is an active structure that responds to the strain by changing its morphology. Abnormal changes in LC morphology are usually associated with, and indicative of, certain pathologies such as glaucoma, intraocular hypertension, and myopia. Recent developments in optical coherence tomography (OCT) have enabled detailed *in vivo* studies about the architectural characteristics of the LC. Structural characteristics of the LC have been widely explored in glaucoma management. However, information about which LC biomarkers could be useful for the diagnosis, and follow-up, of other diseases besides glaucoma is scarce. Hence, this literature review aims to summarize the role of the LC in nonophthalmic and ophthalmic diseases other than glaucoma. PubMed was used to perform a systematic review on the LC features that can be extracted from OCT images. All imaging features are presented and discussed in terms of their importance and applicability in clinical practice. A total of 56 studies were included in this review. Overall, LC depth (LCD) and thickness (LCT) have been the most studied features, appearing in 75% and 45% of the included studies, respectively. These biomarkers were followed by the prelaminar tissue thickness (21%), LC curvature index (5.4%), LC global shape index (3.6%), LC defects (3.6%), and LC strains/deformations (1.8%). Overall, the disease groups showed a thinner LC (smaller LCT) and a deeper ONH cup (larger LCD), with some exceptions. A large variability between approaches used to compute LC biomarkers has been observed, highlighting the importance of having automated and standardized methodologies in LC analysis. Moreover, further studies are needed to identify the pathologies where LC features have a diagnostic and/or prognostic value.

1. Introduction

The lamina cribrosa (LC) is a mesh-like structure localized in the posterior scleral canal of the optic nerve head (ONH), allowing retinal ganglion cell (RGC) axons to pass through to the brain. It is a fenestrated complex that also accommodates vessels that nourish the retina. A large circumpapillary ring of collagen and elastin fibers, in the immediate peripapillary sclera, protects the LC against the mechanical strain, such as that induced by an imbalance between intraocular pressure (IOP) and intracranial pressure (ICP) [1, 2]. Due to its anatomical location, between two differently pressurized compartments, there is a pressure gradient along the LC, denominated translaminar pressure difference (TLPD), which can be calculated as the difference between IOP and ICP in the subarachnoid space (SAS) [3, 4]. Despite

being an extremely relevant structure to the eye's anatomy and function, little is known about the LC. LC morphology plays an important role in the development and progression of ophthalmic pathologies, notably on glaucomatous optic neuropathy, intraocular hypertension, and myopia [5–8]. The structural deformation and the correlated compression across the LC lead to blockade of axonal transport and eventually RGC death [9].

Recent advances in *in vivo* medical imaging techniques, such as optical coherence tomography (OCT), have allowed the visualization of deep connective tissues, including the LC, in greater detail (Figure 1) [10, 11].

Specific developments in OCT software, such as enhanced depth imaging (EDI), and light-attenuation correction software such as adaptive compensation (AC) significantly improved the visibility of the LC without compromising acquisition time. EDI-OCT was originally developed in order to improve the visualization of the choroid, although it has also been adopted to improve cross-sectional images of the LC. AC is a postprocessing technique developed to remove blood vessel shadows and enhance tissue contrast in order to facilitate posterior LC surface detection [12, 13]. In addition to these software developments, several studies have shown that swept-source OCT (SS-OCT) further improves the visualization of the LC [14, 15].

While an increasing number of works have studied the relevance of the LC (and its changes) in glaucoma [16], data on other diseases are still scarce. Hence, this review intends to provide a broader vision and a better comprehension of the measurable laminar structural features that have been identified as relevant for nonglaucomatous pathologies in the published literature.

2. Methods

2.1. Study Selection.
A literature search was conducted in the MEDLINE (PubMed) bibliographic database on 15th May 2020. The search query was (optical coherence tomography NOT angiography) AND (lamina OR cribrosa). Only articles published in English were considered, and no publication date restriction was added. The exclusion criteria were (i) only included glaucomatous eyes in the experimental group; (ii) not conducted in humans; (iii) review articles or case reports; (iv) exclusive focus on imaging techniques and not presenting clinical data; (v) no evaluation of the lamina cribrosa; and (vi) no mention to LC structural parameters and how they were measured/extracted. This led to a total of 408 references, which were narrowed down to 56 after title/abstract screening, followed by a full-text screening (see Figure 2). The 56 included studies provided quantitative values for each of the analyzed features and described how the quantification was performed.

2.2. Data Collection.
In this review, our main aim was to identify potential biomarkers in the morphology of the LC that were associated with, and indicative of, certain pathologies. Therefore, we have opted to only report those that

performed a statistical comparison between an experimental and a control group. The extracted data for each paper consist of the LC structural parameters, their mean and standard deviation (SD), and the p values of the statistical analysis performed between experimental and control groups. Moreover, the image processing methodology applied to compute each feature was taken into account for posterior comparisons.

For all the included articles, the following characteristics are obtained and presented in Table 1: sample size, including the number of patients and eyes per group; age and statistical comparison (p value) between control and experimental groups; OCT device model, manufacturer, and light-source wavelength; cutoff value for the signal strength index (SSI) or similar qualitative image criteria used to exclude patients/eyes; and field of view of the OCT image [17]. Moreover, the procedures followed to measure the LC features, and their respective values, were also collected and compiled.

Data collection comprehended all structural components related to the LC and the surrounding ONH region that were included on the OCT B-scan images. Several locations, planes (superior, middle, and inferior), and sectors were considered for the measurements. The sectors were defined according to the Garway-Heath map [71]. The approach of data extraction by one investigator (ASP) with further verification by a senior author (JBB) has been used, as this has been demonstrated to be as accurate as double independent data extraction [72].

2.3. Data Analysis.
The obtained data were used to calculate the frequency of each LC structural feature in the published literature and to determine the mean values of the most frequently reported features. Statistical relevance, given by the p value, was also taken as a complement for study results and to comprehend the relation and differences found between study groups. To average the data for each LC parameter, pooled mean and pooled SD were determined according to equations (1) and (2), respectively, where N represents the number of eyes included in the study, M the mean value, SD the standard deviation, and n the number of studies analyzed:

$$\text{pooled mean} = \frac{\sum_{i=1}^{n} N_i \times M_i}{\sum_{i=1}^{n} N_i}, \tag{1}$$

$$\text{pooled SD} = \sqrt{\frac{\sum_{i=1}^{n} (N_i - 1) \times \text{SD}_i^2}{\sum_{i=1}^{n} (N_i - 1)}}. \tag{2}$$

3. Results

All structural LC features were analyzed, and the studies were organized in three groups: healthy group ($n = 19$), nonophthalmic disease group ($n = 6$), and ophthalmic (nonglaucomatous) disease group ($n = 31$). Overall, LC depth (LCD) and LC thickness (LCT) have been the most studied features, appearing in 75% and 44.6% from the total articles. Other features, such as prelaminar tissue thickness

(a)   (b)
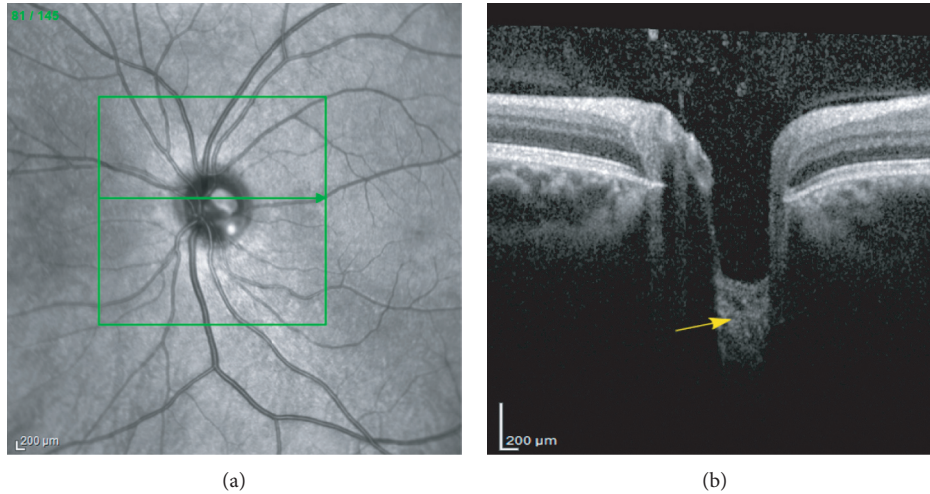
FIGURE 1: Retinal fundus photograph (a) and EDI-OCT B-scan at the optic nerve head (b). The green line denotes the location of the B-scan in the fundus image. The yellow arrow points to the lamina cribrosa region.
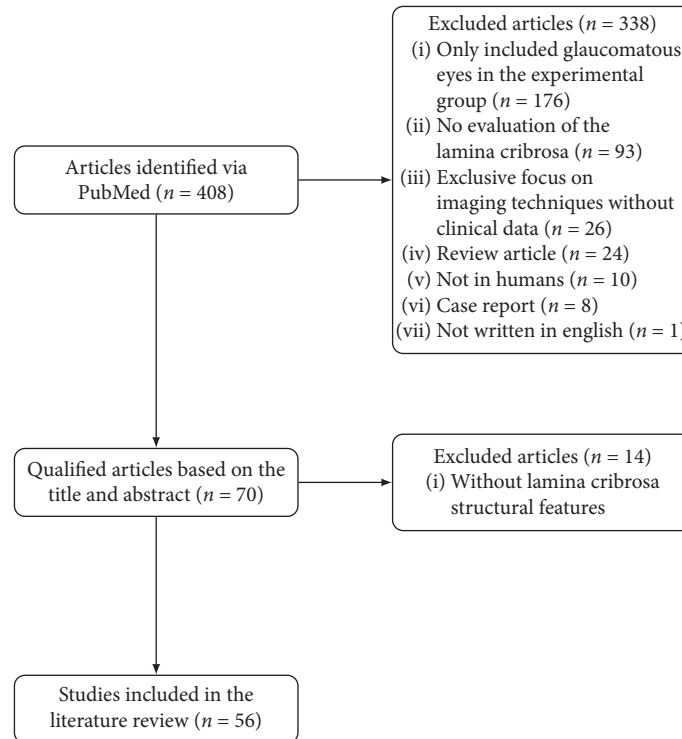
FIGURE 2: Flowchart of the collected data.

(PTT) (21.4%) studied in ophthalmic and nonophthalmic diseases, and lamina cribrosa curvature index (LCCI) (5.4%), LC global shape index (3.6%), LC defects (3.6%), slope of the LC (3.6%), distance between the inner surface of the LC (3.6%), SAS (3.6%), and LC strains/deformations (1.8%) studied in ophthalmic diseases only, are also referenced but in fewer studies.

One bar chart, summarizing the most studied features in the ophthalmic and nonophthalmic disease groups, is presented in Figure 3. Hence, in the following sections, a detailed analysis on how these two biomarkers have been

measured is provided. Moreover, a detailed explanation on how LCD and LCT measurements were carried out in each study is presented in Table 2. The normative values for the groups are also presented and discussed. In cases where more than one measurement was performed for the same feature (e.g., in different planes (superior, middle, or inferior), different scan directions (vertical and horizontal), or 2 eyes (left and right)), the pooled mean and SD were determined according to equations (1) and (2).

Only diseases for which at least 20 eyes were included in the studied group (cumulatively over all the evaluated

TABLE 1: Characteristics of the reviewed studies.

Authors	Group type	Ophthalmic disease	Parameter	No. of patients/eyes	Age (years) and p value	Technique	Device	Light WL (nm)	Image quality cutoff	Field of view
Xiao et al. [20]	Healthy subjects	—	cLCT cALCSD cPTT	Total: 96/96 Control: — Exp.: 96/96	YG: 26.72 ± 6.26 MG: 49.44 ± 5.64 OG: 67.19 ± 6.04 Mean: 50.34 ± 18.20 $p = 0.64$	EDI with SD-OCT	Spectralis	870	Poor image quality affecting the recognition of the boundary of the LC.	Radial scanning protocol comprising 6 angularly equidistant linear scans centering at the center of ONH (scan angle: 20°).
Sousa et al. [34]	Healthy subjects	—	ALCD	Total: 59/59 Control: — Exp.: 59/59	61.7 ± 15.1	EDI with SD-OCT	Spectralis	870	<15.	A 20° 5.8×5.8 mm square covering the optic disc.
Lee et al. [35]	Healthy subjects	—	LCT	Total: 100/189 Control: — Exp.: 100/189	48.6 ± 13.9	EDI with SD-OCT	Spectralis	870	Eyes were excluded when a good-quality image (i.e, quality score >15) could not be obtained for more than five sections. Images did not allow clear delineation of both anterior and posterior borders of the central LC.	Scan line distance is determined automatically by the machine at the center of the ONH.
Bartolomé et al. [19]	Healthy subjects	—	LCD LCT	Total: 81/81 Control: — Exp.: 81/81	28.05 ± 8.4	EDI with SD-OCT	Spectralis	840	Very small optic disc, media opacity, prominent vascular shadow, or significant artefacts.	A 15°×10° vertical rectangle centered on the optic disc.
Leal et al. [36]	Healthy subjects	—	ALCD	Total: 61/120 Control: — Exp.: 61/120	62.1 ± 15.01	EDI with SD-OCT	Spectralis	870	<15.	A 20° 5.8×5.8 mm square covering the optic disc; 2 perpendicular cross-scans (vertical and horizontal) intersected in the optic disc center.

TABLE 1: Continued.

Authors	Group type	Ophthalmic disease	Parameter	No. of patients/eyes	Age (years) and p value	Technique	Device	Light WL (nm)	Image quality cutoff	Field of view
Rhodes et al. [21]	Healthy subjects of African descent (AD) and European descent (ED)	—	LCD	Total: 84/166 Control: — Exp.: 56 AD young 8 AD old 54 ED young 48 AD old $p < 0.001$ between the AD and ED group	58.4 ± 15.5	EDI with SD-OCT	Spectralis	870	<20. Poor centration of the ONH.	20° radial scans centered on the ONH.
Wang et al. [37]	Healthy subjects	—	LC strains (deformations): (i) LC displacements (ii) LC strains	Total: 16/16 Control: — Exp.: 11 PPA 5 non-PPA	25 ± 3	EDI with SD-OCT	Spectralis	870	Poor visibility of the LC.	Rectangular region of 15°×10° centered on the ONH.
Kim et al. [38]	Healthy subjects	—	LC displacement ALCD	Total: 48/48 Control: — Exp.: 48/48	25.6 ± 5.4	EDI with SD-OCT	Carl Zeiss Meditec	NA	<7. Unclear visibility of more than one-quarter of the anterior LC surface of the neural canal opening diameter.	200×200 optic disc cube scan; 5-HD line scans (6 mm length) centered to optic disc; and 1-HD line scan (9 mm length) aligned to the axis connecting the fovea and the center of the optic disc.
Poli et al. [39]	Healthy subjects	—	ALCSD	Total: 8/16 Control: — Exp.: 8/16	52	SS-OCT	Topcon	1050	Good-quality image (i.e., mean success score rate >96/128) allowing clear delineation of the anterior borders of the LC and the posterior border of the choroid.	Horizontal 6-mm line scan centered at the optic disc.
El-Agamy et al. [40]	Healthy subjects	—	ALCSD	Total: 191/191 Control: — Exp.: 191/191	20.76 ± 1.627	SD-OCT	Topcon	840	≤56.	6×6 mm square covering the optic disc.

TABLE 1: Continued.

Authors	Group type	Ophthalmic disease	Parameter	No. of patients/eyes	Age (years) and p value	Technique	Device	Light WL (nm)	Image quality cutoff	Field of view
Park et al. [23]	Healthy subjects	—	LCD	Total: 30/30 Control: — Exp.: 30/30	40 ± 18	EDI with SD-OCT	Spectralis	870	Poor quality because of media opacity or poor patient cooperation, causing diffusely unclear images or significant artifacts.	15°×10° rectangle for horizontal scans (10°×15° rectangle for vertical scans) centered on the optic disc.
Lee et al. [24]	Healthy subjects	—	ALCD LCT	Total: 26/26 Control: — Exp.: 26/26	63.4 ± 8.0	EDI with SD-OCT	Spectralis	870	Poor B-scan quality that did not allow the delineation of the borders of the LC.	Vertical and horizontal B-scan images covering the optic disc, separated by 30–34 μm (the scan-line distance being determined automatically by the instrument).
Bedggood et al. [41]	Healthy subjects	—	Axial shifts of the anterior LC	Total: 21/21 Control: — Exp.: 21/21	33.3 ± 6.8	EDI with SD-OCT	Spectralis	870	<25.	Cubes of extent 10°×15° (horizontal×vertical), with vertical B-scans 0.21° apart (~60 μm) centered on the optic nerve head and oriented vertically.
Lee et al. [42]	Healthy subjects	—	LCCI	Total: 125/250 Control: — Exp.: 125/250	49.02 ± 14.13	EDI with SD-OCT	Spectralis	870	<15.	A 10°×15° rectangle covering of the optic disc.
Seo et al. [43]	Healthy subjects	—	ALCD	Total: 150/300 Control: — Exp.: 150/300	48.31 ± 14.31	EDI with SD-OCT	Spectralis	870	Quality score > 15 could not be obtained at more than five sections.	A 10°×15° rectangle covering the optic disc.
Fazio et al. [44]	Healthy population with different descendents	—	ALCS displacement and depth	Total: 21/42 Control: — Exp.: 12/24 AD 9/18 ED	55.8 ED 45.2 AD $p = 0.065$	EDI with SD-OCT	Spectralis	870	<20.	Radial scans centered on the center of the optic nerve.
Tun et al. [45]	Healthy subjects	—	LCD	Total: 619/619 Control: — Exp.: 619/619	60.23 ± 7.36	EDI with SD-OCT	Spectralis	870	OCT images with a poor scleral visibility.	15°×10° rectangle centered on the ONH.
Thakku et al. [46]	Healthy subjects	—	LC morphology: (i) LC depth (ii) LC curvature	Total: 162/162 Control: — Exp.: 162	58 ± 7	EDI with SD-OCT	Spectralis	870	Poorly visible LC (LC covering less than 70% of the BMO area from en face visualization).	15°×15° rectangular region centered on the ONH.

Table 1: Continued.

Authors	Group type	Ophthalmic disease	Parameter	No. of patients/eyes	Age (years) and p value	Technique	Device	Light WL (nm)	Image quality cutoff	Field of view
Luo et al. [22]	Healthy subjects	—	cLCD	Total: 360/360 Control: — Exp: 357 visible sclera 344 visible lamina 339 visible sclera and lamina	50.6 ± 17.5	EDI with SD-OCT	Spectralis	870	<20.	15° B-scans centered on BMO.
Akkaya et al. [28]	Not ophthalmic Diabetes mellitus	—	AlCD LCT	Total: 70/70 Control: 32/32 Exp:: 38/38	59.1 ± 7.4 diabetes group 58.6 ± 7.7 control group $p = 0.696$	EDI with SD-OCT	Spectralis	870	<20. Unclear image of the fundus or the border of the lamina cribrosa.	15° × 10° rectangle centered on the optic disc.
Eraslan et al. [29]	Not ophthalmic Parkinson's disease (PD)	—	LCT	Total: 47/94 Control: 25/50 Exp:: 22/44	60.56 ± 9.9 control group 60.45 ± 9.1 PD patients $p = 0.976$	SD-OCT	Optovue	840	<50.	6 × 6 mm. The scans passing through the center of the central retinal blood vessels were centered at the optic disc with nasal fixation.
Küçük et al. [30]	Not ophthalmic Obstructive sleep apnea syndrome (OSAS)	—	LCT LCD	Total: 88/88 Control: 43 Exp: 45 13 mild OSAS 17 moderate OSAS 15 severe OSAS	50.30 ± 4.2 control group 50.09 ± 9.7 experimental group $p = 0.931$	EDI with SD-OCT	Spectralis	870	NA.	A 15° × 10° rectangular image centered on the optic disc.
López-de Eguileta et al. [31]	Not ophthalmic Alzheimer's disease (AD) Mild cognitive impairment (MCI)	—	PTT ALCSD	Total: 66/126 Control: 63 Exp: 12 AD 51 MCI	73.28 ± 6.0 control group 73.5 ± 6.0 experimental group $p = 0.998$	SD-OCT	Spectralis	870	The quality of the scans is indicated on a color scale at the bottom of the scanned images. Only scans in the green range were considered of sufficiently good quality for inclusion.	A 15° area scan centered at the ONH.
Lee et al. [32]	Not ophthalmic Alzheimer's disease (AD)	—	LCT	Total: 44/44 Control: 26/26 Exp:: 18/18	63.4 ± 8.0 control group 69.7 ± 7.6 experimental group $p = 0.012$	EDI with SD-OCT	Spectralis	870	B-scan quality that did not allow delineation of the LC borders.	Horizontal and vertical B-scan images covering the optic disc, 30–34 μm apart.

TABLE 1: Continued.

Authors	Group type	Ophthalmic disease	Parameter	No. of patients/eyes	Age (years) and p value	Technique	Device	Light WL (nm)	Image quality cutoff	Field of view
Sirakaya et al. [33]	Not ophthalmic Migraine	—	LCT LCD	Total: 97/97 Control: 35 (group III) Exp.: 27 migraine with aura (group I) 35 migraine patients without aura (group II)	33.0 ± 4.7 group I 33.9 ± 5.4 group II 32.4 ± 4.8 group III $p = 0.460$	EDI with SD-OCT	Spectralis	870	<20.	A $15° \times 10°$ rectangular image centered on the ONH.
Pasaoglu et al. [47]	Ophthalmic	Diopathic intracranial hypertension (IID)	LCT ALCSD	Total: 18/36 Control: 10/20 Exp: 8/16	NA control group 41.1 ± 7.1 experimental group	DRI with SS-OCT	Topcon	1050	NA.	11-horizontal line raster scan protocol.
Villarruel et al. [25]	Ophthalmic	Intracranial hypertension (IIH) Primary open-angle glaucoma (high-tension glaucoma (HTG) and normal-tension glaucoma (NTG))	LCD	Total: 61/88 Control: 37 Exp.: 11 IIH 20 HTG 20 NTG	24.3 ± 4.8 IIH patients 69.8 ± 10.2 glaucoma patients	EDI with SD-OCT	Spectralis	870	<15.	$20° \times 10°$ rectangle scanning covering the ONH.
García-Montesinos et al. [48]	Ophthalmic	Papilledema	LCD PTT	Total: 8/12 Control: — Exp.:6 TLCD <-9.2 mmHg (group 1) 6 TLCD >-9.2 mmHg (group 2)	39 ± 19.9	EDI with SD-OCT	Spectralis	870	Inaccurate images owing to segmentation algorithm errors (failed to detect the edges of the BMO).	Vertical scan closest to the ONH center and where the visibility of the anterior LC surface was more complete.
Demir et al. [49]	Ophthalmic	Angioid streaks (AS)	ALCD LCT	Total: 74/74 Control: 42/42 Exp.: 32/32	53.8 ± 10.2 control group 51.7 ± 8.0 AS patients $p = 0.34$	EDI with SD-OCT	Spectralis	870	NA.	Single line scan centered on the optic disc.
Seo et al. [27]	Ophthalmic	Graves' orbitopathy (GO)	LCD	Total: 42/69 Control: — Exp.: 40 (excluded 19) 15 muscle-dominant 25 fat-dominant	45.2 ± 4.01 muscle-dominant 31.8 ± 1.9 fat-dominant $p = 0.002$	EDI with SD-OCT	Spectralis	870	B-scan images were not well visualized to discriminate the anterior surface of the LC.	$15° \times 10°$ covering the optic disc.

TABLE 1: Continued.

Authors	Group type	Ophthalmic disease	Parameter	No. of patients/eyes	Age (years) and p value	Technique	Device	Light WL (nm)	Image quality cutoff	Field of view
Moghimi et al. [50]	Ophthalmic	Pseudoexfoliation syndrome (PXS)	LCT ALD PLD	Total: 61/61 Control: 29/29 Exp.: 32/32	64.86 ± 7.04 control group 67.94 ± 7.30 PXS group p = 0.10	EDI with SD-OCT	Spectralis	870	<20 inadequate quality as determined by unclear fundus images, interruption of the RNFL, or unclear border of the LC or posterior choroid.	A 15° ×10° rectangle centered on the optic disc.
Soares et al. [51]	Ophthalmic	Spontaneous intracranial hypotension	ALCD	Total: 10/20 Control: 10/10 Exp.: 10/10	36.8 ± 4.6 control group 38 ± 4.18 experimental group	EDI with SD-OCT	Spectralis	870	NA.	B-scan images obtained by dividing the optic disc into 48 equal diagonal slices.
Karaca Adıyeke et al. [52]	Ophthalmic	Central retinal vein occlusion (CRVO)	LCT	Total: 67/67 Control: 35/35 Exp.: 32/32	57.9 ± 13.8 control group 62.2 ± 11.6 experimental group	EDI with SD-OCT	Spectralis	870	Vertical scans without clearly visible borders.	Vertical scans with clearly visible borders centered on ONH.
Son et al. [53]	Ophthalmic	Branch retinal vein occlusion (BRVO)	LCT PTT	Total: 85/85 Control: 35/35 Exp.: 50/50	59.4 ± 12.9 control group 60.9 ± 12.2 experimental group p = 0.615	EDI with SD-OCT	Spectralis	870	The lamina cribrosa margin was not defined.	10° ×15° covering the optic disc.
Sırakaya and Bekir [54]	Ophthalmic	Unilateral branch retinal vein occlusion (BRVO)	LCT LCD	Total: 73/108 Control: 38 Exp.: 35	65.15 ± 9.85 control group 65.48 ± 8.91 experimental group p = 0.882	EDI with SD-OCT	Spectralis	870	<20.	A 15° ×10° rectangular image centered on the optic disc.
Altunel et al. [55]	Ophthalmic	Central retinal vein occlusion	LCT	Total: 80/80 Control: 42/42 Exp.: 38/38	64.5 ± 10.3 control group 65.2 ± 11.0 experimental group p = 0.781	EDI with SD-OCT	Spectralis	870	Scans with invisible LC borders.	A 10° ×15° rectangle covering the optic disc.

TABLE 1: Continued.

Authors	Group type	Ophthalmic disease	Parameter	No. of patients/eyes	Age (years) and p value	Technique	Device	Light WL (nm)	Image quality cutoff	Field of view
Lim et al. [56]	Ophthalmic	Unilateral branch retinal vein occlusion (BRVO)	LCT	Total: 77/77 Control: 31/31 Exp.: 46/46	61.8 ± 11.6 control group 60.5 ± 11.1 experimental group p = 0.635	EDI with SD-OCT	Spectralis	870	< 15.	A 15°×10° rectangular image centered on the ONH.
Akkaya and Küçük [57]	Ophthalmic	Keratoconus	LCT LCD	Total: 101/101 Control: 56/56 Exp.: 45/45	22.5 ± 7.4 control group 24.5 ± 7.2 experimental group p = 0.17	EDI with SD-OCT	Spectralis	870	< 20.	A 15°×10° rectangular image centered on the optic disc.
Lee et al. [58]	Ophthalmic	Myopia	LCT LCD PTT	Total: 40/40 Control: — Exp.: 40/40	28 ± 9	EDI with SD-OCT	Spectralis	870	Images with unclear LC margin, severe shadowing due to overlying vessels, or poor image quality due to cataracts.	A 15°×10° rectangular image centered on the optic disc.
Jnawali et al. [59]	Ophthalmic	Myopia	ALCSD	Total: 52/52 Control: 29/29 Exp.: 23/23	10.16 ± 2.48 control group 12.43 ± 2.31 experimental group p = 0.001	EDI with SD-OCT	Spectralis	880	< 30.	A 12° peripapillary circular scan centered at the optic nerve head.
Ohno-Matsui et al. [60]	Ophthalmic	Myopia	Distance between the inner surface of the LC and the subarachnoid space (SAS)	Total: 108/165 Control: 32 Exp.: 133	Patients with pathologic myopia: 53.2 ± 11.9 subarachnoid space of the optic nerve visible by OCT 59.7 ± 9.3 subarachnoid space of the optic nerve not visible by OCT	SS-OCT	Topcon	1050	Poor image quality because of dense cataract, poor fixation because of macular chorioretinal atrophy, myopic macular holes, or severe visual field defects.	3 × 3 mm and 6×6 mm scans centered on the optic disc.

TABLE 1: Continued.

Authors	Group type	Ophthalmic disease	Parameter	No. of patients/eyes	Age (years) and p value	Technique	Device	Light WL (nm)	Image quality cutoff	Field of view
Miki et al. [61]	Ophthalmic	Myopia glaucoma	LC defects	Total: 108/159 Control: 35 Exp.: 67 high myopia with glaucoma (MG group) 22 glaucoma without high myopia (G group) 35 high myopia without glaucoma (M group)	57.4 ± 16.6 control group 52.4 ± 12.4 MG group 62.3 ± 10.4 G group 55.0 ± 13.5 M group $p = 0.1076$	SS-OCT	Topcon	1600	Poor quality images such as poor contrast images due to media opacity or poorly fixated images. Eyes with poor visibility of the LC, defined as less than 80% visibility of the anterior laminar surface within the ONH area.	A 6 × 6 mm cube centered on the ONH.
Han et al. [18]	Ophthalmic	Myopia with and without open-angle glaucoma	LC defects	Total: 282/282 Control: 58 Exp.: 90 myopic eyes without OAG 134 myopic eyes with OAG	51.3 ± 10.7 control group 46.1 ± 11.0 myopic eyes without OAG 50.9 ± 11.0 myopic eyes with OAG $p = 0.35$	EDI with SD-OCT	Spectralis	870	Scan with <70% of the anterior LC visible due to prelaminar tissue, RPE, or overlying vessels in ≥3 of the 48 radial line scans.	Radial line B-scans (each at an angle of 3.75°) centered on the optic disc.
Rebolleda et al. [62]	Ophthalmic	Nonarteritic anterior ischaemic optic neuropathy (NAION)	ALCSD LCT PTT	Total: 34/34 Control: 17/17 Exp.: 17/17	71.9 ± 10.7 NAION patients	EDI with SD-OCT	Spectralis	870	Inaccurate images due to errors in the segmentation algorithm (failed to detect the edges of the BMO). Scan without retinal vasculature and where borders were more clearly visible was evaluated.	Vertical scan that was closest to the ONH center and where the visibility of the anterior LC surface was complete (without including main vessels).

Table 1: Continued.

Authors	Group type	Ophthalmic disease	Parameter	No. of patients/eyes	Age (years) and p value	Technique	Device	Light WL (nm)	Image quality cutoff	Field of view
Fard et al. [63]	Ophthalmic	Nonarteritic anterior ischaemic optic neuropathy (NAION) Primary open-angle glaucoma (POAG)	ALCS LCT	Total: 91/121 Control: 29 Exp.: 32 POAG 30 NAION patients and their 30 fellow eyes	63.4 ± 7.9 control group 65.6 ± 13.1 POAG 58.4 ± 10.5 NAION $p = 0.01$	EDI with SD-OCT	Spectralis	870	Images with poor centration, segmentation errors, or poor quality (<15 dB).	A 15° × 15° square covering the optic disc.
Lee et al. [64]	Ophthalmic	Normal-tension glaucoma (NTG) Nonarteritic anterior ischemic optic neuropathy (NAION)	LCD PTT	Total: 105/105 Control: 42 Exp.: 21 NAION 42 NTG	60.0 ± 9.7 control group 60.4 ± 9.8 NTG 61.6 ± 10.6 NAION $p = 0.686$	EDI with SD-OCT	Spectralis	870	<15 scans that did not allow clear delineation of the anterior border of the LC.	A 10° × 15° rectangle covering the optic disc.
Rebolleda et al. [26]	Ophthalmic	Nonarteritic anterior ischemic optic (NAION) Primary open-angle glaucoma (POAG)	ALCD PTT	Total: 68/88 Control: 23 Exp.: total: 65 23 NAION 17 fellow unaffected eyes 25 POAG	68.6 ± 10.7 control group 68.6 ± 10.3 NAION 72.3 ± 9.8 POAG $p = 0.53$	EDI with SD-OCT	Spectralis	870	Segmentation errors, poor centration, or poor quality.	A 15° × 10° vertical rectangle centered on the optic disc.
Akkaya et al. [28]	Ophthalmic	Anisometropic Amblyopia	LCT LCD	Total: 95/127 Control: 32 Exp.: 32 hyperopic anisometropic amblyopia and 32 fellow eyes 31 hyperopic nonamblyopic	11.2 ± 2.0 control group 12.0 ± 1.8 amblyopic and fellow eyes 10.7 ± 2.2 hyperopic nonamblyopic p (amblyopia vs. fellow) = 1.0 p (amblyopia vs. control) = 0.58 p (amblyopia vs. hyperopic nonamblyopia) = 0.15	EDI with SD-OCT	Spectralis	870	<20 unclear fundus images and unclear LCT border.	A 15° × 10° rectangular image centered on the optic disc.
Shinohara et al. [65]	Ophthalmic	Tilted disc syndrome (TDS)	Sloping of the lamina cribrosa	Total: 44/54 Control: 16 Exp.: 38	74.9 ± 9.3 control group 66.1 ± 11.2 experimental group	SS-OCT	Topcon	1050	NA.	Scan length: 12 mm centered on the optic disc.

TABLE 1: Continued.

Authors	Group type	Ophthalmic disease	Parameter	No. of patients/eyes	Age (years) and p value	Technique	Device	Light WL (nm)	Image quality cutoff	Field of view
Lee et al. [64]	Ophthalmic	Superior segmental optic nerve hypoplasia (SSOH) Primary open-angle glaucoma (POAG)	LCT LCD	Total: 126/126 Control: 54 Exp.: 35 SSOH 37 POAG	46.1 ± 15.2 control group 29.1 ± 12.5 SSOH 54.7 ± 12.1 POAG $p < 0.001$	EDI with SD-OCT	Spectralis	870	<15 images did not allow clear delineation of both anterior and posterior borders of the central portion of the LC.	Horizontal B-scan section images covering the optic disc, 30 to 34 μm apart (the scan-line distance being determined automatically by the instrument).
Rebolleda et al. [66]	Ophthalmic	Neovascular age-related macular degeneration	LCD PTT	Total: 50/50 Control: 20/20 Exp.: 30/30	74.5 ± 7.7 control group 77.4 ± 6.8 experimental group $p = 0.432$	EDI with SD-OCT	Spectralis	870	Only the highest-quality image and most centered vertical scan without retinal vasculature and where borders were more clearly visible were evaluated.	Vertical scan that was closest to the ONH center and where the visibility of the anterior LC surface was complete (excluding the main vessels).
Hata et al. [67]	Ophthalmic	Compressive optic neuropathy (CON) Glaucomatous optic neuropathy (GON)	LCD PTT	Total: 102/102 Control: 34 Exp.: 34 CON 34 glaucoma	59.4 ± 14.6 control group 59.2 ± 13.2 CON 59.5 ± 13.5 glaucoma $p = 0.94$ (between CON and glaucoma) $p = 0.95$ (between CON and normal subjects)	EDI with SD-OCT	Spectralis	870	NA.	Radial scanning pattern centered on the optic disc (24 high-resolution 15° radial scans).
Kim et al. [7]	Ophthalmic	Normal tension glaucoma (NTG) Autosomal dominant optic atrophy (ADOA)	LCCI LCD	Total: 120/120 Control: 48 Exp.: 24 ADOA 48 NTG	63.38 ± 14.45 control group 63.25 ± 15.66 ADOA 63.42 ± 12.74 NTG $p = 0.894$	EDI with SD-OCT	Spectralis	870	<15.	A 10° ×15° rectangle covering the optic disc.

TABLE 1: Continued.

Authors	Group type	Ophthalmic disease	Parameter	No. of patients/eyes	Age (years) and p value	Technique	Device	Light WL (nm)	Image quality cutoff	Field of view
Yang et al. [68]	Ophthalmic	Diabetic retinopathy with and without panretinal photocoagulation	ALCSD LCT PTT	Total: 206/206 Control: 33 (group I) Exp.: 30 without diabetic retinopathy (group II), 66 nonproliferative diabetic retinopathy (group III), 45 panretinal photocoagulation (group IV), and 32 normal tension glaucoma (group V)	53.5 ± 8.8 group I 55.7 ± 12.3 group II 56.6 ± 10.4 group III 56.2 ± 9.9 group IV 53.8 ± 13.0 group V $p = 0.595$	SS-OCT	Topcon	1500	Unable to visualize the lamina cribrosa and/or peripapillary tissue clearly.	Scans with a scan length of 6 × 6 mm.
Yokota et al. [69]	Ophthalmic	Neovascular glaucoma (NVG) Diabetic retinopathy	ALCT LCT	Total: 46/46 Control: — Exp.: 20 PDR with non-NVG 26 PDR with NVG	66.2 ± 2.4 PDR with the non-NVG group 61.4 ± 2.1 PDR with the NVG group $p = 0.151$	EDI with SD-OCT	Spectralis	870	Eyes with other ocular diseases that might decrease the image quality of OCT were excluded (e.g., vitreous hemorrhage).	Horizontal B-scans at an interval of 50 μm.
Gómez-Mariscal et al. [70]	Ophthalmic	Age-related macular degeneration (AMD) Diabetic macular edema (DME) or retinal venous occlusion (RVO)	LCD PTT	Total: 29/53 Control: 24 Exp.: 29	76.9 ± 6.6 control group 76.8 ± 6.9 experimental group $p = 0.943$	EDI with SD-OCT	Spectralis	870	Presence of media opacities which prevented a good image quality.	Vertical scan selected close to the center of the papilla, and three vertical measurements were performed to obtain a representative value of the relative position and displacement of ONH structures.

LC = lamina cribrosa, LCT = lamina cribrosa thickness, cLCT = central lamina cribrosa thickness, LCD = lamina cribrosa depth, cLCSD = central lamina cribrosa surface depth, PTT = prelaminar tissue thickness, cPTT = central prelaminar tissue thickness, Exp = experimental, YG = young group, MG = middle group, OG = old group, EDI = enhanced depth imaging, SD = spectral domain, SS = swept source, ALCSD = anterior lamina cribrosa surface depth, ONH = optic nerve head, PPA = peripapillary atrophy, LCCI = lamina cribrosa curvature index, PLD = posterior laminar depth, and NA = not available, that is, not mentioned in the article.
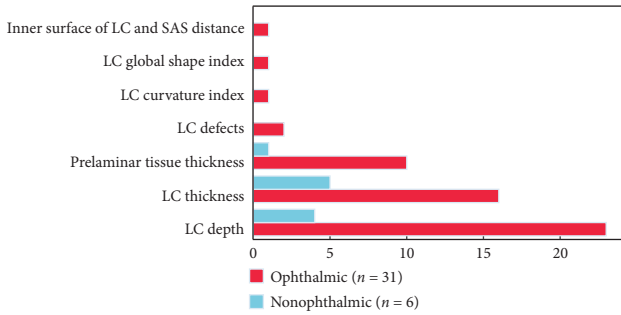
FIGURE 3: Number of occurrences of each lamina cribrosa structural feature published in the literature. The value n corresponds to the total number of studies for each group.

papers) were considered for the average calculations (equations (1) and (2)).

3.1. LCT Measurements.

LCT has been defined in the literature as the distance between the anterior and posterior borders of the highly reflective region visible below the optic disc cup in B-scan cross sections of the ONH (see the red arrow in Figure 4) [18]. However, a discrepancy between the LCT measurements, namely, between the locations used to calculate the LCT average, has been observed and reported in Table 2. For example, Lee et al. [74] considered three locations in each eye (midhorizontal, superior, and inferior midperipheral), with a separation of $100 \mu m$ between the points. Bartolomé et al. [19] determined the points as close as possible to the vertical center of the ONH, which was identified as the point where the trunk of central retinal vessels extends from the ONH, as reported by Park et al. [12]. Other authors, such as Xiao et al. [20], considered LCT as the average of the central and paracentral points (150 μm from the center point in the horizontal and vertical directions).

3.2. LCD Measurements.

In the literature, LCD (also named as anterior lamina cribrosa depth in several studies) is defined as the perpendicular distance from the BMO plane to the maximum depth point of the anterior LC surface. All articles included in this review provide the measurements relative to Bruch's membrane opening (BMO). Only the measurements relative to BMO were considered for the calculations since all articles provide the measurement relative to this plane. Two studies, Rhodes et al. [21] and Luo et al. [22], also considered the scleral plane and the ASCO as the reference for depth measurements. These differences have been shown to lead to measurement bias, as reported by Luo et al. [22], who obtained $402 \pm 91 \mu m$, $309 \pm 88 \mu m$, and $332 \pm 96 \mu m$ for BMO, ASCO, and scleral reference planes, respectively. The number of selected points and B-scan planes to average the measure also influence the precision of the results. Other authors, such as Park et al. [23], obtained measurements as the average from 11 equidistant planes that divided the optic disc diameter into 12 equal parts vertically in each eye. A line was drawn from each of the two LC insertion points perpendicularly to the line connecting the two Bruch's membrane edges (see line D in Figure 4). The area surrounded by these two lines was measured (see area S in Figure 4). The mean LCD was approximated by dividing S by the length of D for each of the 11 horizontal OCT scans. Finally, Lee et al. [24] defined LCD as the mean of 3 values obtained from the 3 upper B-scans (1st to the 3rd scan), the 3 central B-scans (5th to the 7th scan), and at the 3 lower B-scans (from the 9th to the 11th scan) passing through the ONH. Commonly, temporal adjacent points were selected because the maximally depressed point was often close to the central vessel trunk, and its shadow obscured the LC [25].

3.3. Features' Applicability and Measurements.

This section details the mean values for the two dominating LC structural features (LCT and LCD) in the three groups (healthy controls, ophthalmic, and nonophthalmic diseases). The values were calculated based on the articles presented in Table 2 for each group and disease, and the mean and SD values for each group are summarized in Figure 5.

3.3.1. Healthy Group Measurements.

Analysis of healthy subjects is very important to establish normative values for the healthy population, and hence facilitate the diagnosis and follow-up of the pathology. The studies that included only healthy subjects, as well as those comparing patients to a healthy control group, were selected, and the LCT and LCD average values were determined. The observed averages were $261 \pm 39 \mu m$ (range: 211–323 μm) and $386 \pm 91 \mu m$ (range: 293–441 μm) for the LCT and LCD, respectively. Figures 5(a) and 5(b) show a comparison between the three groups for both features. These parameters seem to be influenced by several factors, such as age and racial ancestry. Rhodes et al. [21] conducted a study in healthy eyes and concluded that the LC was significantly anteriorly displaced with increasing age in those with European ancestry in contrast to those with African ancestry.

3.3.2. Ophthalmic Disease Group Measurements.

The ophthalmic disease group represented the largest group ($n = 31$) and included a large number of conditions, the most common being myopia, retinal vein occlusion (RVO), nonarteritic anterior ischaemic optic neuropathy (NAION), pseudoexfoliation syndrome (PXS), superior segmental optic nerve hypoplasia (SSOH), compressive optic neuropathy (CON), age-related macular degeneration (AMD), autosomal dominant optic atrophy (ADOA), and diabetic macular edema (DME). For ophthalmic patients, mean LCT and LCD were $211 \pm 33 \mu m$ and $403 \pm 90 \mu m$, respectively (Figure 5). The graphics in Figure 6 presents the mean values for different ophthalmic diseases in comparison with the healthy population (horizontal dashed green line). Regarding the LCT, its mean was lower for every pathology in this group except for SSOH (Figure 6(a)). Overall, the studies that reported LCD in nonglaucomatous ophthalmic diseases showed a slightly higher mean LCD compared with healthy controls (Figure 5(b)). Nonetheless, this trend is not

TABLE 2: Approach used for the measurement and reported values for the lamina cribrosa thickness and depth.

Authors	Measurement	Results
Xiao et al. [20]	(i) cCLT was defined as "the distance between the anterior lamina cribrosa surface (ALCactS) and posterior lamina cribrosa surface (PLCS). cLCT was calculated from the average value of the LCT in the ONH center point and paracentral points (150 μm from the center point in the horizontal and vertical directions)." (ii) cALCSD was defined as "the distance between the ALCS and the reference plane (the connection of the terminal of Bruch's membrane was defined as the reference plane). The cALCSD was calculated from the average value of ALCSD in the ONH center point and paracentral points (150 μm from the center point in the horizontal and vertical directions)."	(i) cLCT (μm): 235.18 $\pm$ 41.27; $p < 0.001$ between the 3 groups (YG/MG/OG) (ii) cALCSD (μm): 358.02 $\pm$ 93.80; $p = 0.11$ between the 3 groups (YG/MG/OG)
Sousa et al. [34]	ALCD was defined as "the prependicular distance from the BMO plane to the maximum depth point of the anterior LC border. A mean of the 2 measurements was used."	(i) Vertical scan (μm): 456.2 $\pm$ 84.3 (right eye)/444.5 $\pm$ 92.2 (left eye); $p = 0.19$ (ii) Horizontal scan (μm): 436.7 $\pm$ 81.6 (right eye) 427.6 $\pm$ 82.7 (left eye); $p = 0.13$ (iii) Pool mean + SD (μm): 441.5 $\pm$ 82.5
Lee et al. [35]	"LCT was measured as the distance between the levels of the anterior and posterior borders in the B-scan images. LCT was measured at the midpoint between the opening of Bruch's membrane and two additional points that were 150 μm from either side of the midpoint."	273.19 $\pm$ 34.74 μm
Bartolomé et al. [19]	(i) "LCD was measured in 11 horizontal B-scans that were spaced equally along the vertical diameter of the optic disc. The line connecting both Bruch's membrane opening (BMO) edges was used as a reference plane for all depth measurements. A line perpendicular to this reference line was drawn from each BMO edge to the anterior surface of the lamina cribrosa. When one of these two perpendicular lines did not meet the anterior laminar surface because of disc tilting and associated lateral lamina displacement, a line was drawn from the anterior lamina cribrosa insertion point perpendicularly to the line connecting the two BMO edges. The area defined by these two perpendicular lines, the line connecting the BMO edges and the anterior laminar surface, was measured area S. Mean LCD depth in each of the 11 horizontal EDI-OCT scans was defined by area S divided by length D." (ii) LCT was defined as "the distance between the anterior and posterior borders of the highly reflective region at the vertical center of the ONH. LCT was determined as close as possible to the vertical center of the ONH, which was identified as the site where the trunk of central retinal vessels extends from the ONH."	(i) LCD (μm): 329.15 $\pm$ 60.85 (male: 351.03 $\pm$ 63.83/female: 319.01 $\pm$ 57.39; $p = 0.057$) (ii) LCT (μm): 323.25 $\pm$ 56.02 (male: 344.75 $\pm$ 48.73/female: 313.07 $\pm$ 71.14; $p = 0.094$)
Leal et al. [36]	"ALCD was defined as the maximum perpendicular distance between the line connecting both ends of Bruch's membrane and the maximum depth point of the anterior border of the LC. The anterior border of the LC was defined by a highly reflective structure below the optic cup."	(i) Right eye vertical (REV) scan (μm): 456.16 $\pm$ 84.32 (ii) Left eye vertical (LEV) scan (μm): 444.53 $\pm$ 92.19 (iii) Right eye horizontal (REH) scan (μm): 436.66 $\pm$ 81.57 (iv) Left eye horizontal (LEH) scan (μm): 427.56 $\pm$ 82.71 (v) Pool mean + SD (μm): 441.23 $\pm$ 85.20

TABLE 2: Continued.

Authors	Measurement	Results
	"LCD measures the distance of the LC from a reference plane, either a BMO plane (LDBMO) or a scleral plane (LDAS). The definition and computation of mean LD require the definition of a reference structure against which to measure depth, a surface reconstruction and sampling for mean depth, and the use of a suitable coordinate frame for the manually delineated point clouds. The Bruch structure (BMO plane, BMO ellipse, and laminar half-space) is computed, and the LC moved to a Bruch frame. The LC sections are uniformly resampled; an optimal mesh is built from these LC sections; and mean LDBMO is computed as a weighted average of the mesh centroid depths. The scleral structure is built using an interior disk-like region (the region of the AS between 1700 and	(i) LD BMO (μm): 413.88 ± 75.06 (AD young) 365.38 ± 64.48 (AD old) 382.43 ± 93.29 (ED young) 337.73 ± 82.41 (ED old)
Rhodes et al. [21]	1800 μm from the axis of the BMO cylinder, the right elliptic cylinder defined by the BMO ellipse, orthogonal to the BMO plane). Like the BMO, this region is almost planar. The scleral representative of an AS half-section is the mean of the samples that lie between 1700 and 1800 μm from the axis of the BMO cylinder (using Euclidean, not geodesic distance). The mean is used (as opposed to the point at 1750 μm, e.g.) as a smoothing operation. The scleral plane (ellipse) is the best-fitting plane (ellipse) of the point cloud of scleral representatives, analogous to the BMO plane/ellipse. Replacing the BMO plane by the scleral plane, we have LD based on a scleral reference plane (distance of LC from the scleral plane, LDAS). These measurements are again simplified by using a special frame, where depth becomes the z-coordinate."	Pool mean + SD: 379.29 ± 82.70 (ii) LD AS (μm): 333.61 ± 83.84 (AD young) 353.75 ± 60.32 (AD old) 316.39 ± 87.60 (ED young) 309.20 ± 78.69 (ED old)
Kim et al. [38]	Anterior LC depth (LCD) was defined as "the maximal vertical distance between the reference plane connecting Bruch's membrane openings (BMO) and the anterior LC surface."	463.4 ± 118.8 μm
El-Agamy et al. [40]	"ALCSD was measured at all planes, defined as the distance from the line connecting the two Bruch's membrane opening (BMO) edges (reference line) to the anterior LC surface. It was measured in the direction perpendicular to the reference plane at three points: the maximum depth point and two additional points (100 and 200 μm apart from the maximum depth point to the temporal direction). Only the temporally adjacent points were selected because the LC at the maximally depressed point was masked by the shadow of the central vessel trunk. The average of three measurements was taken as the ALCSD of each plane. The average of the ALCSDs from all planes was defined as the mean of ALCSD of the eye."	(i) Mean of ALCSD (μm): 371.88 ± 114.62 (ii) Superior plane (μm): 368.08 ± 116.04 (iii) Middle plane (μm): 379.86 ± 117.12 (iv) Inferior plane (μm): 366.59 ± 120.98 Significant difference between superior and middle planes ($p = 0.004$) and middle and inferior planes ($p = 0.013$) but no significant difference between superior and inferior planes ($p = 0.820$)

Table 2: Continued.

Authors	Measurement	Results
Lee et al. [24]	(i) "LCD was determined by measuring the distance from the Bruch's membrane (BM) opening plane to the level of the anterior LC surface in 11 equidistant planes that divided the optic disc diameter into 12 equal parts vertically in each eye. A reference line connecting the two termination points of the BM was drawn on each B-scan image. The distance from the reference line to the level of the anterior border of the LC was measured at three points: the maximally depressed point and two additional points (100 and 200 μm from the maximally depressed point in a temporal direction). Only the temporally adjacent points were selected because the maximally depressed point was often close to the central vessel trunk, the shadow of which obscured the LC. When there was insufficient space for measuring the LCD at three points (e.g., the uppermost or lowermost B-scans or B-scans with a prominent vascular shadow), adjacent scans were used. The measurements from the 11 planes were used to calculate the mean LCD of the eye. The superior LCD was defined as the mean of 3 values obtained at the 3 uppermost B-scan images (from the 1st to the 3rd scan), the central LCD as that obtained at the 3 central-most B-scan images (from the 5th to the 7th scan), and the inferior LCD as that obtained at the 3 lowermost B-scans (from the 9th to the 11th scan)." (ii) "LCT was measured at three locations in each eye (the midhorizontal and the superior and inferior midperipheral regions of the ONH) using thin-slab maximum-intensity-projection (MIP) images."	(i) LCT (μm): overall subjects: 250.4 ± 41.6 244.9 ± 47.2 (male)/255.1 ± 37.3 (female); $p = 0.544$ (ii) LCD (μm): overall subjects: 425.9 ± 100.2 486.2 ± 91.4 (male)/372.0 ± 80.6 (female); $p = 0.002$
Seo et al. [43]	"After the 3D image was reconstructed, seven B-scan images that divided the optic disc diameter into eight equal parts vertically were selected for each eye. These seven B-scan lines were defined as plane 1 to plane 7 (top to bottom). In this model, plane 4 corresponds to the midhorizontal plane, and planes 2 and 6 correspond to the superior and inferior midperiphery, respectively. The ALCSD was measured at each plane and defined as the distance from the Bruch's membrane opening level to the anterior LC surface."	402.06 ± 101.46 μm
Tun et al. [45]	LCD was defined as "the distance from each anterior LC point to the peripapillary scleral (PPS) reference plane line in the central one-third of the length of BMO. The PPS reference plane was defined as a line connecting the outermost points of the anterior surface of the PPS ring. The mean depth of all LC points on the anterior LC surface was reported as the mean LC depth."	363.65 ± 95.36 μm
Thakku et al. [46]	LCD was defined as "the distance of the reconstructed anterior LC from the BMO plane. The mean depth of all points on the surface was reported as the mean LC depth. Additionally, mean depths of points along the nasal-temporal (N-T) and superior-inferior (S-I) cross sections were reported."	403 ± 90 μm

TABLE 2: Continued.

Authors	Measurement	Results
Luo et al. [22]	"Mean depth of the segmented points within the central 24 anterior scleral canal opening (ASCO) subsectors regardless of the reference plane was used for the depth measurement. Quantification of all parameters derived from the manually segmented points was performed within custom software (MATLAB version 7.3.0.267). A BMO reference plane was determined based on the 48 BMO points (2 points in each of 24 radial B-scans) as for the ASCO reference plane. Peripapillary BM and peripapillary scleral reference planes were separately defined by fitting a plane to 48 points 1700 μm distal to the BMO centroid (for the BM points) and ASCO centroid (for the scleral points)."	(i) Central LD BMO (μm): 402 ± 91 (ii) Central LD BM (μm): 498 ± 123 (iii) Central LD ASCO (μm): 309 ± 88 (iv) Central LD sclera (μm): 332 ± 96
Akkaya et al. [28]	(i) ALCSD was defined as "the distance between the Bruch's membrane opening and the anterior border of the lamina cribrosa." (ii) LCT: "anterior and posterior borders of the highly reflective region at the vertical center of the optic nerve head in horizontal SD-OCT cross sections were defined as lamina cribrosa borders, and the distance between them was defined as LCT."	(i) LCT (μm): control group: 248.50 ± 5.40 experimental group: 271.61 ± 33.96 $p < 0.001$ (ii) ALCSD (μm): control group: 420.32 ± 90.26 experimental group: 351.45 ± 58.61 $p = 0.003$
Eraslan et al. [29]	"LCT was measured manually on vertical lines lying between the inner and outer boundaries of the hyperreflective area temporal to the central retinal vessels. In cases where the hyporeflective image created by the nerve fibers passing through the laminar pores was too close to the temporal of the central retinal vessels in patients with thinner LCs, the measurement was performed at the points at which the inner and outer boundaries of the LC could be most clearly seen."	Control group: 292.5 ± 33.7 μm Experimental group: 209.4 ± 40.2 μm $p < 0.001$
Küçük et al. [30]	(i) LCT was defined as "the distance between the LCT borders, which were the anterior and posterior borders of the highly reflective region at the vertical center of the ONH in the horizontal SD-OCT cross section." (ii) LCD was defined as "the distance between Bruch's membrane opening and the anterior border of the LCT."	(i) LCT (μm): control group: 300.49 ± 42.6 Experimental group (OSAS): 213.38 ± 30.7; $p < 0.001$ Mild OSAS: 223.23 ± 36.7/moderate OSAS: 219.79 ± 27.8/severe OSAS: 198.8 ± 23.1; $p = 0.068$ (ii) LCD (μm): control group: 411.67 ± 101.4 Experiemental group (OSAS): 397.21 ± 85.6; $p = 0.506$ Mild OSAS: 408.46 ± 101.8/moderate OSAS: 404.13 ± 86.7/severe OSAS: 379.36 ± 70.2; $p = 0.639$
Lee et al. [32]	"LCT was measured at three locations in each eye (the midhorizontal and the superior and inferior midperipheral regions of the ONH) using thin-slab maximum-intensity-projection (MIP) images."	Control group: 247.95 ± 37.55 μm Experimental group: 242.46 ± 31.93 μm; $p = 0.616$
Sirakaya et al. [33]	(i) LCT was designated as "the area between the outer and inner lines of the hyperreflective region at the vertical center of the optic nerve head; LC thickness was the perpendicular distance between those borders." (ii) LCD was defined as "the distance between the BMO and the anterior margin of the LC."	(i) LCT (μm): control group (group III): 279.91 ± 49.61 Experimental group (groups I and II): group I: 237.48 ± 38.53 group II: 241.42 ± 36.89; $p = 0.684$ (group I versus group II); $p = 0.001$ (group versus group III); $p < 0.001$ (group II versus group III) (ii) LCD (μm): control group (group III): 355.34 ± 65.53 Experimental group (groups I and II): group I: 412.15 ± 58.80 Group II: 405.57 ± 55.39; $p = 0.653$ (group I versus group II); $p = 0.001$ (group I versus group III); $p = 0.001$ (group II versus group III)

TABLE 2: Continued.

Authors	Measurement	Results
Pasaoglu et al. [47]	"LCD and LCT were measured at the 7 locations equidistant across the vertical optic disc diameter. These seven horizontal B-scan lines were defined as planes 1–7 (from superior to inferior). The average LC depth and thickness were determined as the mean values of the measurements made at seven points of the LC. ALS was defined as the anterior border of the highly reflective region beneath the internal limiting membrane at the optic disc cup on the B-scans. Distance between the reference line connecting both edges of the Bruch membrane and anterior surface of the LC at the maximally depressed point was defined as the ALS depth. The distance between the same reference line and the posterior surface of the LC again at the maximally depressed point was defined as the PLS depth. The difference between the PLS and ALS depth was taken to be the LC thickness."	(i) ALCSD (μm): control group: 359.40 ± 105.38 Experimental group: 225.00 ± 58.57 $p < 0.01$ (ii) LCT (μm): control group: 210.70 ± 36.93 Experimental group: 224.75 ± 45.98 $p = 0.42$
Villarruel et al. [25]	"LCD was defined as the distance between the reference line connecting both edges of the Bruch membrane (Bruch membrane opening plane) and the anterior surface of the LC. The anterior LC surface was defined as the anterior border of the highly reflective region beneath the internal limiting membrane at the optic disc cup on the B-scans. On the selected B-scans, the LC depth was measured at 3 points: the maximally depressed point and 2 additional points (100 and 200 μm apart from the maximally depressed point in a temporal direction). Temporal adjacent points were selected because the maximally depressed point often was close to the central vessel trunk, which cast a shadow obscuring the LC. The average of these 3 values was defined as the LC depth of the B-scan. The LC depth of each of the B-scans was then averaged and defined as the mean LC depth for that eye."	Control group: 387.8 ± 53.9 μm Patients with IIH: 325.2 ± 92.1 μm; $p < 0.01$ (comparative to the control group) Patients with HTG: 493.0 ± 115.2 μm; $p < 0.001$ (comparative to the control group)
Demir et al. [49]	(i) ALCSD was defined as "the distance between the BMO reference plane and the anterior border of the LC." (ii) LCT was defined as "the distance between the anterior and posterior borders of the LC. The anterior and posterior borders of the LC were defined using a highly reflective structure below the optic cup."	(i) ALCSD (μm): control group: 432.5 ± 82.1 Experimental group: 350.9 ± 70.8; $p = 0.003$ (ii) LCT (μm): control group: 241.3 ± 43.2 Experimental group: 166.3 ± 41.0; $p < 0.001$
Seo et al. [27]	LCD value was "determined by measuring the distance from the Bruch membrane opening (BMO) plane to the level of the anterior LC surface. The anterior surface of the LC was defined by the highly reflective structure below the optic cup. A reference line connecting the two termination points of the Bruch membrane was drawn on each B-scan image. The distance from the reference line to the level of the anterior border of the LC was then measured at three points: the maximally depressed point and two additional points located 100 μm from the maximally depressed point in the temporal and nasal directions, respectively. The distance was measured on the line perpendicular to the reference line. The average value of these three points was considered as the LCD."	Muscle-domain group: 462.79 ± 95.96 μm Fat-domain group: 621.39 ± 78.39 μm $p = 0.007$

TABLE 2: Continued.

Authors	Measurement	Results
Moghimi et al. [50]	"The anterior and posterior borders of the highly reflective region at the vertical center of the ONH in the horizontal SD-OCT cross section were defined as the borders of the LC, and the distance between these two borders was defined as LC thickness." (i) "Anterior laminar depth (ALD) and posterior laminar depth (PLD) were defined as the distance between the BMO and the anterior border and posterior border of the LC, respectively. The laminar thickness was defined as the distance between the anterior surface of the optic cup and the anterior border of the LC and the distance between the BMO and the internal limiting membrane (surface of the optic cup)."	(i) ALCSD (μm): control group: central: 321.14 $\pm$ 106.72/superior: 324.05 $\pm$ 87.68/ inferior: 280.33 $\pm$ 92.38/pool mean+SD: 308.51 $\pm$ 95.59 Experimental group: central: 330.12 $\pm$ 90.23; $p = 0.74$/superior: 380.0 $\pm$ 81.51; $p = 0.04$/inferior: 350.82 $\pm$ 99.73; $p = 0.05$/pool mean+SD: 353.65 $\pm$ 90.49 (ii) LCT (μm): control group: central: 273.3 $\pm$ 57.97/superior: 267.50 $\pm$ 93.66/ inferior: 253.90 $\pm$ 59.52/pool mean+SD: 264.90 $\pm$ 70.38 Experimental group: central: 207.8 $\pm$ 47.76; $p < 0.001$/superior: 182.31 $\pm$ 48.53; $p = 0.004$/inferior: 176.52 $\pm$ 42.02; $p = 0.004$/pool mean+SD: 188.88 $\pm$ 46.10
Soares et al. [51]	"ALCSD was defined as the distance between the plane of Bruch's membrane opening (BMO) and the ALCS. The BMO plane was established with a line joining the limits of the BM. Three measurements of ALCS depth were made on three planes perpendicular to the BM plane: the first plane in the maximal depth of ALCS, the second plane 100 μm temporal to the first plane, and the third plane 200 μm temporal to the first plane. Three depth measurements were obtained, and their mean value was considered to be the final depth for each eye in both groups."	Control group: 292.56 $\pm$ 40.71 μm Experimental group: 447.96 $\pm$ 118.51 μm $p = 0.001$
Karaca Adiyeke et al. [52]	LCT was defined as "the distance between the anterior and posterior margins of the LC, which were determined as a highly reflective structure below the optic cup."	Control group: 266.4 $\pm$ 10.7 μm Experimental group: 285.2 $\pm$ 12.7 μm (affected eye) and 283.5 $\pm$ 12.6 μm (fellow eye); $p < 0.01$
Son et al. [53]	LCT was defined as "the thickness of the highly reflective region. If the lamina cribrosa margin was not defined, the auto contrast was used which was included in the program. The measurement point was the midpoint of the line connecting Bruch's membrane openings. If vascular shadows disturbed visualization of the lamina cribrosa, the measurement points were determined as centrally on the midpoint as possible where there was the least likelihood of vascular shadows."	Control group: 260.41 $\pm$ 43.25 μm Experimental group: 208.26 $\pm$ 33.36 μm (affected eye of unilateral BRVO); $p = 0.000$ (comparative to the control group); 204.97 $\pm$ 37.57 μm (fellow eye of unilateral BRVO); $p = 0.000$ (comparative to the control group)
Sirakaya and Bekir [54]	"Bruch's membrane opening (BMO) was defined as the distance of the line between the two endpoints of Bruch's membrane; LC is the area between the outer and inner lines of the hyperreflective region in the vertical center of the ONH." (i) LCT was defined as "the perpendicular distance between those borders." (ii) LCD was defined as "the distance between the BMO and anterior margin of the LC."	(i) LCT (μm): control group: 251.9 $\pm$ 37.2 Experimental group: 212.5 $\pm$ 33.3 (affected eyes); $p < 0.001$ (comparative to the control group); 226.7 $\pm$ 28.8 (unaffected eyes); $p = 0.002$ (comparative to the control group) (ii) LCD (μm): control group: 369.3 $\pm$ 52.3 Experimental group: 411.6 $\pm$ 71.3 (affected eyes); $p = 0.005$ (comparative to the control group); 403.31 $\pm$ 50.49 (unaffected eyes); $p = 0.006$ (comparative to the control group)
Altunel et al. [55]	"Anterior and posterior regions of the LC were defined by highly reflective structures below the ONH." LCT was defined as "the distance between the anterior and posterior regions of the LC."	Control group: 228.0 $\pm$ 7.1 μm Experimental group: 204.4 $\pm$ 8.8 μm (affected eyes); $p < 0.001$ (comparative to the control group) 205.3 $\pm$ 9.3 μm (fellow eyes); $p < 0.001$ (comparative to the control group)

TABLE 2: Continued.

Authors	Measurement	Results
Lim et al. [56]	"LCT was measured at the vertical center of the ONH using a horizontal cross-sectional B-scan. The LCT was defined as the distance between the anterior and posterior borders of the highly reflective region. LCT was obtained from three points: the midsuperior, center, and midinferior locations. LCT was defined as the average value of the LCT at the center of the midsuperior, central, and midinferior horizontal B-scans of the ONH."	Control group: 274.0 ± 29.4 μm Experimental group: 237.0 ± 37.0 μm (affected eye); $p < 0.001$ (comparative to the control group) 241.4 ± 33.2 μm (unafected eye); $p < 0.001$ (comparative to the control group)
Akkaya and Küçük [57]	"3 frames were defined: center, midsuperior, and midinferior, which passed through the ONH, and the parameters of thickness were measured in each of these frames. During measurements of thickness, full weight to the center of the LCT plate was assigned." LCD was defined as "the distance between the BMO and the anterior border of LCT."	(i) LCT (μm): control group: 249.1 ± 4.9 Experimental group: 174.9 ± 11.4 $p < 0.001$ (ii) LCD (μm): control group: 422.0 ± 90.7 Experimental group: 403.2 ± 91.1 $p = 0.3$
Lee et al. [58]	(i) LC thickness was defined as "the shortest distance between the anterior border and the posterior border of the LC. The anterior and posterior LC margins were defined by a highly reflective structure below the optic cup. Anterior and posterior LC margins were defined as the line that connected the peripheral points of the anterior and posterior LC margins. The line that connected the two termination points of Bruch's membrane was used as a baseline reference." (ii) LC depth was measured by "calculating the average at each periphery of the anterior LC margin."	(i) LCT (μm): inferior: 218 ± 10/middle: 218 ± 10/superior: 219 ± 10/pool mean + SD: 218 ± 10 (ii) LCD (μm): inferior: 426 ± 38/middle: 435 ± 41/superior: 427 ± 37/pool mean + SD: 429.33 ± 38.67
Rebolleda et al. [62]	"A reference line connecting the two Bruch's membrane limit points was drawn, and three equidistant points, corresponding to one-half and one-third of the reference, were highlighted and connected to the anterior face of the prelaminar tissue (PT) and the anterior and posterior surfaces of the LC. LCT and anterior LCD were measured at the aforementioned three points. The arithmetic mean of the three measurements was considered as the average. LCT was defined as the difference between the position of the anterior and posterior borders of the LC. LCD was determined by measuring the distance from the reference line to the level of the anterior LC surface."	(i) ALCSD (μm): control group: 347.5 ± 120.9; experimental group: 390.2 ± 120.1; $p = 0.196$ (ii) LCT (μm): control group: 241.2 ± 49.9; experimental group: 245.5 ± 47.4; $p = 0.720$
Fard et al. [63]	"The anterior and posterior borders of the highly reflective region at the vertical center of the ONH in the horizontal SD-OCT cross section were defined as the borders of the LC, and the distance between these two borders was defined as LC thickness. Anterior laminar cribrosa depth (ALD) was measured at the anterior LC surface as the perpendicular distance from BMO distance. Anterior lamina cribrosa depth and LC thicknesses were measured at central, midsuperior, and midinferior sections of the ONH."	(i) ALD (μm): control group: central: 321 ± 107/midsuperior: 324 ± 8/midinferior: 280 ± 92/pool mean + SD: 308.33 ± 95.67; NAION: central: 339 ± 93; $p = 0.61$/midsuperior: 380 ± 83; $p = 0.53$/midinferior: 373 ± 133; $p = 0.30$/pool mean + SD: 364 ± 103 (ii) LCT (μm): control group: central: 273 ± 58/midsuperior: 268 ± 94/midinferior: 254 ± 60/pool mean + SD: 265 ± 70.67; NAION: central: 250 ± 62; $p = 0.42$/midsuperior: 228 ± 52; $p = 0.17$/midinferior: 235 ± 44; $p = 0.16$/pool mean + SD: 237.67 ± 52.67
Lee et al. [64]	LCD was measured on "the three horizontal B-scans. A horizontal reference line was drawn by connecting the two termination points of Bruch's membrane opening (BMO) in each B-scan image. The LCD was then measured from the reference line to the level of the anterior border of the LC at the maximally depressed point and two additional points that were 100 and 200 μm from the maximally depressed point in the temporal direction."	Control group: 427.3 ± 94.1 μm NAION: 390.1 ± 111.8 μm NTG: 494.2 ± 92.8 μm $p = 0.001$

TABLE 2: Continued.

Authors	Measurement	Results
Rebolleda et al. [26]	"Reference line connecting the two ends of the BMO was defined as the BMO diameter. Three equidistant points (inferior, middle, and superior), corresponding to one-half and one-third of the reference, were highlighted and connected from this reference line to the anterior face of the prelaminar tissue (PT) and the anterior surface of the LC. Prelaminar tissue thickness (PTT) was defined as the distance between the anterior surfaces of the PT and LC. Lamina cribrosa depth (LCD) was defined as the distance from the reference line to the anterior surface of the LC. The arithmetic mean of the three measurements was registered as the average."	Control group: 404.1 ± 70.7 μm NAION: 292.1 ± 77.4 and 316.5 ± 98.5 μm (unaffected fellow eye); $p \leq 0.001$ (comparative to the control group)
Akkaya [73]	"Lamina cribrosa borders were defined as the posterior and anterior borders of the highly reflective area at the ONH's perpendicular center in the horizontal SD-OCT cross section." (i) LCT was defined as "the distance between these two borders." (ii) LCD was defined as "the distance between the BMO and the anterior border of the lamina cribrosa."	(i) LCT (μm): control group: 240.2 ± 15.8 Hyperopic nonamblyopic eyes: 251.6 ± 27.3 Amblyopic eyes: 180.9 ± 29.4 and 247.7 ± 19.0 (fellow eyes) $p < 0.001$ (amblyopia vs. control) (ii) LCD (μm): control group: 391.1 ± 87.7 Hyperopic nonamblyopic eyes: 397.4 ± 75.7 Amblyopic eyes: 371.7 ± 85.8 and 272.1 ± 51.6 (fellow eyes) $p = 0.84$ (amblyopia vs. control)
Lee et al. [64]	(i) LCT was measured at "3 locations in each eye (superior midperiphery, central, and inferior midperiphery regions of the ONH) using thin-slab maximum-intensity-projection (MIP) images. LCT was measured as the distance between the anterior and posterior borders at the central 3 points (with a separation of 100 mm between the points) in each MIP thin-slab image in the direction perpendicular to the anterior LC surface at the measurement point. The measurements obtained from the 3 thin-slab images were used to calculate the mean LCT of each eye." (ii) Anterior LCD was measured in "5 horizontal B-scans (superior, superior midperiphery, center, inferior midperiphery, and inferior regions). LCD was determined by measuring the distance from the BMO plane to the level of the anterior LC surface. A reference line connecting the 2 termination points of Bruch's membrane was drawn on each B-scan image. The distance from the reference line to the level of the anterior border of the LC was measured at 3 points: the maximally depressed point and 2 additional points (100 and 200 μm from the maximally depressed point in a temporal direction). The measurements from the 3 planes were used to calculate the mean LCD of the eye."	(i) LCT (μm): control group: 247.08 ± 32.70 POAG: 193.15 ± 22.19 SSOH: 260.84 ± 38.62 $p < 0.001$ (ii) ALCD (μm): control group: 299.32 ± 39.78 POAG: 511.57 ± 105.36 SSOH: 421.98 ± 111.38 $p < 0.001$
Rebolleda et al. [66]	"A reference line connecting the two Bruch's membrane termination points was drawn, and three equidistant points (inferior, middle, and superior), corresponding to one-half and one-third of this reference, were highlighted and connected to the anterior face of the prelaminar tissue and anterior surface of the LC. The arithmetic mean of the three measurements (inferior, middle, and superior) was considered as the average. Lamina cribrosa depth was determined by measuring the distance from the reference line to the level of the anterior LC surface."	400.1 ± 102.7 μm

TABLE 2: Continued.

Authors	Measurement	Results
Hata et al. [67]	"The BMO was defined as the termination of the Bruch's membrane, and we measured the diameter of BMO. The BMO-anterior LC was defined as the vertical distance between the reference line connecting BMO and the anterior laminar surface."	(i) LCD (μm): CON: 376.26 ± 102.6; $p = 0.47$ (comparative to the control group)
Kim et al. [7]	"LCDs on horizontal SD-OCT B-scan images were measured at seven locations equidistant across the vertical optic disc diameter. The seven B-scan lines from the superior to the inferior regions were defined as planes 1 to 7 with plane 4 corresponding to the midhorizontal plane and planes 2 and 6 corresponding to the superior and inferior midperiphery planes, respectively. To determine the LCD, a line connecting the edges of the BMO was set as the reference plane (BMO reference line), and the LCD was measured in the direction perpendicular to the reference plane at the maximally depressed point."	Control group: 405.88 ± 81.13 μm NTG: 500.37 ± 118.97 μm ADOA: 383.00 ± 85.39 μm $p < 0.001$
Yang et al. [68]	"The measurement points were selected by dividing the total length of the reference line by 2 or 4 depending on the midsuperior, midinferior, or midtemporal point of the disc center. The LCD was measured from the reference line to the anterior surface of the lamina cribrosa at each point. At the same point, the LCT was defined as the minimum vertical length between the anterior and posterior surface of the prelaminar tissue and the anterior and posterior surface of the lamina cribrosa, respectively."	(i) ALCD (μm): control group: 440.9 ± 61.3; group II: 451.7 ± 74.6; group III: 455.2 ± 91.7; group IV: 464.6 ± 106.8; group V: 528.8 ± 101.8; $p = 0.001$ (ii) LCT (μm): control group: 212.7 ± 37.4; group II: 218.4 ± 44.0; group III: 215.0 ± 40.5; group IV: 179.2 ± 25.5; group V: 159.0 ± 14.5; $p < 0.001$
Yokota et al. [69]	"Three frames, center, midsuperior, and midinferior, which passed through the optic nerve disc were selected from these B-scans." (i) ALD was defined as "the distance between the line connecting both ends of Bruch's membrane and the anterior border of the lamina cribrosa." (ii) The LCT was defined as "the distance between the anterior and posterior borders of the lamina cribrosa. The anterior and posterior borders of the lamina cribrosa were defined by a highly reflective structure below the optic cup. To minimize the variation, the mean data of the three frames (center, midsuperior, and midinferior) for the ALD and the LCT analyses were considered."	(i) ALCD (μm): PDR with no-NVG: 407.0 ± 22.9; PDR with NVG: 403.9 ± 20.1; $p = 0.919$ (ii) LCT (μm): PDR with no-NVG: 155.0 ± 4.7; PDR with NVG: 156.9 ± 4.2; $p = 0.757$
Gómez-Mariscal et al. [70]	"Three vertical and equidistant lines localized at one-half and one-third of the BMO diameter were drawn from the reference line to the anterior ONH surface and the anterior LC surface, defining the cup depth (CD) and the lamina cribrosa depth (LCD)."	Control group: 362.7 ± 98.2 μm Experimental group: 369.9 ± 102.9 μm $p = 0.532$

LC = lamina cribrosa, LCT = lamina cribrosa thickness, cLCT = central laminacribrosa thickness, LCD = lamina cribrosa depth, ALCS = anterior lamina cribrosa surface depth, cLCSD = central anterior lamina cribrosa surface depth, BMO = Bruch's membrane opening, ONH = optic nerve head, ASCO = anterior scleral canal opening, OSAS = obstructive sleep apnea syndrome, IIH = intracranial hypertension, HTG = high-tension glaucoma, NTG = normal-tension glaucoma, BRVO = branch retinal vein occlusion, NAION = nonarteritic anterior ischaemic optic neuropathy, SSOH = superior segmental optic nerve hypoplasia, POAG = primary open-angle glaucoma, CON = compressive optic neuropathy, ADOA = autosomal dominant optic atrophy, PDR = proliferative diabetic retinopathy, and NVG = neovascular glaucoma.
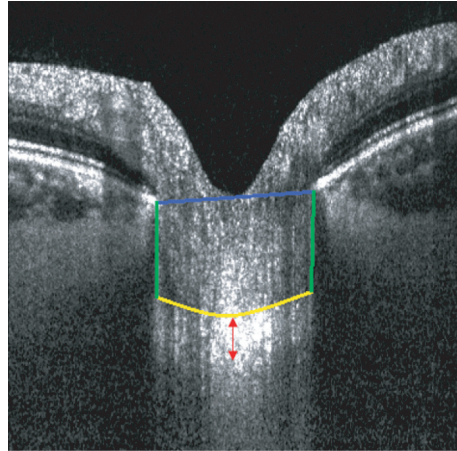
FIGURE 4: OCT B-scan showing the points used to compute the LCD. Line D in blue connects the two Bruch's membrane opening (BMO) edges. The two lines perpendicular to D in green are defined from the BMO edges to the anterior LC insertion points. The anterior LC surface is demarcated in yellow, enclosing the area S where the LC is measured. The red arrow measures the distance between the anterior and posterior margins of the LC, defined as the LCT.

significant because the standard deviations of all the diseases cross the standard deviation of the healthy LCD (Figure 6(b)). For example, Rebolleda et al. [26] found a lower average LCD in the superior, middle, and inferior planes in eyes with NAION compared to healthy eyes ($p < 0.001$), which was also true between unaffected fellow eyes when compared to healthy eyes ($p < 0.05$). The maximum value for LCD was found in cases of Graves' orbitopathy with proptosis and/or compressive optic neuropathy. Seo et al. [27] conducted a study in these patients and reported $462.79 \pm 95.96\,\mu m$ and $621.39 \pm 78.39\,\mu m$ values, at baseline, for the muscle-dominant and fat-dominant group, respectively.

3.3.3. Nonophthalmic Disease Group Measurements. The number of studies in this group was smaller than in the other groups. The registered diseases were diabetes mellitus [28], Parkinson's disease (PD) [29], obstructive sleep apnea syndrome (OSAS) [30], Alzheimer's disease (AD) [31, 32], mild cognitive impairment (MCI) [31], and migraine [33]. The mean LCT and LCD were $234 \pm 36\,\mu m$ and $390 \pm 68\,\mu m$, respectively, as shown in Figure 5. The graphics in Figure 7 presents LCT and LCD for each pathology in comparison to the healthy population (horizontal dashed green line).

LCT measurements seem to be lower relative to the healthy group, with the exception of diabetes mellitus. Akkaya et al. [28] described a significantly higher mean LCT in diabetic patients when compared to a healthy group, $271.61 \pm 33.96\,\mu m$ vs. $248.50 \pm 5.40\,\mu m$, respectively ($p < 0.001$). Regarding LCD, diabetes mellitus showed significantly lower mean values in comparison to healthy controls in one study [28] ($351 \pm 59\,\mu m$ vs. $420 \pm 90\,\mu m$; $p = 0.003$). The maximum mean LCD absolute value (deepest ONH cup) was described in patients with migraine (see Figure 7(b)). Sirakaya et al. [33] reported significantly higher mean LCD values for both migraine groups

($412.15 \pm 58.80\,\mu m$ with aura and $405.57 \pm 55.39\,\mu m$ without aura) when compared to the healthy group ($355.34 \pm 65.53\,\mu m$; $p = 0.001$).

4. Discussion

The present study highlights which LC structural parameters have been analyzed in the literature with a focus on nonglaucomatous diseases. Overall, the most commonly studied parameters were LCD and LCT. The disease groups (ophthalmic and nonophthalmic) presented lower values for mean LCT, relative to the healthy population (Figure 5(a)). In parallel, mean LCD values were higher (deeper ONH cup) for these groups (Figure 5(b)). An exception in the nonophthalmic disease group was DM, which presented a shallower cup and thicker LC, when compared to healthy subjects. Akkaya et al. proposed that this evidence supports the "neuroprotective effect of DM on glaucomatous optic neuropathy and suggests that LCT and lamina cribrosa position mediate this protective effect." [28]

This study shows that LC structural features are significantly different between healthy patients and some (nonglaucomatous) ocular and systemic pathologies. As such, there is a potential to add them as additional clinical features for clinical diagnosis. Nonetheless, being patient-specific features, LC features might hold an even better role for patient follow-up, signalling disease status' change. Unfortunately, we did not find any longitudinal studies focusing on this matter in this review. This fact highlights the need for longitudinal studies linking LC parameters and diseases, similarly to what is now common in glaucoma-related studies [75].

LC features are influenced by factors such as age, race, and also by the way measurements are carried out. However, these factors were not used as segmentation criteria in this study due to the lack of this information in several studies. For future works in this field, it is important to take into account these factors when analysing
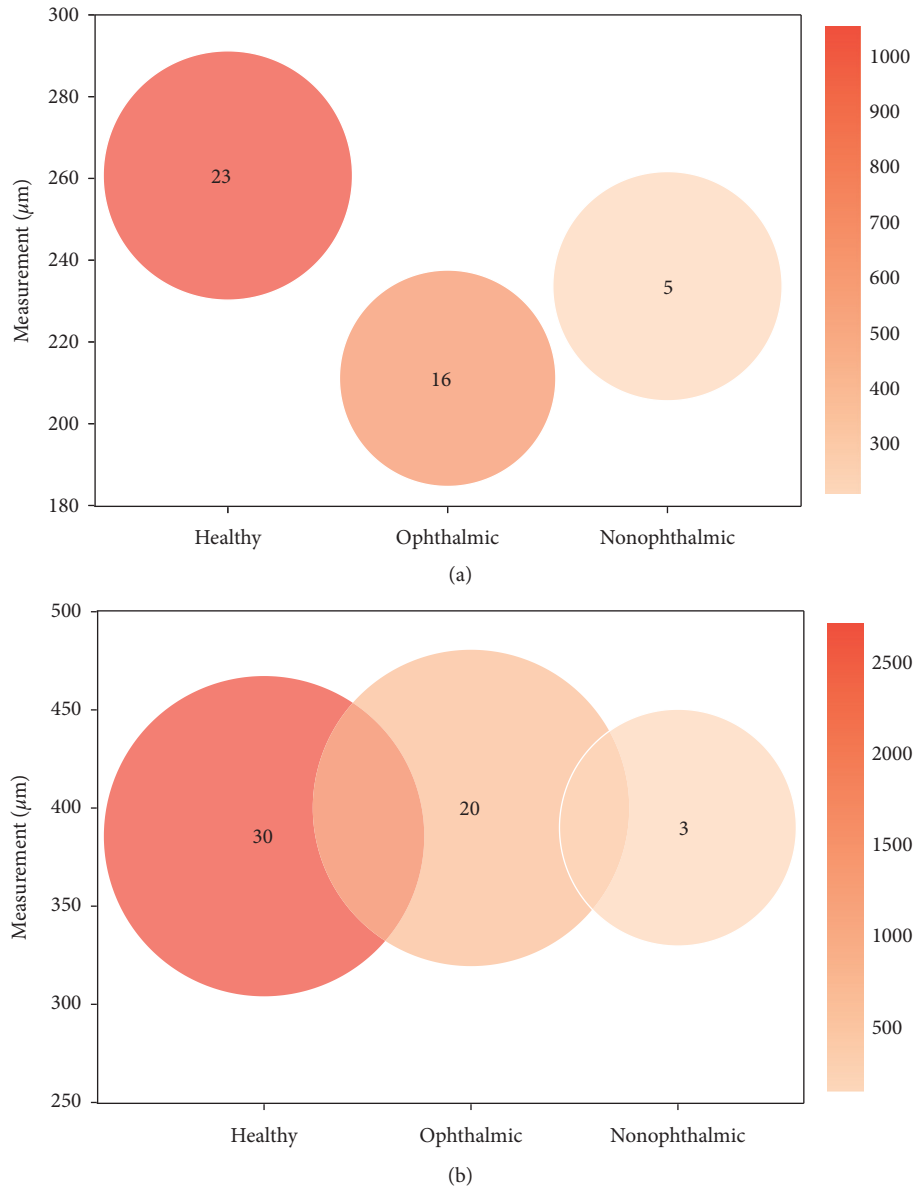
Figure 5: Comparison of lamina cribrosa (a) thickness (LCT) and (b) depth (LCD) between healthy controls, ophthalmic, and non-ophthalmic diseases. The number in the circle represents the amount of studies used for calculating the averaged measurements for each group. The color scale shows the number of eyes comprised in the studied groups, and the radius of each circle denotes the standard deviation of the averaged values.

and comparing results between studies since they are a potential source of bias. Moreover, the current methods are heterogeneous (see Table 2), which may lead to imprecise comparisons between studies. For depth measurements, the consensus is to use the BMO plane as a reference, but the way the feature is measured is not consistent among research groups. One of the causes for this heterogeneity is the fact that the analysis of LC features still requires a considerable amount of manual input. This causes measurement bias due to the inherent difficulty of the manual delineation of the structure. This lack of automation increases the likelihood that each research group adopts their own reference points and methods. Besides,

studies usually report averages of a limited number of B-scans without capturing the whole LC. The distance between these B-scan slices, as well as their number and position, may also be a source of discrepancies when comparing studies. Finally, some authors have pointed out the fact that the BMO reference place might be biased due to choroidal thickness changes and that perhaps the anterior sclera reference plane would be better suited for these calculations [76, 77]. Ideally, similar measurement methods should be adopted across all research groups. Currently, the measurement of the LC features is laborious and time consuming. As such, automation might hold the key to reduce bias in LC feature measurement. There is

(a)

(b)
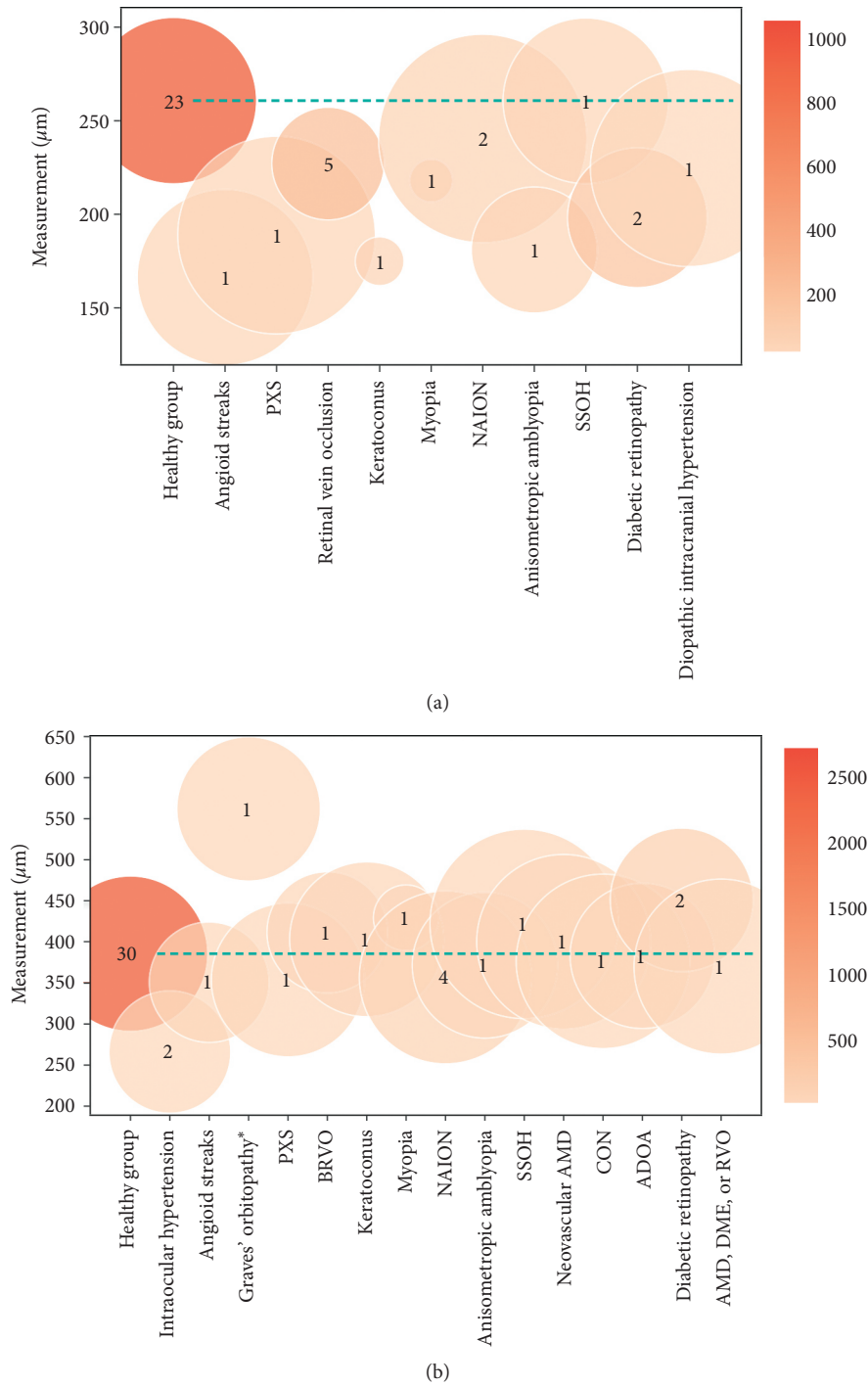
FIGURE 6: Comparison of lamina cribrosa (a) thickness (LCT) and (b) depth (LCD) for the ophthalmic disease group. The dashed green line represents the mean for the healthy population. Only pathologies that included more than 20 eyes among all articles are considered for the analysis. *With proptosis and/or compressive optic neuropathy.

a need for easy-to-use software that can automatically measure LC features (possibly starting with LCT and LCD), ideally capturing all the information from OCT volumes, instead of selecting some of the B-scans. Providing such a tool with a fast and repeatable computation would contribute to making LC features a part of everyday clinical practice.

The main limitation of this review is the reduced number of studies, mainly in the nonophthalmic disease group, which precludes definite conclusions. Moreover, due to the lack of individual study data, it was not possible to perform statistical comparisons between groups and pathologies. As such, our results point towards differences that need to be better clarified. Nonetheless, LC features'

(a)

(b)
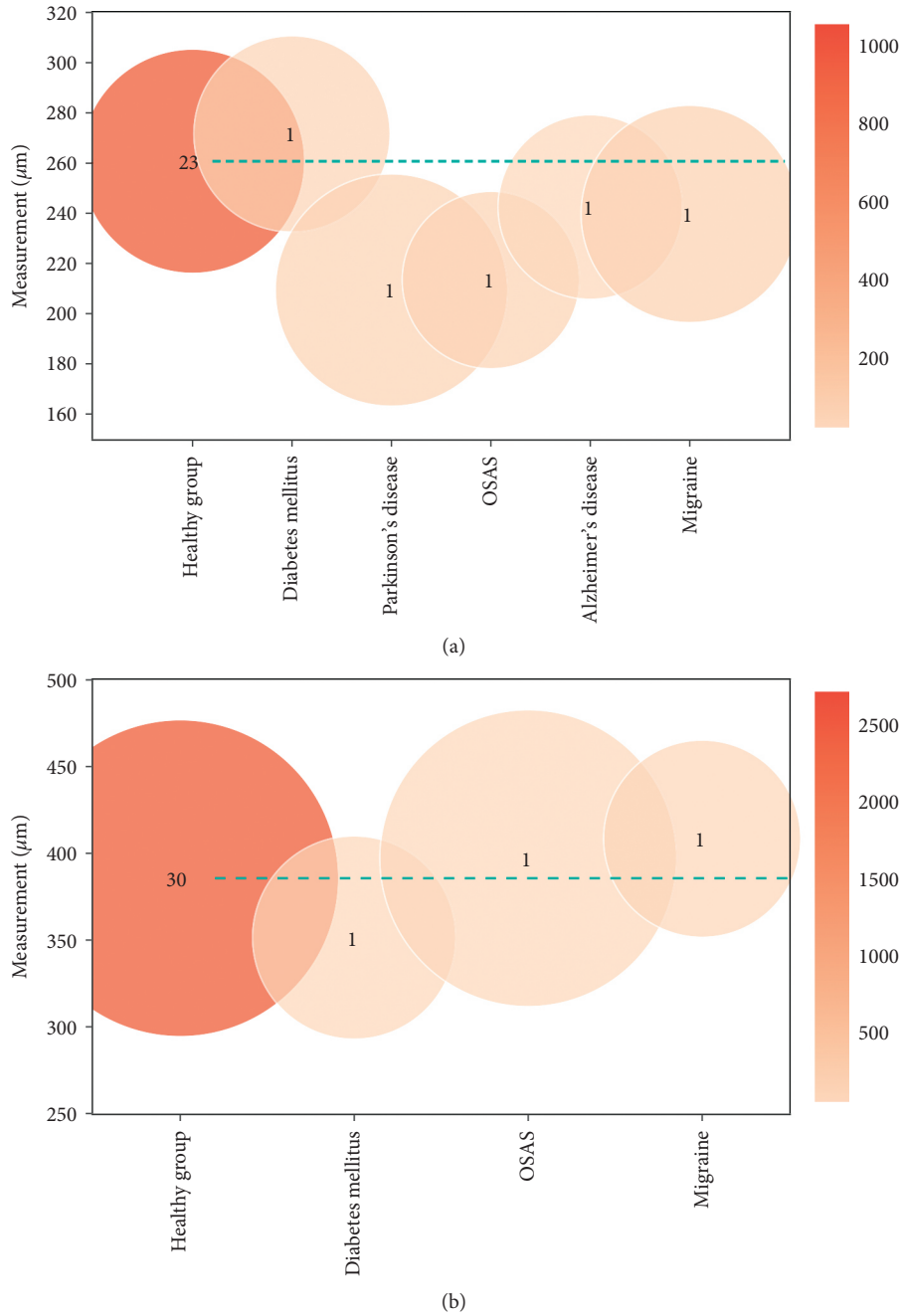
FIGURE 7: Comparison of lamina cribrosa (a) thickness (LCT) and (b) depth (LCD) for the nonophthalmic disease group. The green dashed line represents the mean for the healthy population. Only pathologies that included more than 20 eyes among all articles are considered for the analysis.

ability to discriminate between these groups is supported by results presented by several individual studies, as reported in Table 2. Lastly, it is noteworthy to mention that the statistical analysis performed on groups (ophthalmic and nonophthalmic diseases) may be biased by different pathologies comprised in each group.

5. Conclusion

There is a growing interest in LC features outside the glaucoma field. The results of this meta-analysis show

several promising features (mainly, LCT and LCD) that may be relevant for clinical practice. Nevertheless, further studies are needed to validate these findings, and longitudinal data are needed to clarify the potential for use in patient follow-up. Moreover, efforts should be employed to develop automated tools that can capture LC features from OCT data in a standardized manner, thus allowing more accurate comparisons between studies. These efforts should enable to further explore the potential of LC parameters for use in daily clinical practice.

Conflicts of Interest

The authors declare that they have no conflicts of interest.

Acknowledgments

References

[1] I. A. Sigal, H. Yang, M. D. Roberts et al., "IOP-induced lamina cribrosa deformation and scleral canal expansion: independent or related?" *Investigative Opthalmology & Visual Science*, vol. 52, no. 12, pp. 9023–9032, 2011.

[2] R. Grytz, M. A. Fazio, V. Libertiaux et al., "Age- and race-related differences in human scleral material properties," *Investigative Ophthalmology & Visual Science*, vol. 55, no. 12, pp. 8163–8172, 2014.

[3] H. Quigley and D. R. Anderson, "The dynamics and location of axonal transport blockade by acute intraocular pressure elevation in primate optic nerve," *Investigative Ophthalmology*, vol. 15, no. 8, pp. 606–616, 1976.

[4] H. A. Quigley, E. M. Addicks, W. R. Green, and A. E. Maumenee, "Optic nerve damage in human glaucoma. the site of injury and susceptibility to damage," *Archives of Ophthalmology*, vol. 99, no. 4, pp. 635–649, 1981.

[5] S. H. Lee, T.-W. Kim, E. J. Lee, M. J. A. Girard, and J. M. Mari, "Diagnostic power of lamina cribrosa depth and curvature in glaucoma," *Investigative Opthalmology & Visual Science*, vol. 58, no. 2, pp. 755–762, 2017.

[6] X. Wang, T. A. Tun, M. E. Nongpiur et al., "Peripapillary sclera exhibits a v-shaped configuration that is more pronounced in glaucoma eyes," *British Journal of Ophthalmology*, 2020, In press.

[7] G.-N. Kim, J.-A. Kim, M.-J. Kim et al., "Comparison of lamina cribrosa morphology in normal tension glaucoma and autosomal-dominant optic atrophy," *Investigative Ophthalmology & Visual Science*, vol. 61, no. 5, p. 9, 2020.

[8] J. C. Han, S. H. Cho, D. Y. Sohn, and C. Kee, "The characteristics of lamina cribrosa defects in myopic eyes with and without open-angle glaucoma," *Investigative Opthalmology & Visual Science*, vol. 57, no. 2, pp. 486–494, 2016.

[9] D. S. Minckler and M. O. M. Tso, "A light microscopic, autoradiographic study of axoplasmic transport in the normal rhesus optic nerve head," *American Journal of Ophthalmology*, vol. 82, no. 1, pp. 1–15, 1976.

[10] A. Bhandari, L. Fontana, F. W. Fitzke, and R. A. Hitchings, "Quantitative analysis of the lamina cribrosa in vivo using a scanning laser opthalmoscope," *Current Eye Research*, vol. 16, no. 1, pp. 1–8, 1997.

[11] A. S. Vilupuru, N. V. Rangaswamy, L. J. Frishman, E. L. Smith III, R. S. Harwerth, and A. Roorda, "Adaptive optics scanning laser ophthalmoscopy for in vivo imaging of lamina cribrosa," *Journal of the Optical Society of America A*, vol. 24, no. 5, pp. 1417–1425, 2007.

[12] H.-Y. L. Park, S. H. Jeon, and C. K. Park, "Enhanced depth imaging detects lamina cribrosa thickness differences in normal tension glaucoma and primary open-angle glaucoma," *Ophthalmology*, vol. 119, no. 1, pp. 10–20, 2012.

[13] J. M. Mari, N. G. Strouthidis, S. C. Park, and M. J. A. Girard, "Enhancement of lamina cribrosa visibility in optical coherence tomography images using adaptive compensation," *Investigative Opthalmology & Visual Science*, vol. 54, no. 3, pp. 2238–2247, 2013.

[14] B. Nuyen, K. Mansouri, and R. N. Weinreb, "Imaging of the lamina cribrosa using swept-source optical coherence tomography," *Journal of Current Glaucoma Practice*, vol. 6, no. 3, pp. 113–119, 2012.

[15] S. C. Park and R. Ritch, "High resolution in vivo imaging of the lamina cribrosa," *Saudi Journal of Ophthalmology*, vol. 25, no. 4, pp. 363–372, 2011.

[16] T.-W. Kim, L. Kagemann, M. J. A. Girard et al., "Imaging of the lamina cribrosa in glaucoma: perspectives of pathogenesis and clinical applications," *Current Eye Research*, vol. 38, no. 9, pp. 903–909, 2013.

[17] A. Bekkers, N. Borren, E. Vera et al., "Microvascular damage assessed by optical coherence tomography angiography for glaucoma diagnosis: a systematic review of the most discriminative regions," *Acta Ophthalmologica*, vol. 98, no. 6, pp. 537–558, 2020.

[18] J. C. Han, D.-Y. Choi, Y. K. Kwun, W. Suh, and C. Kee, "Evaluation of lamina cribrosa thickness and depth in ocular hypertension," *Japanese Journal of Ophthalmology*, vol. 60, no. 1, pp. 14–19, 2016.

[19] F. P. Bartolomé, J. M. Martínez de la Casa, I. C. Bosca et al., "Correlating corneal biomechanics and ocular biometric properties with lamina cribrosa measurements in healthy subjects," *Seminars in Ophthalmology*, vol. 33, no. 2, pp. 223–230, 2018.

[20] H. Xiao, X.-Y. Xu, Y.-M. Zhong, and X. Liu, "Age related changes of the central lamina cribrosa thickness, depth and prelaminar tissue in healthy Chinese subjects," *International Journal of Ophthalmology*, vol. 11, no. 11, pp. 1842–1847, 2018.

[21] L. A. Rhodes, C. Huisingh, J. Johnstone et al., "Variation of laminar depth in normal eyes with age and race," *Investigative Ophthalmology & Visual Science*, vol. 55, no. 12, pp. 8123–8133, 2014.

[22] H. Luo, H. Yang, S. K. Gardiner et al., "Factors influencing central lamina cribrosa depth: a multicenter study," *Investigative Ophthalmology & Visual Science*, vol. 59, no. 6, pp. 2357–2370, 2018.

[23] S. C. Park, S. Kiumehr, C. C. Teng et al., "Horizontal central ridge of the lamina cribrosa and regional differences in laminar insertion in healthy subjects," *Investigative Opthalmology & Visual Science*, vol. 53, no. 3, pp. 1610–1616, 2012.

[24] D. S. Lee, E. J. Lee, T.-W. Kim et al., "Influence of translaminar pressure dynamics on the position of the anterior lamina cribrosa surface," *Investigative Opthalmology & Visual Science*, vol. 56, no. 5, pp. 2833–2841, 2015.

[25] J. M. Villarruel, X. Q. Li, D. Bach-Holm, and S. Hamann, "Anterior lamina cribrosa surface position in idiopathic intracranial hypertension and glaucoma," *European Journal of Ophthalmology*, vol. 27, no. 1, pp. 55–61, 2017.

[26] G. Rebolleda, A. Pérez-Sarriegui, L. Díez-Álvarez et al., "Lamina cribrosa position and bruch's membrane opening differences between anterior ischemic optic neuropathy and open-angle glaucoma," *European Journal of Ophthalmology*, vol. 29, no. 2, pp. 202–209, 2018.

[27] Y. Seo, W. B. Shin, H. W. Bae, and J. S. Yoon, "Effects of orbital decompression on lamina cribrosa depth in patients

with Graves' orbitopathy," *Korean Journal of Ophthalmology*, vol. 33, no. 5, pp. 436–445, 2019.

[28] S. Akkaya, B. Küçük, H. K. Doğan, and E. Can, "Evaluation of the lamina cribrosa in patients with diabetes mellitus using enhanced depth imaging spectral-domain optical coherence tomography," *Diabetes and Vascular Disease Research*, vol. 15, no. 5, pp. 442–448, 2018.

[29] M. Eraslan, C. Eren, S. Yildiz Balci et al., "The choroid and lamina cribrosa is affected in patients with Parkinson's disease: enhanced depth imaging optical coherence tomography study," *Acta Ophthalmologica*, vol. 94, no. 1, pp. 68–75, 2016.

[30] B. Küçük, E. Sırakaya, and Ş Delibaş, "Posterior segment assessment in patients with obstructive sleep apnea syndrome," *Sleep & Breathing*, vol. 23, no. 3, pp. 997–1005, 2019.

[31] A. López-de Eguileta, C. Lage, S. López-García et al., "Ganglion cell layer thinning in prodromal Alzheimer's disease defined by amyloid pet," *Alzheimer's & Dementia*, vol. 5, pp. 570–578, 2019.

[32] E. J. Lee, T.-W. Kim, D. S. Lee et al., "Increased CSF tau level is correlated with decreased lamina cribrosa thickness," *Alzheimer's Research & Therapy*, vol. 8, no. 6, 2016.

[33] E. Sirakaya, B. Kucuk, A. Agadayi, and N. Yilmaz, "Evaluation of the lamina cribrosa thickness and depth in patients with migraine," *International Ophthalmology*, vol. 40, no. 1, pp. 89–98, 2020.

[34] D. C. Sousa, I. Leal, C. Marques-Neves, F. Pinto, and L. Abegão Pinto, "Relationship between intraocular pressure and anterior lamina cribrosa depth: a cross-sectional observational study in a healthy Portuguese population," *European Journal of Ophthalmology*, vol. 27, no. 3, pp. 295–300, 2017.

[35] E. J. Lee, T.-W. Kim, R. N. Weinreb, M. H. Suh, and H. Kim, "Lamina cribrosa thickness is not correlated with central corneal thickness or axial length in healthy eyes: central corneal thickness, axial length, and lamina cribrosa thickness," *Graefe's Archive for Clinical and Experimental Ophthalmology*, vol. 251, no. 3, pp. 847–854, 2013.

[36] I. Leal, D. C. Sousa, F. Pinto, C. Marques-Neves, and L. Abegão Pinto, "Intra- and inter-rater agreement of anterior lamina cribrosa depth measurements using enhanced-depth imaging optical coherence tomography," *Ophthalmic Research*, vol. 57, no. 2, pp. 92–99, 2017.

[37] X. Wang, M. R. Beotra, T. A. Tun et al., "In vivo 3-dimensional strain mapping confirms large optic nerve head deformations following horizontal eye movements," *Investigative Opthalmology & Visual Science*, vol. 57, no. 13, pp. 5825–5833, 2016.

[38] Y. W. Kim, M. J. A. Girard, J. M. Mari, and J. W. Jeoung, "Anterior displacement of lamina cribrosa during valsalva maneuver in young healthy eyes," *PLoS One*, vol. 11, no. 7, Article ID e0159663, 2016.

[39] M. Poli, P. Denis, E. Sellem, L.-S. Aho-Glélé, and A. M. Bron, "Is the optic nerve head structure impacted by a diagnostic lumbar puncture in humans?" *Journal of Glaucoma*, vol. 26, no. 11, pp. 1036–1040, 2017.

[40] A. El-Agamy, F. Oteaf, and M. Berika, "Anterior lamina cribrosa surface depth in healthy saudi females," *Clinical Ophthalmology*, vol. 11, pp. 1045–1050, 2017.

[41] P. Bedggood, F. Tanabe, A. M. McKendrick, A. Turpin, A. J. Anderson, and B. V. Bui, "Optic nerve tissue displacement during mild intraocular pressure elevation: its relationship to central corneal thickness and corneal hysteresis," *Ophthalmic and Physiological Optics*, vol. 38, no. 4, pp. 389–399, 2018.

[42] S. H. Lee, T.-W. Kim, E. J. Lee et al., "Lamina cribrosa curvature in healthy Korean eyes," *Scientific Reports*, vol. 9, no. 1, p. 1756, 2019.

[43] J. H. Seo, T.-W. Kim, and R. N. Weinreb, "Lamina cribrosa depth in healthy eyes," *Investigative Opthalmology & Visual Science*, vol. 55, no. 3, pp. 1241–1251, 2014.

[44] M. A. Fazio, J. K. Johnstone, B. Smith, L. Wang, and C. A. Girkin, "Displacement of the lamina cribrosa in response to acute intraocular pressure elevation in normal individuals of African and European descent," *Investigative Opthalmology & Visual Science*, vol. 57, no. 7, pp. 3331–3339, 2016.

[45] T. A. Tun, X. Wang, M. Baskaran et al., "Variation of peripapillary scleral shape with age," *Investigative Opthalmology & Visual Science*, vol. 60, no. 10, pp. 3275–3282, 2019.

[46] S. G. Thakku, Y.-C. Tham, M. Baskaran et al., "A global shape index to characterize anterior lamina cribrosa morphology and its determinants in healthy indian eyes," *Investigative Opthalmology & Visual Science*, vol. 56, no. 6, pp. 3604–3614, 2015.

[47] I. Pasaoglu, B. Satana, C. Altan et al., "Lamina cribrosa surface position in idiopathic intracranial hypertension with swept-source optical coherence tomography," *Indian Journal of Ophthalmology*, vol. 67, no. 7, pp. 1085–1088, 2019.

[48] J. García-Montesinos, F. J. Muñoz-Negrete, V. de Juan, and G. Rebolleda, "Relationship between lamina cribrosa displacement and trans-laminar pressure difference in papilledema," *Graefe's Archive for Clinical and Experimental Ophthalmology*, vol. 255, no. 6, pp. 1237–1243, 2017.

[49] G. Demir, C. Altan, S. Cakmak et al., "Evaluation of lamina cribrosa in angioid streaks using spectral-domain optical coherence tomography enhanced depth imaging," *Journal Français d'Ophtalmologie*, vol. 42, no. 6, pp. 586–591, 2019.

[50] S. Moghimi, M. Mazloumi, M. Johari et al., "Evaluation of lamina cribrosa and choroid in nonglaucomatous patients with pseudoexfoliation syndrome using spectral-domain optical coherence tomography," *Investigative Opthalmology & Visual Science*, vol. 57, no. 3, pp. 1293–1300, 2016.

[51] A. Soares, N. Lopes, G. Morgado et al., "Study of lamina cribrosa depth and optic nerve in patients with spontaneous intracranial hypotension," *European Journal of Ophthalmology*, vol. 29, no. 6, pp. 659–663, 2019.

[52] S. Karaca Adıyeke, N. Kutlu, H. Aytogan et al., "Thickness of sclera and lamina cribrosa in patients with central retinal vein occlusion," *Retina*, vol. 40, no. 10, pp. 2050–2054, 2019.

[53] Y. Son, S. Lee, and J. Park, "Measurement of lamina and prelaminar thicknesses of both eyes in patients with unilateral branch retinal vein occlusion," *Graefe's Archive for Clinical and Experimental Ophthalmology*, vol. 255, no. 3, pp. 503–508, 2017.

[54] E. Sırakaya and K. Bekir, "Thickness of the lamina cribrosa, retinal nerve fiber layer, and peripapillary choroid in patients with branch retinal vein occlusion," *Ophthalmologica*, vol. 243, no. 4, pp. 288–296, 2019.

[55] O. Altunel, M. Atas, and S. Demircan, "Evaluation of lamina cribrosa thickness in patients diagnosed with central retinal vein occlusion," *Graefe's Archive for Clinical and Experimental Ophthalmology*, vol. 257, no. 10, pp. 2087–2093, 2019.

[56] S.-H. Lim, M. Kim, W. Chang, and M. Sagong, "Comparison of the lamina cribrosa thickness of patients with unilateral branch retinal vein occlusion and healthy subjects," *Retina*, vol. 37, no. 3, pp. 515–521, 2017.

[57] S. Akkaya and B. Küçük, "Lamina cribrosa thickness in patients with keratoconus," *Cornea*, vol. 36, no. 12, pp. 1509–1513, 2017.

[58] S. Lee, D.-Y. D. Choi, D. H. Lim, T. Y. Chung, J. C. Han, and K. C. Lim, "Lamina cribrosa changes after laser in situ keratomileusis in myopic eyes," *Korean Journal of Ophthalmology*, vol. 32, no. 2, pp. 95–102, 2018.

[59] A. Jnawali, H. Mirhajianmoghadam, G. Musial et al., "The optic nerve head, lamina cribrosa, and nerve fiber layer in non-myopic and myopic children," *Experimental Eye Research*, vol. 195, 2020.

[60] K. Ohno-Matsui, M. Akiba, M. Moriyama, T. Ishibashi, T. Tokoro, and R. F. Spaide, "Imaging retrobulbar subarachnoid space around optic nerve by swept-source optical coherence tomography in eyes with pathologic myopia," *Investigative Opthalmology & Visual Science*, vol. 52, no. 13, pp. 9644–9650, 2011.

[61] A. Miki, Y. Ikuno, T. Asai, S. Usui, and K. Nishida, "Defects of the lamina cribrosa in high myopia and glaucoma," *PLoS One*, vol. 10, no. 9, Article ID e0137909, 2015.

[62] G. Rebolleda, J. García-Montesinos, E. De Dompablo, N. Oblanca, F. J. Muñoz-Negrete, and J. J. González-López, "Bruch's membrane opening changes and lamina cribrosa displacement in non-arteritic anterior ischaemic optic neuropathy," *British Journal of Ophthalmology*, vol. 101, no. 2, pp. 143–149, 2017.

[63] M. A. Fard, M. Afzali, P. Abdi et al., "Optic nerve head morphology in nonarteritic anterior ischemic optic neuropathy compared to open-angle glaucoma," *Investigative Opthalmology & Visual Science*, vol. 57, no. 11, pp. 4632–4640, 2016.

[64] E. J. Lee, Y. J. Choi, T.-W. Kim, and J.-M. Hwang, "Comparison of the deep optic nerve head structure between normal-tension glaucoma and nonarteritic anterior ischemic optic neuropathy," *PLoS One*, vol. 11, no. 4, Article ID e0150242, 2016.

[65] K. Shinohara, M. Moriyama, N. Shimada et al., "Analyses of shape of eyes and structure of optic nerves in eyes with tilted disc syndrome by swept-source optical coherence tomography and three-dimensional magnetic resonance imaging," *Eye*, vol. 27, no. 11, pp. 1233–1242, 2013.

[66] G. Rebolleda, B. Puerto, V. de Juan, M. Gómez-Mariscal, F. J. Muñoz-Negrete, and A. Casado, "Optic nerve head biomechanic and IOP changes before and after the injection of aflibercept for neovascular age-related macular degeneration," *Investigative Opthalmology & Visual Science*, vol. 57, no. 13, pp. 5688–5695, 2016.

[67] M. Hata, K. Miyamoto, A. Oishi et al., "Comparison of optic disc morphology of optic nerve atrophy between compressive optic neuropathy and glaucomatous optic neuropathy," *PLoS One*, vol. 9, no. 11, Article ID e0112403, 2014.

[68] H. S. Yang, J.-G. Kim, J. B. Cha et al., "Quantitative analysis of neural tissues around the optic disc after panretinal photocoagulation in patients with diabetic retinopathy," *PLoS One*, vol. 12, no. 10, Article ID e0186229, 2017.

[69] S. Yokota, Y. Takihara, Y. Takamura, and M. Inatani, "Circumpapillary retinal nerve fiber layer thickness, anterior lamina cribrosa depth, and lamina cribrosa thickness in neovascular glaucoma secondary to proliferative diabetic retinopathy: a cross-sectional study," *BMC Ophthalmology*, vol. 17, no. 1, p. 57, 2017.

[70] M. Gómez-Mariscal, B. Puerto, F. J. Muñoz-Negrete, V. de Juan, and G. Rebolleda, "Acute and chronic optic nerve head biomechanics and intraocular pressure changes in patients receiving multiple intravitreal injections of anti-vegf," *Graefe's Archive for Clinical and Experimental Ophthalmology*, vol. 257, no. 10, pp. 2221–2231, 2019.

[71] D. F. Garway-Heath, D. Poinoosawmy, F. W. Fitzke, and R. A. Hitchings, "Mapping the visual field to the optic disc in normal tension glaucoma eyes," *Ophthalmology*, vol. 107, no. 10, pp. 1809–1815, 2000.

[72] T. Li, I. J. Saldanha, J. Jap et al., "A randomized trial provided new evidence on the accuracy and efficiency of traditional vs. electronically annotated abstraction approaches in systematic reviews," *Journal of Clinical Epidemiology*, vol. 115, pp. 77–89, 2019.

[73] S. Akkaya, "Lamina cribrosa thickness in children with hyperopic anisometropic amblyopia," *International Journal of Ophthalmology*, vol. 11, no. 10, pp. 1663–1667, 2018.

[74] E. J. Lee, T.-W. Kim, and R. N. Weinreb, "Improved reproducibility in measuring the laminar thickness on enhanced depth imaging sd-oct images using maximum intensity projection," *Investigative Opthalmology & Visual Science*, vol. 53, no. 12, pp. 7576–7582, 2012.

[75] N. Y. Q. Tan, Y.-C. Tham, S. G. Thakku et al., "Changes in the anterior lamina cribrosa morphology with glaucoma severity," *Scientific Reports*, vol. 9, no. 6612, 2019.

[76] H. Quigley, K. Arora, S. Idrees et al., "Biomechanical responses of lamina cribrosa to intraocular pressure change assessed by optical coherence tomography in glaucoma eyes," *Investigative Opthalmology & Visual Science*, vol. 58, no. 5, pp. 2566–2577, 2017.

[77] J. R. Vianna, V. R. Lanoe, J. Quach et al., "Serial changes in lamina cribrosa depth and neuroretinal parameters in glaucoma: impact of choroidal thickness," *Ophthalmology*, vol. 124, no. 9, pp. 1392–1402, 2017.

Research Article

Discordance in Retinal and Choroidal Vascular Densities in Patients with Type 2 Diabetes Mellitus on Optical Coherence Tomography Angiography

Ho Ra, Nam Yeo Kang, Jiyun Song, Junhyuck Lee, Inkee Kim, and Jiwon Baek ⓘ

Department of Ophthalmology, Bucheon St. Mary's Hospital, College of Medicine, The Catholic University of Korea, Seoul, Republic of Korea

Correspondence should be addressed to Jiwon Baek; md.jiwon@gmail.com

Purpose. In the present study, the retinal and choroidal vascular densities (VDs) in type 2 diabetes mellitus (DM) patients were analyzed using optical coherence tomography angiography (OCTA). *Methods*. The study included 282 eyes of 152 patients with type 2 DM (114 without retinopathy, 79 nonproliferative diabetic retinopathy (NPDR), 48 severe NPDR, and 41 proliferative diabetic retinopathy (PDR) eyes). The superficial and deep retinal vessel, choriocapillaris, and choroidal VDs were measured using a binarization method on OCTA images. VDs were compared based on retinopathy severity. Correlations among densities were analyzed. *Results*. Retinal and choriocapillaris VDs were lower in PDR than in NPDR (all $P < 0.05$). Correlation analysis showed significant positive correlations among densities of superficial and deep retinal vessels and choriocapillaris (all $P < 0.001$). Choroidal VD showed a negative correlation with superficial and deep retinal vessels and choriocapillaris (all $P < 0.001$). Retinal and choriocapillaris VDs showed a negative correlation with diabetic retinopathy (DR) grade (all $P < 0.001$); however, the choroidal VD showed a weak positive correlation ($P = 0.030$). *Conclusion*. Choroidal VD increased as retinal and choriocapillaris VDs decreased, indicating that the outer layer of the choroid is less affected by DR severity and VD of larger choroidal vessels may even be increased as a compensatory mechanism for decreased retinal and choriocapillaris VDs in type 2 DM patients.

1. Introduction

Diabetic retinopathy (DR) is a major cause of blindness in adults worldwide [1]. Although the pathogenic mechanism of DR is not fully understood due to its complexity, upregulation of angiogenic cytokines and inflammatory mediators caused by metabolic disturbances is considered a core mechanism resulting in a chain of pathological processes in DR [2]. Retinal vessels are influenced by a hypoxic state which is caused by chronic hyperglycemic status in DR eyes. Hypoxia-driven angiogenic factors, including vascular endothelial growth factor (VEGF), cause vasodilation and leakage of retinal capillaries and may eventually lead to proliferation of new vessels [3].

Vascular involvement in DR pathogenesis has previously been studied. In recent years, the introduction of optical coherence tomography angiography (OCTA) has facilitated investigations on retinal vessels as well as choriocapillaris and large choroidal vessels. An important finding in vasculature changes in DR using OCTA includes enlargement of the foveal avascular zone [4]. In addition, lower retinal vascular density (VD) in DR eyes has consistently been reported in previous studies [5–7]. Furthermore, retinal VD was shown associated with disease severity or visual function [6].

Although vascular features of the retina in diabetes mellitus (DM) patients are similar to the above-described changes, the VD change of retina and choroid and their direct correlations have not yet been clarified. In the current

study, superficial and deep retinal vessel, choriocapillaris, and choroidal vessel densities in type 2 DM patients were quantitatively analyzed using OCTA and compared based on retinopathy severity. In addition, the correlation among densities was investigated.

2. Materials and Methods

This retrospective cross-sectional case series study was performed in the Department of Ophthalmology at Bucheon St. Mary's Hospital, The Catholic University of Korea (Gyeonggi-do, Republic of Korea). The study was approved by the hospital's institutional review board and conducted according to the Declaration of Helsinki. Informed consent was waived due to the retrospective nature of the study.

2.1. Patients. The study group consisted of consecutive type 2 DM patients who visited the ophthalmology outpatient department at Bucheon St. Mary's Hospital between December 2019 and February 2020. All patients included in the study were diagnosed with type 2 DM by doctors in the endocrinology department of the hospital. Type 2 DM was diagnosed if the patient exhibited a fasting plasma glucose level of ≥126 mg/dl or a 2 h postglucose level of ≥200 mg/dl after a 75 g oral glucose tolerance test [8]. The severity of DR was evaluated in accordance with the Early Treatment Diabetic Retinopathy Study standard grading protocols by two retinal specialists with an experience in DR over 10 years (H.R. and J.B.) [9].

Each patient underwent a complete ophthalmologic examination, including measurement of best-corrected visual acuity (BCVA), slit-lamp examination, and dilated fundus examination using mydriatic ultra-widefield color fundus photography (Optos California P200DTx icg; Optos, Dunfermline, United Kingdom) and Heidelberg HRA2 Spectralis OCTA device (Heidelberg Engineering®, Germany). DR grade was determined based on the modified Early Treatment Diabetic Retinopathy Study grade [9].

Demographic and clinical data including age, sex, coexistence of hypertension, duration of DM, systolic and diastolic blood pressures, serum levels of random glucose, and hemoglobin A1c (HbA1c) were collected.

Exclusion criteria were as follows: (1) low-quality images due to significant cataract, corneal opacities, vitreous hemorrhages, or poor cooperation and images with Q score lower than 30; (2) eyes with diabetic macular edema (i.e., central macular thickness (CMT) of 350 μm or more and/or eyes with intra- or subretinal fluids) to eliminate interference of macular fluid on the vessel density analysis; (3) receiving any prior treatment for DR including anti-VEGF therapy, intraocular or periocular steroid, laser photocoagulation, or vitrectomy; and (4) presence of any significant retinal pathology other than PDR (including pathologic myopia, retinal vessel occlusion, other vasculitis symptoms, or retinal detachment).

2.2. Image Analysis. En face $3 \times 3 \, mm^2$ macular area OCTA images of superficial vascular complex (SVC), deep vascular complex (DVC), choriocapillaris, and choroid, centered at the fovea were obtained. Each slab was automatically obtained using predefined settings of Spectralis OCTA system. SVC consisted of nerve fiber layer vascular plexus and superficial vascular plexus, and DVC consisted of intermediate capillary plexus and deep capillary plexus. Choriocapillaris slab is generated by segmentation of 10 to 30 μm below Bruch's membrane and choroid is defined as choroidal areas below the choriocapillaris up to chorioscleral junction. Image binarization was performed using Niblack's method with a 30° radius using FIJI software (an expanded version of ImageJ version 1.51a, available at fiji.sc, free of charge). The white region was considered the vascular area in SVC, DVC, and choriocapillaris slabs and the black region was considered vascular area in choroid slab. The number of pixels was obtained and flow density was calculated by dividing the number of pixels of the vascular area by the total region of interest (Figure 1). Choroidal VD on OCTA was compared and validated with choroidal VD measured on the structural *en face* image.

2.3. Statistical Analysis. Statistical analysis was performed with SPSS for Windows (version 23.0.1; SPSS Inc., Chicago, IL, USA). For statistical analysis, the Snellen BCVA was converted to a logarithm of the minimal angle of resolution (logMAR). Values of continuous variables are presented as means ± standard deviation. One-way analysis of variance (ANOVA) was used to compare continuous variables among and between groups. Mann-Whitney and Kruskal-Wallis tests were used when a normal distribution could not be confirmed. Post hoc analysis was conducted using the Bonferroni test. Categorical variables between groups were compared using the chi-square test. Standardized adjustment was used as the post hoc test after the chi-square test. Pearson's correlation analysis was used to determine the coefficients of correlation between each VD and VDs and clinical parameters following confirmation of normal distribution. Spearman's correlation was used when normal distribution was not confirmed. Multivariate linear regression analysis was done for relevant variables. A P value < 0.05 was considered statistically significant.

3. Results

3.1. Demographic and Clinical Features. Of 295 consecutive eyes, we excluded 7 eyes due to poor image quality and 6 eyes due to concomitant macular diseases. In total, the present study included 282 eyes of 152 type 2 DM patients. Among the 282 eyes, 114 eyes did not show retinopathy, 79 had nonproliferative diabetic retinopathy (NPDR), 48 eyes had severe NPDR, and 41 eyes had proliferative diabetic retinopathy (PDR). All patients were Korean. The mean age was 60.12 ± 12.17 years, 57% were male, and 57% and 13% had comorbid hypertension (HTN) and chronic kidney disease (CKD), respectively. The mean duration of DM was 9.67 ± 7.91 years. The mean BCVA was 0.13 ± 0.29 logMAR. Age, sex distribution, DM duration, comorbid HTN and CKD, BCVA, random serum glucose level, and CMT did not differ significantly between DR grades (all $P \geq 0.084$). DM duration was significantly shorter in patients without DR

(a)

(b)

(c)

(d)
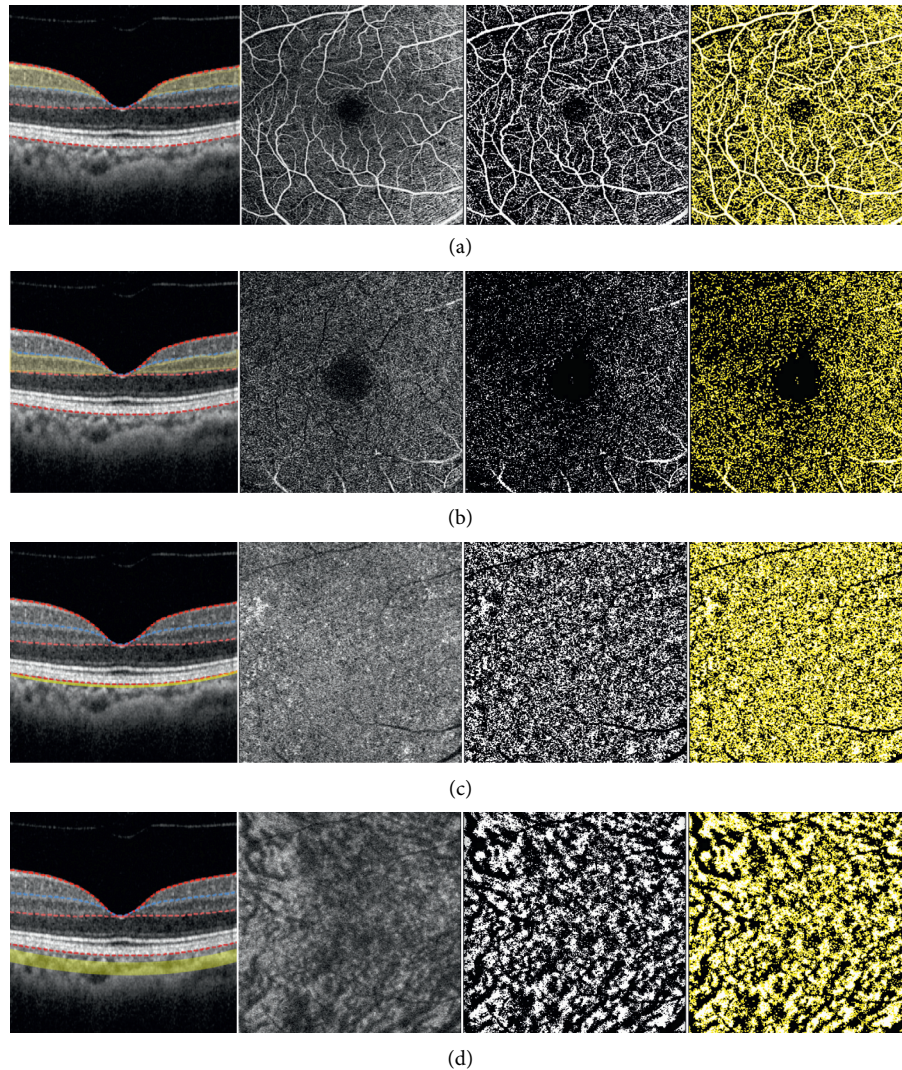
FIGURE 1: Vessel density measurements of each layer. En face 3×3 mm2 optical coherence tomography angiography (OCTA) images of (a) superficial vascular complex (SVC), (b) deep vascular complex (DVC), (c) choriocapillaris, and (d) choroid were analyzed. Each slab was automatically obtained using predefined settings of the Spectralis OCTA system. SVC consisted of nerve fiber layer vascular plexus and superficial vascular plexus, and DVC consisted of intermediate capillary plexus and deep capillary plexus. Choriocapillaris slab is generated by segmentation of 10 to $30 \mu m$ below Bruch's membrane and choroid is defined as choroidal areas below the choriocapillaris up to choriscleral junction (first and second column). Image binarization was performed using Niblack's method with a $30°$ radius (third column). The white region was considered the vascular area in SVC, DVC, and choriocapillaris slabs and the black region was considered the vascular area in choroid slab (forth column). The number of pixels was obtained, and flow density was calculated by dividing the number of pixels of the vascular area by the total region of interest.

compared with other grades (all $P < 0.001$) and longer in patients with PDR than without DR or NPDR ($P < 0.001$ and $P = 0.034$, respectively). Baseline demographic and clinical features of the study eyes are summarized in Table 1.

3.2. Comparing Vessel Densities of Different Retinal and Choroidal Layers among DR Grades. The mean VD of each layer was 0.28 ± 0.03, 0.31 ± 0.04, 0.32 ± 0.02, and 0.69 ± 0.02 for SVC, DVC, choriocapillaris, and choroidal vessels, respectively. It was 0.69 ± 0.2 for choroidal vessel measured in structural *en face* image. The choroidal VDs measured in OCTA and structural *en face* showed a strong positive

correlation with a high intraclass correlation coefficient of 0.852 ($r = 0.743$; $P < 0.001$). The ANOVA analysis showed that VDs of SVC, DVC, and choriocapillaris differed based on DR grade (all $P < 0.001$). Post hoc analysis showed that severe NPDR and PDR eyes had lower VDs of SVC and DVC compared with their previous grades (all $P < 0.001$, Figure 2). PDR eyes also showed lower choriocapillaris VD compared with lower DR grades (all $P < 0.008$).

3.3. Correlation between Vessel Densities and Clinical Parameters. Vessel densities of SVC, DVC, and choriocapillaris were negatively correlated with DR grade ($r = -0.573$,

Table 1: Clinical characteristics of study eyes.

Variables	Total eyes	No DR	NPDR	Severe NPDR	PDR	P value
N	282	114	79	48	41	
Age (years), mean ± SD	60.12 ± 12.17	59.16 ± 12.82	61.51 ± 11.47	59.31 ± 12.19	61.05 ± 11.73	0.537
Sex (male, n) (%)	160 (57)	152 (54)	166 (59)	168 (60)	152 (54)	0.778
DM duration (years)	9.67 ± 7.91	6.12 ± 6.33	10.59 ± 7.34	12.42 ± 6.92	14.51 ± 9.73	>0.001*
HTN (n) (%)	160 (57)	147 (52)	178 (63)	149 (53)	200 (71)	0.084
CKD (n) (%)	37 (13)	28 (10)	54 (19)	42 (15)	20 (7)	0.175
BCVA (LogMAR), mean ± SD	0.13 ± 0.29	0.15 ± 0.33	0.09 ± 0.21	0.12 ± 0.28	0.18 ± 0.33	0.436
HbA1c (%), mean ± SD	7.19 ± 1.43	6.84 ± 1.37	7.49 ± 1.5	7.34 ± 1.41	7.39 ± 1.35	0.009*
Glucose (mg/dL), mean ± SD	152.67 ± 60.66	147.13 ± 46.25	157.11 ± 71.28	156.06 ± 64.03	155.51 ± 70.23	0.658
CMT (um), mean ± SD	264.41 ± 43.24	262.96 ± 39.85	268.27 ± 42.2	268.35 ± 44.46	256.41 ± 52.3	0.467

DR: diabetic retinopathy; NPDR: nonproliferative diabetic retinopathy; PDR: proliferative diabetic retinopathy; SD: standard deviation; DM: diabetes mellitus; HTN: hypertension; CKD: chronic kidney disease; BCVA: best-corrected visual acuity; HbA1c: hemoglobin A1c; CMT: central macular thickness. *Statistically significant value. *P value for DM duration should be < 0.001.
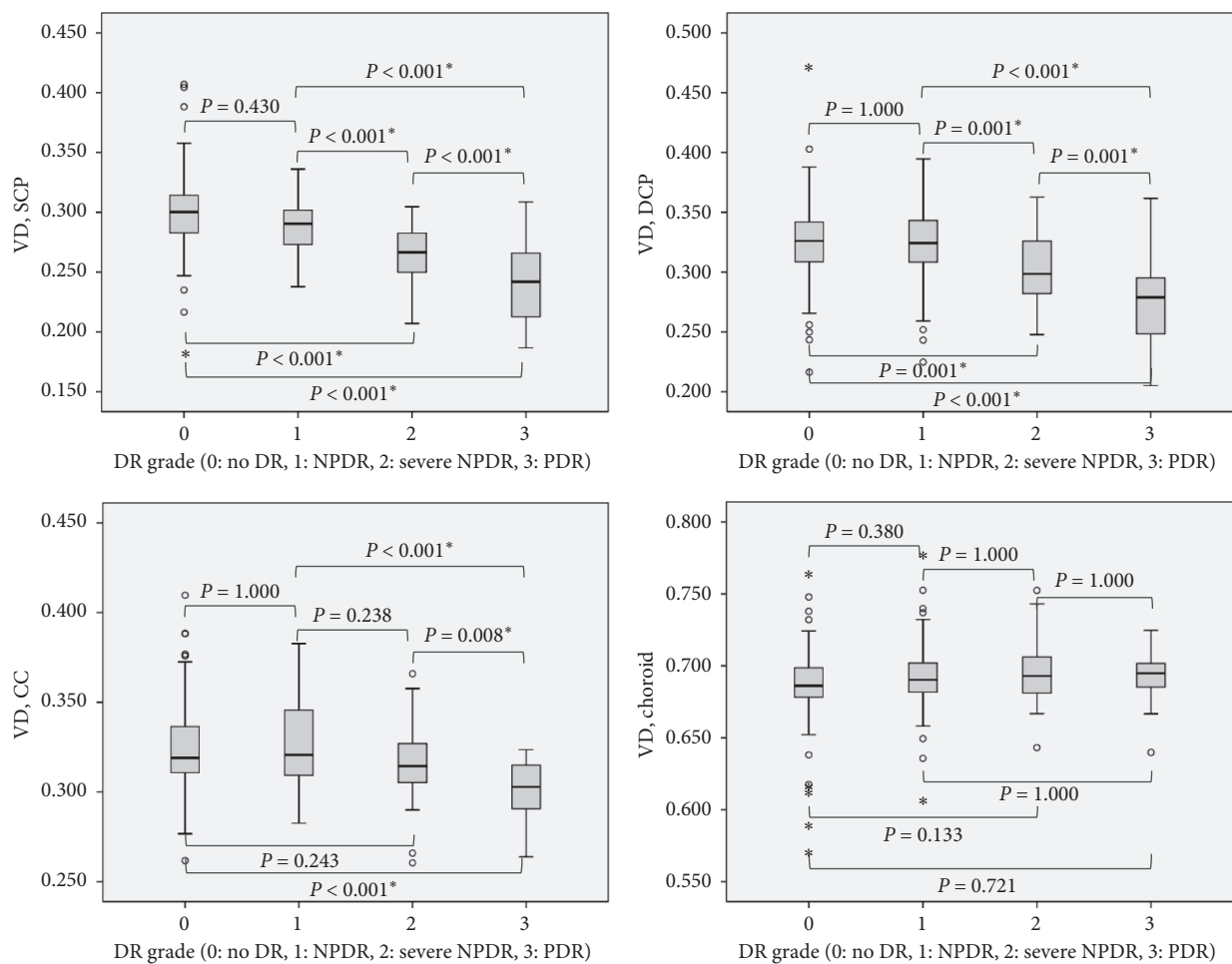
Figure 2: Comparison of vessel densities and grades of diabetic retinopathy (DR). Vascular densities (VDs) of superficial vascular complex (SVC), deep vascular complex (DVP), and choriocapillaris differed based on DR grades (all $P < 0.001$). Post hoc analysis showed that severe nonproliferative diabetic retinopathy (NPDR) and proliferative diabetic retinopathy (PDR) eyes had lower VDs of SVC and DVC compared with their previous grades (all $P < 0.001$). PDR eyes also showed lower choriocapillaris VD compared with lower DR grades (all $P < 0.008$). *Statistically significant P value.

−0.441, and −0.309, respectively; all $P < 0.001$; Figure 3); however, choroidal VD was positively correlated with DR grade ($r = 0.129$; $P = 0.030$). Age was negatively correlated with VD of SVC ($r = -0.120$; $P = 0.043$). Vessel densities of SVC and DVC were negatively correlated with DM duration

and comorbid HBP ($r = -0.213$ and -0.165; $P < 0.001$ and $= 0.005$ for SVC, respectively, and $r = -0.142$ and -0.148; $P = 0.017$ and $= 0.013$ for DVC, respectively). The correlation between VDs and clinical parameters is summarized in Table 2. Multivariate regression analysis including DR grade,
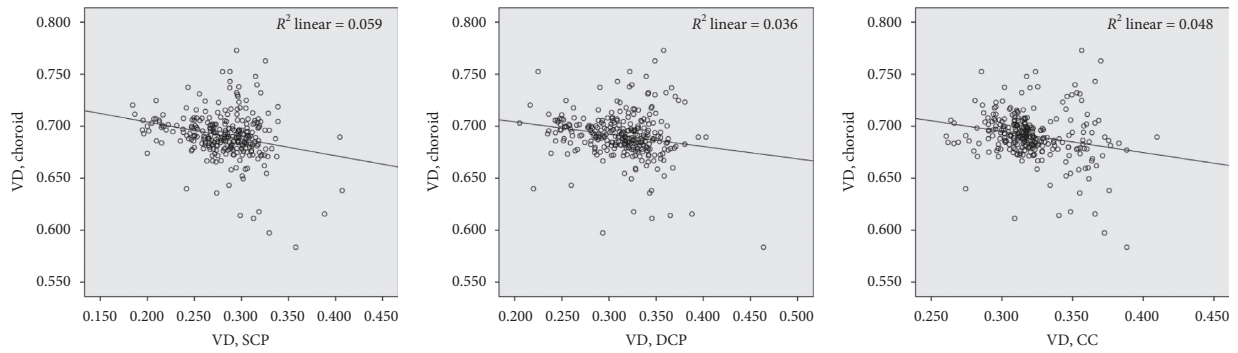
FIGURE 3: Correlation between choroidal vascular densities (VDs) and VDs of other layers. Choroidal vascular density (VD) showed weak negative correlations with VDs of other layers ($r = -0.243$, -0.189, and -0.220; $P < 0.001$, $= 0.001$, and < 0.001, for superficial capillary complex (SVC), deep capillary complex (DVC), and choriocapillaris, respectively).

TABLE 2: Correlation between vessel densities and clinical parameters.

Layers		DR grade	Age	Sex	DM duration	HTN	CKD	BCVA	HbA1c	Glucose	CMT
VD; SVC	Pearson correlation	−0.573*	−0.120*	0.075	−0.213*	−0.165*	0.023	−0.0092	0.047	0.115	0.094
	Sig. (2-tailed)	<0.001	0.043	0.212	<0.001	0.005	0.696	0.126	0.436	0.054	0.115
VD; DVC	Pearson correlation	−0.441*	−0.013	0.073	−0.142*	−0.148*	0.002	−0.059	0.028	0.078	0.066
	Sig. (2-tailed)	<0.001	0.831	0.224	0.017	0.013	0.967	0.323	0.640	0.193	0.267
VD; choriocapillaris	Pearson correlation	−0.309*	0.104	0.010	−0.069	−0.035	0.047	−0.022	0.102	0.057	0.022
	Sig. (2-tailed)	<0.001	0.081	0.861	0.248	0.554	0.431	0.715	0.088	0.343	0.715
VD; choroid	Pearson correlation	0.129*	−0.008	−0.089	0.031	0.063	0.060	0.005	0.032	0.063	−0.017
	Sig. (2-tailed)	0.030	0.892	0.137	0.605	0.288	0.319	0.937	0.589	0.290	0.777

DR: diabetic retinopathy; DM: diabetes mellitus; HTN: hypertension; CKD: chronic kidney disease; BCVA: best-corrected visual acuity; HbA1c: hemoglobin A1c; CMT: central macular thickness; VD: vessel density; SVC: superficial vascular complex; DVP: deep vascular complex; CC: choriocapillaris. *Statistically significant value.

age, DM duration, and HTN showed that DR grade was an independent factor associated with VDs of SVC and DVC ($B = -0.019$ and -0.015; $P < 0.001$ and < 0.001, resp.). Age correlated with DM duration ($r = 0.343$; $P < 0.001$) and DM duration correlated with DR grades ($r = 0.390$; $P < 0.001$).

3.4. Correlation between Vessel Densities of Different Retinal and Choroidal Layers.
Vessel densities of SVC, DVC, and choriocapillaris were strongly positively correlated (all $P < 0.001$, Table 3). Negative correlations were observed between choroidal VD and VDs of other layers ($r = -0.243$, -0.189, and -0.220; $P < 0.001$, $= 0.001$, and < 0.001, for SVC, DVC, and choriocapillaris, respectively).

4. Discussion

Measuring VDs using OCTA is useful for investigating the pathophysiology of retinal disease including DR in which vascular changes are the main process of the disease. In the present study, VDs of SVC, DVC, choriocapillaris, and choroid were analyzed in type 2 DM patients. The results showed a significant negative correlation between VDs of retinal layers with DR grades. However, VDs of larger choroidal vessels showed different association with the DR grades. The association between each VD of retinal layers and larger choroidal also revealed some differences.

The VDs of SVC, DVC, and choriocapillaris were significantly decreased as the severity of DR increased. Age and DM duration were also associated with VD which is in agreement with findings from previous studies. Retinal VDs were associated with DR severity, older age, higher HbA1c level, and the presence of DME in previous studies [7, 10]. In the present study, eyes with DME were excluded because DME can affect VDs as well as causing inaccurate measurement of VD. Age strongly correlated with DM duration and DM duration strongly correlated with DR grades; therefore, multivariate analysis showed that only DR severity was an independent factor associated with VDs of SVC and DVC. Definitive correlation was not observed between VDs and HbA1c level in the present study. This discordance might have been caused by different medical management strategies for DM. Further prospective controlled studies are warranted to clarify the correlation between HbA1c and VDs.

A significant association of DR with retinal, SVC, and DVC VDs has been reported in many previous studies and decreases in vessel densities in DR have been suggested

TABLE 3: Correlation between vessel densities of different retinal and choroidal layers.

Layers		VD; SVC	VD; DVC	VD; CC	VD; choroid
VD; SCP	Pearson correlation*	1	0.714	0.439	−0.243
	Sig. (2-tailed)		0.000	0.000	0.000
VD; DVC	Pearson correlation*	0.714	1	0.611	−0.189
	Sig. (2-tailed)	0.000		0.000	0.001
VD; CC	Pearson correlation*	0.439	0.611	1	−0.220
	Sig. (2-tailed)	0.000	0.000		0.000
VD; choroid	Pearson correlation*	−0.243	−0.189	−0.220	1
	Sig. (2-tailed)	0.000	0.001	0.000	

VD: vessel density; SVC: superficial vascular complex; DVP: deep vascular complex; CC: choriocapillaris. *Statistically significant value (P-value <0.05).

[7, 11, 12]. Because the retina has nonanastomotic end arteries, the pathophysiology of DM affects retinal vessels [13, 14]. However, choroidal vessels can also be affected by DR status. Choriocapillaris perfusion was decreased in DM patients even without retinopathy in studies using OCTA, indicating that decreased choriocapillaris perfusion may exist before clinically detectable DR [7, 12, 15, 16]. In addition, the decrease in choriocapillaris VD was correlated with DR severity [7]. In the current study, choriocapillaris VD also decreased with increasing severity of DR. This finding is supported by other previous histopathological study results showing that a decrease in the alkaline phosphatase enzyme activity is associated with choriocapillaris loss in DM eyes [17, 18].

Conversely, choroidal VD did not significantly differ among various DR grades and even had a positive correlation with DR grades based on correlation analysis. The choroidal VD also negatively correlated with VDs of SVC, DVC, and choriocapillaris; however, other layers were positively correlated. Choroidal vascularity index (CVI) had been calculated in DR eyes and decreased CVI in PDR eyes was reported [19, 20]. In the current study, choriocapillaris VD was decreased with increased severity of DR, similar to other studies; however, choroidal VD was not decreased. Measurement of CVI includes all layers of the choroid including choriocapillaris as well as Sattler's and Haller's layers. The feasibility of layer-by-layer analysis is a distinctive advantage of OCTA including analysis for choroidal sublayer [21, 22]. The choroid slab used in the present study included choroidal area under the choriocapillaris and, therefore, represented the larger choroidal vessel status. In addition, CVI measurements are usually performed in one B-scan image which crosses the fovea. The *en face* image of OCTA can represent the general status of the larger choroidal vessel at a $3 \times 3 \, mm^2$ macular area. The main physiological function of the choroid is to provide oxygen and nutrients to the highly metabolic outer retinal layers [23]. The positive correlation of choroidal VD with DR grade may suggest a compensatory mechanism of deep choroidal vessels in response to hypoxic status and hypoxic damage occurs in the retina. Alternatively, dilation of choroidal venule could be a reactive change to the occlusion choriocapillaris, as a shunt in retinal capillary occlusion may lead to venous beading in the diabetic retina [24].

The present study had several limitations. First, due to the retrospective design, factors that could affect clinical parameters, such as HbA1c and glucose levels, could not be controlled. Second, selection bias may have existed due to the exclusion of eyes with DME; however, we believe that disadvantages from excluding DME are outweighed by improved clarity of analysis. Third, the sample size of the current study was not large. Research with larger sample sizes is required to validate the results of this study. In addition, this study did not utilize an additional method for projection artifact reduction or not analyze the impact of signal strength, which can cause errors in VD analysis. Nonetheless, we minimized the error by including images with high Q score and excluding images with considerable artifacts. Also, the Spectralis OCTA system itself provides projection artifact removal. To the best of our knowledge, the association between choroidal vessel and DR grades or direct correlation among densities of retinal and choroidal vessels has not yet been reported in any study. The correlation between clinical parameters, as well as retinal and choroidal VDs, is a strength of the current study.

In conclusion, choroidal VD increased as retinal and choriocapillaris VDs decreased, indicating that the choroidal large vessel layer is less affected by DR severity, and larger choroidal vessel VD may even be increased as a compensatory mechanism for decreased retinal and choriocapillaris VDs in type 2 DM patients. However, interpretation of the results should be made with caution because the correlation was not strong. We believe that the results of this study can improve the understanding of the hemodynamics associated with DR.

Data Availability

The datasets generated and/or analyzed in the current study are available from the corresponding author upon reasonable request.

Ethical Approval

This study was approved by the institutional review board of Bucheon St. Mary's Hospital and conducted according to the Declaration of Helsinki.

Conflicts of Interest

The authors have no conflicts of interest to declare.

Authors' Contributions

Junhyuck Lee contributed to the preparation of data and data analysis; Nam Yeo Kang contributed to the conceptualization and data analysis; Inkee Kim and Ho Ra contributed to the collection of data and data analysis; Jiwon Baek contributed to the conception and design of the study, writing manuscript text, preparing figures, collection and assembly of data, data analysis and interpretation, and supervision. All authors reviewed the manuscript. Ho Ra and Nam Yeo Kang contributed equally to this work.

Acknowledgments

References

[1] R. Lee, T. Y. Wong, and C. Sabanayagam, "Epidemiology of diabetic retinopathy, diabetic macular edema and related vision loss," *Eye and Vision*, vol. 2, no. 1, p. 17, 2015.

[2] P. Kroll, E. Büchele Rodrigues, and S. Hoerle, "Pathogenesis and classification of proliferative diabetic vitreoretinopathy," *Ophthalmologica*, vol. 221, no. 2, pp. 78–94, 2007.

[3] R. Simo, E. Carrasco, M. Garcia-Ramirez, and C. Hernandez, "Angiogenic and antiangiogenic factors in proliferative diabetic retinopathy," *Current Diabetes Reviews*, vol. 2, no. 1, pp. 71–98, 2006.

[4] F. Bandello, E. Corbelli, A. Carnevali, L. Pierro, and G. Querques, "Optical coherence tomography angiography of diabetic retinopathy," *Developments in Ophthalmology*, vol. 56, pp. 107–112, 2016.

[5] A. Y. Kim, Z. Chu, A. Shahidzadeh, R. K. Wang, C. A. Puliafito, and A. H. Kashani, "Quantifying microvascular density and morphology in diabetic retinopathy using spectral-domain optical coherence tomography angiography," *Investigative Opthalmology and Visual Science*, vol. 57, no. 9, pp. 362–370, 2016.

[6] H. R. AttaAllah, A. A. M. Mohamed, and M. A. Ali, "Macular vessels density in diabetic retinopathy: quantitative assessment using optical coherence tomography angiography," *International Ophthalmology*, vol. 39, no. 8, pp. 1845–1859, 2019.

[7] G. Ryu, I. Kim, and M. Sagong, "Topographic analysis of retinal and choroidal microvasculature according to diabetic retinopathy severity using optical coherence tomography angiography," *Graefe's Archive for Clinical and Experimental Ophthalmology*, vol. 259, no. 1, p. 61, 2020.

[8] K. G. M. M. Alberti and P. Z. Zimmet, "Definition, diagnosis and classification of diabetes mellitus and its complications. Part 1: diagnosis and classification of diabetes mellitus. Provisional report of a WHO Consultation," *Diabetic Medicine*, vol. 15, no. 7, pp. 539–553, 1998.

[9] "Fundus photographic risk factors for progression of diabetic retinopathy. ETDRS report number 12. Early Treatment Diabetic Retinopathy Study Research Group," *Ophthalmology*, vol. 98, pp. 823–833, 1991.

[10] N. Xie, Y. Tan, S. Liu et al., "Macular vessel density in diabetes and diabetic retinopathy with swept-source optical coherence tomography angiography," *Graefe's Archive for Clinical and Experimental Ophthalmology*, vol. 258, no. 12, p. 2671, 2020.

[11] G. Dimitrova, E. Chihara, H. Takahashi, H. Amano, and K. Okazaki, "Quantitative retinal optical coherence tomography angiography in patients with diabetes without diabetic retinopathy," *Investigative Opthalmology & Visual Science*, vol. 58, no. 1, pp. 190–196, 2017.

[12] Y. Dai, H. Zhou, Z. Chu et al., "Microvascular changes in the choriocapillaris of diabetic patients without retinopathy investigated by swept-source OCT angiography," *Investigative Opthalmology & Visual Science*, vol. 61, no. 3, p. 50, 2020.

[13] S. A. M. Kolman, A. M. van Sijl, F. A. van der Sluijs, and M. A. van de Ree, "Consideration of hypertensive retinopathy as an important end-organ damage in patients with hypertension," *Journal of Human Hypertension*, vol. 31, no. 2, pp. 121–125, 2017.

[14] A. Campos, E. J. Campos, J. Martins, A. F. Ambrósio, and R. Silva, "Viewing the choroid: where we stand, challenges and contradictions in diabetic retinopathy and diabetic macular oedema," *Acta Ophthalmologica*, vol. 95, no. 5, pp. 446–459, 2017.

[15] J. Yang, E. Wang, X. Zhao et al., "Optical coherence tomography angiography analysis of the choriocapillary layer in treatment-naïve diabetic eyes," *Graefe's Archive for Clinical and Experimental Ophthalmology*, vol. 257, no. 7, pp. 1393–1399, 2019.

[16] D. S. McLeod and G. A. Lutty, "High-resolution histologic analysis of the human choroidal vasculature," *Investigative Ophthalmology and Visual Science*, vol. 35, no. 11, pp. 3799–3811, 1994.

[17] G. A. Lutty and D. S. McLeod, "Phosphatase enzyme histochemistry for studying vascular hierarchy, pathology, and endothelial cell dysfunction in retina and choroid," *Vision Research*, vol. 45, no. 28, pp. 3504–3511, 2005.

[18] I. Fukushima, D. S. McLeod, and G. A. Lutty, "Intrachoroidal microvascular abnormality: a previously unrecognized form of choroidal neovascularization," *American Journal of Ophthalmology*, vol. 124, no. 4, pp. 473–487, 1997.

[19] M. Kim, M. J. Ha, S. Y. Choi, and Y.-H. Park, "Choroidal vascularity index in type-2 diabetes analyzed by swept-source optical coherence tomography," *Scientific Reports*, vol. 8, no. 1, p. 70, 2018.

[20] C. Gupta, R. Tan, C. Mishra et al., "Choroidal structural analysis in eyes with diabetic retinopathy and diabetic macular edema-A novel OCT based imaging biomarker," *PLoS One*, vol. 13, no. 12, Article ID e0207435, 2018.

[21] F. Siegfried, F. Rommel, M. Rothe et al., "Evaluating diurnal changes in choroidal sublayer perfusion using optical coherence tomography angiography," *Acta Ophthalmologica*, vol. 97, no. 8, pp. e1062–e1068, 2019.

[22] O. Gal-Or, K. K. Dansingani, D. Sebrow, R. Dolz-Marco, and K. B. Freund, "Inner choroidal flow signal attenuation in pachychoroid disease," *Retina*, vol. 38, no. 10, pp. 1984–1992, 2018.

[23] S. S. Hayreh, "Blood flow in the optic nerve head and factors that may influence it," *Progress in Retinal and Eye Research*, vol. 20, no. 5, pp. 595–624, 2001.

[24] B. Fagrell, G. Jorneskog, and M. Intaglietta, "Disturbed microvascular reactivity and shunting - a major cause for diabetic complications," *Vascular Medicine*, vol. 4, no. 3, pp. 125–127, 1999.

Research Article

Spectral-Domain Optical Coherence Tomography-Based Morphofunctional Characterization of Dome-Shaped Maculopathy in Indian Population

Naresh Babu Kannan [ID], **Sagnik Sen** [ID], **Prithviraj Udaya** [ID], **Obuli Ramachandran** [ID], **and Kim Ramasamy**

Department of Retina & Vitreous Services, Aravind Eye Hospital, Madurai, India

Correspondence should be addressed to Naresh Babu Kannan; cauveryeye@gmail.com

Purpose. To study the clinicodemographic profile of dome-shaped maculopathy (DSM) eyes in the Indian population and characterization using spectral-domain optical coherence tomography (SD-OCT). *Methods*. This observational cross-sectional study included 25 eyes of 14 patients diagnosed with DSM. All eyes underwent SD-OCT for characterization of the dome profile and also to measure central macular thickness (CMT), subfoveal choroidal thickness (SFCT), and dome height (DH) and to detect the presence of subretinal fluid (SRF). *Results*. The mean age of patients was 48.36 ± 14.23 years (range, 28–65 years). Eleven patients had bilateral involvement. Mean axial length of all eyes was 24.25 ± 1.95 mm and mean spherical equivalent -4.23 ± 3.79 DS. Overall, 11/25 eyes (44%) had round domes, 9/25 eyes (36%) had horizontal domes, and 5/25 eyes (20%) had vertical domes, with a mean dome height at fovea of $500.54 \pm 291.58\,\mu$m. Vertical domes had higher DH compared to horizontal or combined domes ($p = 0.02$). Six eyes (6/25, 24%) showed the presence of SRF; 60% of vertical domes had SRF, and 22.2% of horizontal domes had SRF. The eyes having SRF had significantly higher CMT ($p = 0.017$) and DH ($p = 0.001$), especially in horizontal domes ($p = 0.023$). The eyes with thicker SFCT tended to have higher DH and poorer visual acuity. *Conclusion*. Indian DSM eyes may have relatively lesser amounts of myopia. Choroidal thickening may play a role in development of DSM and may also be related to development of subretinal fluid in such eyes.

1. Introduction

Myopia is one of the leading causes of visual morbidity around the world [1, 2], with a particularly high prevalence in the Eastern and the southeastern global population [3–9]. Dome-shaped maculopathy (DSM) is an unusual clinical entity, first described in 2008 by Gaucher and associates as an abnormal forward convex bulge of the macula within concavity of posterior staphyloma in highly myopic eyes [10–12]. Although the prevalence of DSM has not been reported by any population-based study, incidence of DSM in highly myopic eyes has been estimated as 20% in Japan [13], 16% in Turkey [14], and 11% in Europe [15]. DSM has been documented in adults, adolescents, and children in

many other parts of the world, namely, Canada [11], USA [16, 17], UK [18, 19], Europe [10, 15, 20, 21], Korea [22, 23], and Japan [16, 24]. Although, DSM was initially believed to occur exclusively in high myopic eyes with staphyloma, it has also been described in emmetropes, hypermetropes [18], and eyes without staphyloma [16]. The field of retinal imaging by optical coherence tomography (OCT), especially enhanced depth imaging and swept source OCT for deeper penetration into choroid and the sclera, has especially aided in describing the topographic attributes of DSM [16, 24].

After a thorough literature review, we came to the conclusion that no study has been performed to describe the clinical and demographic profile of DSM in the Indian population. Hence, the current study was performed with the

purpose of providing an insight into the clinical picture of dome-shaped maculopathy and relationship between its structural profile and visual function in the Indian population.

2. Methodology

This observational cross-sectional study was performed at a tertiary care ophthalmic center in South India. The study adhered to the Declaration of Helsinki, and ethical clearance was obtained from the Institutional Ethics Committee. Any eye diagnosed as DSM between January 2018 and December 2019 was included for evaluation. Eyes with macular degeneration due to any cause, macular holes, diabetic retinopathy, and significant media opacity obstructing image capturing and patients with subretinal fluid due to any specific retinal conditions such as choroidal neovascularization and diabetic macular edema were excluded.

A complete ophthalmological examination was performed for all subjects, including best corrected visual acuity (BCVA) with Snellen chart and anterior and posterior segment examination and spectral-domain optical coherence tomography (SD-OCT) with enhanced depth imaging (Heidelberg Spectralis, Heidelberg, Germany). All cases of DSM with SRD detected on SD-OCT underwent simultaneous fluorescein angiography and indocyanine green angiography (Heidelberg Spectralis, Heidelberg, Germany) to rule out any underlying choroidal neovascularization. SD-OCT examination was performed in both the eyes of each subject. SD-OCT images were analyzed for measuring the central macular thickness, subfoveal choroidal thickness, dome height, and subretinal fluid height if present. The OCT thickness measurements were all performed between 10am and 2pm during the day for all included patients, to rule out variability of choroidal thickness. Axial length of each eye was measured using partial coherence interferometry (IOLMaster 500, Carl Zeiss Meditec, Jena, Germany).

Dome-shaped maculopathy was defined as a convex elevation of the sclero-choroido-retinal macular complex seen in horizontal and/or vertical SD-OCT scans. Three-dimensional OCT topography was used to identify the orientation of the dome in the posterior pole in addition to the raster scans, and accordingly, types of domes were defined as horizontal oval (when dome was more convex along the vertical axis), vertical oval (when dome was more convex along the horizontal axis), and round (when dome was symmetric along the vertical and horizontal axis). This was performed based on the classification by Caillaux et al. [20]. Dome height (DH) was determined by drawing a line passing through the center of the fovea (line 1), perpendicular to another line (line 2) passing horizontally tangential to the outer border of the line corresponding to the retinal pigment epithelium (RPE) at the edges of the dome [20]. DH was defined as the distance between the intersection of line 1 with RPE and intersection of lines 1 and 2 (Figure 1).

2.1. Statistical Analysis. Data were entered in a Microsoft Excel spreadsheet. Data normality was checked using histograms. Statistical analysis was performed using SPSS for Windows software (version 20.0, International Business Machines Corp.). Mean (±standard deviation) and frequency (percentage) were used to describe continuous and categorical variables, respectively. Quantitative data were compared using the t test for parametric and Mann–Whitney U test for nonparametric variables. Statistical significance was taken at 2-tailed p value of less than 0.05.

3. Results

We analyzed 25 eyes of 14 patients who presented to our center between January 2018 and December 2019 and diagnosed as having dome-shaped maculopathy. The mean age of patients was 48.36 ± 14.23 years (range, 28–65 years). Eleven patients had bilateral involvement (22 eyes). Baseline visual acuity of all eyes was 0.33 ± 0.3 logMAR (Snellen equivalent 6/9). Mean axial length of all eyes was 24.25 ± 1.95 mm (range, 21.4–28.7 mm). The mean spherical equivalent (SE) of 25 eyes was -4.23 ± 3.79 DS (range, +0.50–−13 DS). 44% of eyes (11) had myopia less than −3 DS. The mean SE of 22 eyes showing bilateral involvement was -4.65 ± 3.86 DS (median, −3.50 DS). Three eyes showing unilateral involvement had a median SE of −1.25 DS. 23 eyes had myopia, 1 eye had hyperopia, and 1 eye had no significant refractive error. Demographic characteristics of the study population are summarized in Table 1.

The mean dome height at fovea was $500.54 \pm 291.58 \mu m$ (range, 116–1311 μm). None of the eyes exhibited vitreomacular traction, and only 1 eye had an epiretinal membrane. A total of 11/25 eyes (44%) had round domes, 9/25 eyes (36%) had horizontal domes, and 5/25 eyes (20%) had vertical domes. On comparison of clinical characteristics among the three different types of domes (Table 2), we observed that the domes differed significantly in terms of dome height, with vertical domes having higher dome height as compared to horizontal or combined domes ($p = 0.02$). There was no difference in the dome height between horizontal domes and round domes ($p = 0.9$). Rest all clinical parameters among the groups were comparable.

A total of 6/25 eyes (24%) showed the presence of subretinal fluid (SRF) and associated neurosensory detachment. 60% of vertical domes had SRF, and 22.2% of horizontal domes had SRF. Only 1 eye with round dome had SRF. The clinical summary of eyes based on presence of SRF is shown in Table 3.

We observed that eyes having SRF showed significantly higher CMT ($p = 0.017$) and dome height ($p = 0.001$), especially in horizontal domes ($p = 0.023$). The overall dome height was significantly higher in the eyes having SRF, and this difference was significant in horizontal domes, and vertical domes also showed a trend towards higher dome height in the presence of SRF (Table 2). Of the eyes with SRF, 3 eyes were treated with subthreshold micropulse yellow laser and 2 eyes were injected with 1.25 mg/0.05 mL of intravitreal bevacizumab. After a follow-up period of 3 months, the SRF had reduced in all of these eyes, however, still persisted. One eye with SRF was observed, and the SRF persisted till the last follow-up.
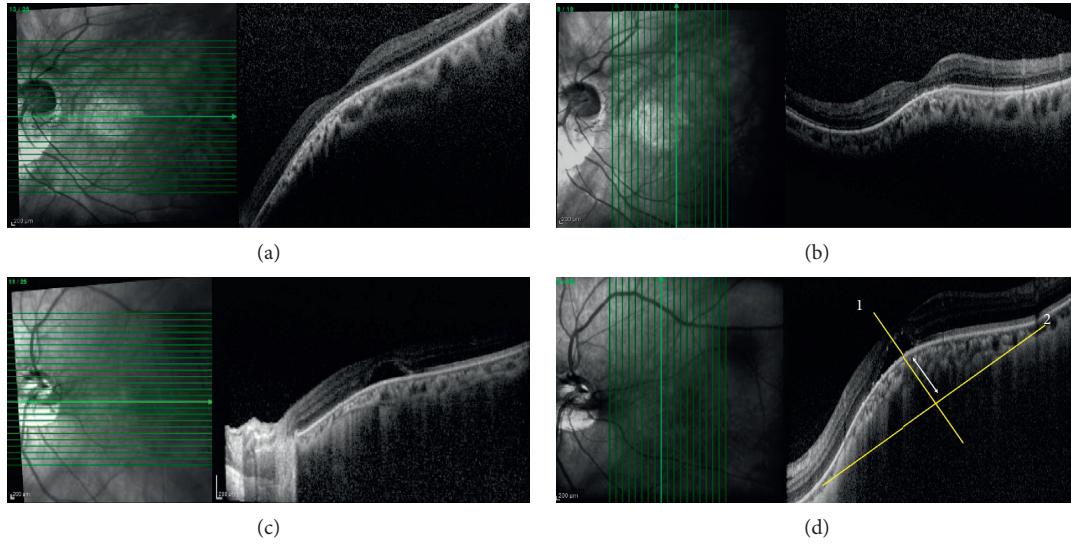
(a)

(b)

(c)

(d)

FIGURE 1: Horizontal (a and c) and vertical (b and d) spectral-domain optical coherence tomography (SD-OCT) scans at the fovea of a vertical dome (upper panel) and a horizontal dome with subretinal fluid (SRF) (lower panel). (d) Measurement of dome height in a horizontal dome with SRF on SD-OCT scan—line 1 is a line passing through the center of the fovea, perpendicular to line 2 passing tangential to the outer border of the retinal pigment epithelium (RPE) at the edges of the dome. The distance between the intersection of line 1 with RPE and intersection of lines 1 and 2 represents the dome height.

TABLE 1: Clinical characteristics of study population.

Variable	Mean ± SD	Range
Number of eyes/number of patients	25/14	—
Sex	8 female/6 male	—
Age (years)	48.36 ± 14.23	28–65
Best corrected visual acuity (logMAR)	0.33 ± 0.30	0–1
Spherical equivalent (DS)	−4.23 ± 3.79	−13.0–0.5
Axial length (mm)	24.25 ± 1.95	21.4–28.7
Subfoveal choroidal thickness (μm)	275.08 ± 82.83	83–422
Central macular thickness (μm)	256.76 ± 108.17	70–455
Dome height (μm)	500.54 ± 291.58	116–1311

TABLE 2: Comparison of parameters among different orientations of myopic domes.

Variable	Horizontal	Vertical	Round	p value
Number of eyes	9	5	11	—
Sex	5 M/1 F	1 M/2 F	5 F	—
Age (years)	42.33 ± 15.98	48 ± 14.93	55.8 ± 10.15	0.318
Best corrected visual acuity (logMAR)	0.35 ± 0.28	0.2 ± 0.44	0.36 ± 0.26	0.198
Spherical equivalent (DS)	−3.78 ± 4.99	−4.2 ± 3.25	−4.61 ± 3.14	0.413
Axial length (mm)	23.75 ± 2.34	24.06 ± 2.06	24.74 ± 1.59	0.312
Subfoveal choroidal thickness (μm)	234.0 ± 97.01	303.6 ± 66.82	295 ± 69.15	0.181
Central macular thickness (μm)	245.2 ± 116.88	318.2 ± 111.86	238.2 ± 98.80	0.627
Dome height (μm)	412.22 ± 247.97	811.2 ± 338.5	424.7 ± 209.49	**0.02**∗
Subretinal fluid (present/absent)	2/7	3/2	1/10	0.095
Foveoschisis (present/absent)	0/9	0/5	2/9	0.670

∗Bonferroni post hoc test for dome height: horizontal vs. vertical, −0.03; vertical vs. combined, −0.03; horizontal vs. combined, −0.9.

We tried to find an association among different eye characteristics. We found that logMAR visual acuity showed a trend towards a negative association with the subfoveal choroidal thickness (SFCT) ($\rho = 0.307$), indicating that with an increase of choroidal thickness, VA tended to worsen (Figure 2(a)). Moreover, dome height showed a trend towards a positive association with both SFCT ($\rho = 0.366$) and CMT ($\rho = 0.401$) (Figures 2(b) and 2(c)). The associations were, however, not found statistically significant.

TABLE 3: Impact of SRF on morphological and functional parameters.

	Overall			Vertical			Horizontal		
	SRF		p	SRF		p	SRF		p
	No	Yes		No	Yes		No	Yes	
Number	19	6		2	3		7	2	
VA (logMAR)	0.29 ± 0.24	0.44 ± 0.47	0.69	0	0.33 ± 0.58	0.99	0.29 ± 0.17	0.59 ± 0.59	0.67
Spherical equivalent (DS)	-4.41 ± 4.01	-3.67 ± 3.25	0.73	-1 ± 0.35	-6.33 ± 2.02	0.2	-4.71 ± 5.34	-0.5 ± 0.71	0.22
Central macular thickness (μm)	226.58 ± 96.46	352.33 ± 90.79	**0.017**	242 ± 1.41	369 ± 123.89	0.218	209.71 ± 106.15	369.5 ± 44.55	**0.028**
Subfoveal choroidal thickness (μm)	264.37 ± 86.61	309 ± 64.12	0.201	299.5 ± 30.41	306.33 ± 91.87	0.914	218.43 ± 105.48	289.5 ± 26.16	0.15
Dome height (μm)	361.16 ± 160.5	900.5 ± 211.96	**0.001**	495.5 ± 21.92	1021.67 ± 250.64	0.066	309.14 ± 156.28	773 ± 103.23	**0.023**

VA, visual acuity; SRF, subretinal fluid. *Analysis of round dome was not performed since only 1 eye had presence of SRF. The values in bold are statistically significant at $p < 0.05$.

(a)

(b)

(c)
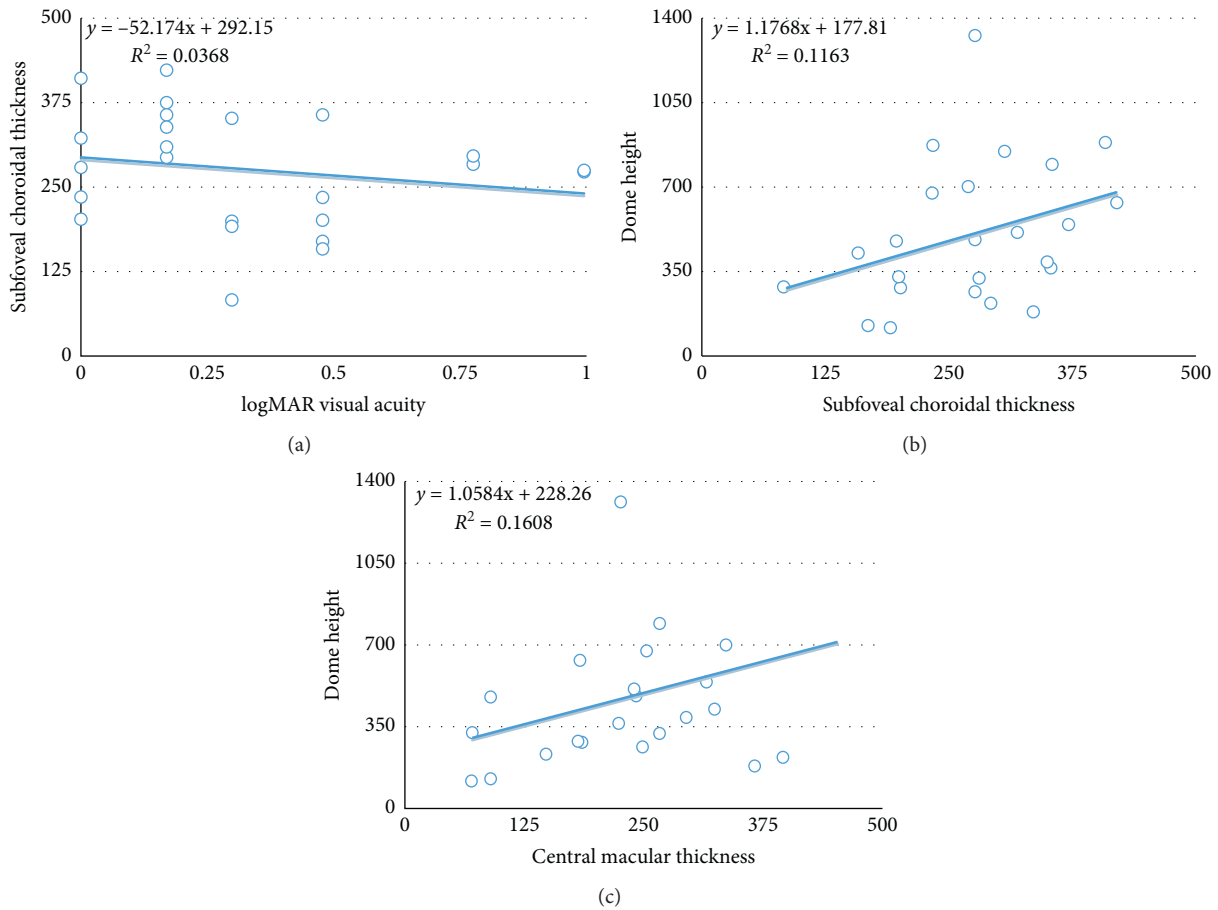
FIGURE 2: (a) Visual acuity (logMAR) showing a negative trend with subfoveal choroidal thickness ($\rho = 0.307$). (b)-(c) Dome height showing a positive trend with SFCT ($\rho = 0.366$) and CMT ($\rho = 0.401$).

4. Discussion

In this study, we have documented the clinical characteristics of Indian eyes with DSM. A noteworthy proportion of DSM eyes, in our study, is that 44% had myopia less than -3 DS, signifying the fact DSM in Indians may be present in low to moderate myopic eyes as well, which may be a different presentation as has been observed in the Eastern countries. Previously, authors have reported refractive errors of -13.6 DS, -15.5 DS, and -15.8 DS in Asian eyes [13, 16, 25].

The pathomechanism of DSM remains ambiguous with several theories postulated: rigid alteration in the scleral biomechanics with progressing staphyloma, dynamic vitreomacular traction (VMT), locally confined subfoveal choroidal thickening, scleral infolding through collapse of

the posterior portion of the eyewall, compensatory mechanism to myopic globe expansion, adjustment to minimize defocus at the macula, and hypotony in the area of staphyloma [10, 16, 26–28]. Imamura et al. [16] suggested DSM is linked with a localised variation of subfoveal scleral thickness, while it was confirmed later by Ellabban et al. [29] that DSM in high myopes is indeed associated with parafoveal scleral thinning. Thickened sclera can compress the underlying choroidal vasculature with subsequent alterations in retinal pigment epithelium and eventual atrophy [16]. Probably in Indian eyes, localised macular choroidal thickening seems to play a role, as around 1/4th of domes in our series had underlying SFCT greater than 350 μm. Our data also show that our population may have DSM at a lesser refractive error, which goes against the concept of DSM development secondary to defocus at the macula [27]. Moreover, normal intraocular pressure in all eyes of our series along with the absence of biomicroscopic/OCT signs of vitreomacular traction contravenes the theories of hypotony, scleral collapse, and tangential VMT behind development of DSM. Hence, the pathogenesis of DSM in the Indian population may be different.

OCT imaging has proven to be pivotal in diagnosis of DSM, as domes can be easily missed on routine funduscopic examination [10, 30]. Caillaux et al. affirmed the relevance of methodical multidirectional SD-OCT scans with at least one horizontal and one vertical scan to diagnose and optimally image the topographic attributes of DSM [20]. In their report, 21% of eyes had round domes, 16% of eyes had vertically oriented oval dome, and 63% of eyes had horizontally oriented oval dome [20]. In our study, round dome was seen to be the most common DSM morphology (44% of eyes), followed by horizontal dome (36% of eyes) and vertical dome (20% of eyes). Contrary to the previous finding that horizontal domes are the most commonly observed DSM pattern [13, 14, 20], we found them to be less common than round domes in our Indian cohort. This might represent a regional variation, although only studies with larger sample size can confirm this observation. We compared the clinical parameters between the three different morphological dome patterns. There was no difference in BCVA and CMT among the three types of domes. The dome height varied among the groups but was significantly higher in vertical domes. The other clinical characteristics were comparable between the groups.

DSM can be associated with a diverse spectrum of vision-threatening macular complications that include serous retinal detachment (SRD), choroidal neovascularization (CNV), pigment epithelial detachment (PED), retinal pigment epithelium (RPE) atrophy, foveoschisis, macular hole (MH), and lamellar MH (LMH) [13, 16, 20, 24, 26, 30–32]. DSM has been observed in about 18% of eyes with myopic choroidal neovascularization [33]. SRD as a macular complication is reportedly very frequent in eyes with DSM [16, 26, 32, 34]. It is also seen commonly in DSM eyes without choroidal neovascularization [20, 31].

A review of literature suggests that there is a marked variation in the incidence of SRF in DSM eyes among different studies, ranging from 1.8% to 66.7% [10, 13, 20, 24, 26, 30, 34].

In our study, SRF was present in 24% of eyes at baseline. CNVM was ruled out by angiography. Lorenzo et al. [11] observed that a lower magnitude of myopia (less than −6 D) may be an important factor influencing the development of SRF. 64% of our study eyes had myopia less than −6 D. We found contrasting results of refractive error in vertical and horizontal domes with SRF (Table 3). Overall, the eyes with SRF were likely to have a significantly greater dome height. Horizontal domes had a significantly lower dome height compared to the vertical domes; however, horizontal domes with a higher dome height were found to be more likely to be complicated by the presence of SRF. For vertical domes, there was no difference in clinical parameters between the eyes with SRF and the eyes without SRF, except for a higher dome height. In keeping with other reports [20, 34], there was a high proportion of vertical domes with SRF (60%). Contrary to the report by Pilotto et al. [34], SRF was least frequently found in round domes in our study (9%).

The precise mechanism behind accumulation of SRF is uncertain. It may be attributable to higher dome height, as suggested by our study. Some of the hypotheses put forward to explain SRF in DSM include altered dynamics of choroidal blood flow and RPE function consequent to a local subfoveal scleral thickening and a central serous chorioretinopathy-like mechanism, wherein locally confined subfoveal choroidal thickening can further enhance slow fluid leakage across the RPE [16]. In our series, although 24% of eyes showed choroidal thickness greater than 350 μm, only 2 of these eyes had SRF at baseline; hence, it would be difficult for us to exactly establish the relationship between SRF and choroidal thickness.

The various treatment approaches pursued to resolve DSM-related SRF with variable results include observation, anti-VEGF, photodynamic therapy, subthreshold micropulse laser, and mineralocorticoid receptor antagonists [11, 19, 21, 35–37]. A combined treatment approach has been proposed to target both choroidal and RPE dysfunction using half-fluence and half-dose PDT followed by subthreshold 577 nm micropulse laser therapy, wherein SRF diminished in all cases and had completely resolved in 45.4% of the eyes at 6 months [38]. In our series, 5/6 eyes with SRF were given some form of treatment; however, SRF still persisted at the final follow-up of 3 months.

Interestingly, our results also suggest that SRF is not likely to influence visual acuity. There have been contrasting reports regarding outcome of SRF on visual acuity [11, 20, 21, 29, 31, 32, 34, 36, 39, 40]. It has been postulated that shallow serous retinal detachments in DSM eyes might aid sustenance of photoreceptors by ensuring adequate oxygen and nutrient diffusion from the choriocapillaris to the photoreceptors [36]. When the presence of SRF did not significantly impact the vision compared to eyes without SRF in our series, any attempt to reduce SRF by treatment can be questionable. However, only longer periods of follow-up may confirm these findings in a real-world scenario.

5. Conclusions

In summary, dome-shaped maculopathy in Indian population may be seen in eyes with relatively less myopia than

seen globally. Optical coherence tomography helps us in not only characterizing DSM but also in identifying specific features which may be associated with the prognosis of these eyes like the dome height. Choroidal thickening may play a role in development of DSM and may also be related to development of subretinal fluid in such eyes.

Data Availability

The data used to support the findings of this study are available from Dr. Sagnik Sen and Dr. Prithviraj Udaya upon request.

Conflicts of Interest

The authors declare that they have no conflicts of interest.

References

[1] I. G. Morgan, K. Ohno-Matsui, and S.-M. Saw, "Myopia," *The Lancet*, vol. 379, no. 9827, pp. 1739–1748, 2012.

[2] S. Resnikoff, D. Pascolini, S. P. Mariotti, and G. P. Pokharel, "Global magnitude of visual impairment caused by uncorrected refractive errors in 2004," *Bulletin of the World Health Organization*, vol. 86, no. 1, pp. 63–70, 2008.

[3] H. Matsumura and H. Hirai, "Prevalence of myopia and refractive changes in students from 3 to 17 years of age," *Survey of Ophthalmology*, vol. 44, pp. S109–S115, 1999.

[4] K.-C. Yoon, G.-H. Mun, S.-D. Kim et al., "Prevalence of eye diseases in South Korea: data from the Korea national health and nutrition examination survey 2008-2009," *Korean Journal of Ophthalmology*, vol. 25, no. 6, pp. 421–433, 2011.

[5] D. S. P. Fan, D. S. C. Lam, R. F. Lam et al., "Prevalence, incidence, and progression of myopia of school children in Hong Kong," *Investigative Opthalmology & Visual Science*, vol. 45, no. 4, pp. 1071–1075, 2004.

[6] L. L. Lin, Y. F. Shih, C. K. Hsiao, and C. J. Chen, "Prevalence of myopia in Taiwanese schoolchildren: 1983 to 2000," *Annals of the Academy of Medicine Singapore*, vol. 33, no. 1, pp. 27–33, 2004.

[7] G. V. Murthy, S. K. Gupta, L. B Ellwein et al., "Refractive error in children in an urban population in New Delhi," *Investigative Ophthalmology & Visual Science*, vol. 43, no. 3, pp. 623–631, 2002.

[8] S. Ghosh, U. Mukhopadhyay, D. Maji, and G. Bhaduri, "Visual impairment in urban school children of low-income families in Kolkata, India," *Indian Journal of Public Health*, vol. 56, no. 2, pp. 163–167, 2012.

[9] R. Saxena, P. Vashist, R. Tandon et al., "Prevalence of myopia and its risk factors in urban school children in Delhi: the North India myopia study (NIM Study)," *PLoS ONE*, vol. 10, no. 2, Article ID e0117349, 2015.

[10] D. Gaucher, A. Erginay, A. Lecleire-Collet et al., "Dome-shaped macula in eyes with myopic posterior staphyloma," *American Journal of Ophthalmology*, vol. 145, no. 5, pp. 909–914, 2008.

[11] D. Lorenzo, L. Arias, N. Choudhry et al., "Dome-shaped macula in myopic eyes," *Retina*, vol. 37, no. 4, pp. 680–686, 2017.

[12] J. Fajardo Sánchez, C. E. Chau Ramos, J. A. Roca Fernández, and J. L. Urcelay Segura, "Clinical, fundoscopic, tomographic and angiographic characteristics of dome shaped macula classified by bulge height," *Archivos de la Sociedad Española de Oftalmología (English Edition)*, vol. 92, no. 10, pp. 458–463, 2017 Oct.

[13] I.-C. Liang, N. Shimada, Y. Tanaka et al., "Comparison of clinical features in highly myopic eyes with and without a dome-shaped macula," *Ophthalmology*, vol. 122, no. 8, pp. 1591–1600, 2015.

[14] M. Hocaoglu, M. G. Ersoz, I. Sayman Muslubas, S. Arf, and M. Karacorlu, "Factors associated with macular complications in highly myopic eyes with dome-shaped macular configuration," *Graefe's Archive for Clinical and Experimental Ophthalmology*, vol. 257, no. 11, pp. 2357–2365, 2019.

[15] A. Chebil, B. Ben Achour, N. Chaker, L. Jedidi, F. Mghaieth, and L. El Matri, "Épaisseur choroïdienne fovéolaire au SD-OCT dans la myopie forte avec macula bombée," *Journal Français d'Ophtalmologie*, vol. 37, no. 3, pp. 237–241, 2014.

[16] Y. Imamura, T. Iida, I. Maruko, S. A. Zweifel, and R. F. Spaide, "Enhanced depth imaging optical coherence tomography of the sclera in dome-shaped macula," *American Journal of Ophthalmology*, vol. 151, no. 2, pp. 297–302, 2011.

[17] A. C. S. Tan, S. Yzer, K. B. Freund, K. K. Dansingani, N. Phasukkijwatana, and D. Sarraf, "Choroidal changes associated with serous macular detachment in eyes with staphyloma, dome-shaped macula or tilted disk syndrome," *Retina*, vol. 37, no. 8, pp. 1544–1554, 2017.

[18] M.-H. Errera, M. Michaelides, P. A. Keane et al., "The extended clinical phenotype of dome-shaped macula," *Graefe's Archive for Clinical and Experimental Ophthalmology*, vol. 252, no. 3, pp. 499–508, 2014.

[19] T. R. Burke, A. D. Wu, Y. Shen, and R. Rajendram, "Longitudinal follow-up of dome-shaped macula," *Eye*, vol. 34, pp. 1903–1908, 2020.

[20] V. Caillaux, D. Gaucher, V. Gualino, P. Massin, R. Tadayoni, and A. Gaudric, "Morphologic characterization of dome-shaped macula in myopic eyes with serous macular detachment," *American Journal of Ophthalmology*, vol. 156, no. 5, pp. 958–967.e1, 2013.

[21] G. Soudier, A. Gaudric, V. Gualino et al., "Long-term evolution of dome-shaped macula," *Retina*, vol. 36, no. 5, pp. 944–952, 2016.

[22] E. Shin, K.-A. Park, and S. Y. Oh, "Dome-shaped macula in children and adolescents," *PLoS ONE*, vol. 15, no. 1, Article ID e0227292, 2020.

[23] G. W. Lee, J. H. Kim, S. W. Kang et al., "Structural profile of dome-shaped macula in degenerative myopia and its association with macular disorders," *BMC Ophthalmology*, vol. 20, p. 202, 2020.

[24] A. A. Ellabban, A. Tsujikawa, A. Matsumoto et al., "Three-dimensional tomographic features of dome-shaped macula by swept-source optical coherence tomography," *American Journal of Ophthalmology*, vol. 155, no. 2, pp. 320–328, 2013.

[25] Y. Ikuno and Y. Tano, "Retinal and choroidal biometry in highly myopic eyes with spectral-domain optical coherence tomography," *Investigative Opthalmology & Visual Science*, vol. 50, no. 8, pp. 3876–3880, 2009.

[26] H. Ohsugi, Y. Ikuno, K. Oshima, T. Yamauchi, and H. Tabuchi, "Morphologic characteristics of macular complications of a dome-shaped macula determined by swept-source optical coherence tomography," *American Journal of Ophthalmology*, vol. 158, no. 1, pp. 162–170.e1, 2014.

[27] P. A. Keane, A. Mitra, I. J. Khan, F. Quhill, and S. M. Elsherbiny, "Dome-shaped macula: a compensatory mechanism in myopic anisometropia?" *Ophthalmic Surgery, Lasers & Imaging*, vol. 43, pp. e52–e54, 2012.

[28] M. Mehdizadeh and M. H. Nowroozzadeh, "Dome-shaped macula in eyes with myopic posterior staphyloma," *American Journal of Ophthalmology*, vol. 146, no. 3, pp. 478-479, 2008.

[29] A. A. Ellabban, A. Tsujikawa, Y. Muraoka et al., "Dome-shaped macular configuration: longitudinal changes in the sclera and choroid by swept-source optical coherence tomography over two years," *American Journal of Ophthalmology*, vol. 158, no. 5, pp. 1062–1070, 2014.

[30] R. M. Coco, M. R. Sanabria, and J. Alegría, "Pathology associated with optical coherence tomography macular bending due to either dome-shaped macula or inferior staphyloma in myopic patients," *Ophthalmologica*, vol. 228, no. 1, pp. 7–12, 2012.

[31] F. Sanabria, L. Dell'Arti, E. Benatti et al., "Choroidal findings in dome-shaped macula in highly myopic eyes: a longitudinal study," *American Journal of Ophthalmology*, vol. 159, no. 1, pp. 44–52, 2015.

[32] A. García-Ben, M. J. M. Sanchez, A. G. Gómez, I. García-Basterra, A. S. García, and J. M. García-Campos, "Factors associated with serous retinal detachment in highly myopic eyes with vertical oval-shaped dome," *Retina*, vol. 39, no. 3, pp. 587–593, 2019.

[33] L. Ceklic, U. Wolf-Schnurrbusch, M. Gekkieva, and S. Wolf, "Visual acuity outcome in RADIANCE study patients with dome-shaped macular features," *Ophthalmology*, vol. 121, no. 11, pp. 2288-2289, 2014.

[34] E. Pilotto, F. Guidolin, M. Parravano et al., "Morphofunctional evaluation in dome-shaped macula," *Retina*, vol. 38, no. 5, pp. 922–930, 2018.

[35] I. Arapi, P. Neri, C. Mariotti et al., "Considering photodynamic therapy as a therapeutic modality in selected cases of dome-shaped macula complicated by foveal serous retinal detachment," *Ophthalmic Surgery, Lasers and Imaging Retina*, vol. 46, no. 2, pp. 217–223, 2015.

[36] M. Battaglia Parodi, P. Iacono, and F. Bandello, "Subthreshold laser treatment for serous retinal detachment in dome-shaped macula associated with pathologic myopia," *Retina*, vol. 38, no. 2, pp. 359–363, 2018.

[37] A. Dirani, A. Matet, T. Beydoun, F. Behar Cohen, and I. Mantel, "Resolution of foveal detachment in dome-shaped macula after treatment by spironolactone: report of two cases and mini-review of the literature," *Clinical Ophthalmology*, vol. 8, pp. 999–1002, 2014.

[38] V. Pirani, P. Pelliccioni, A. Giovannini, M. Nicolai, C. Cesari, and C. Mariotti, "Photodynamic therapy and subthreshold micropulse laser treatment-a novel combined approach for the treatment of serous retinal detachment in dome-shaped macula," *Photodiagnosis and Photodynamic Therapy*, vol. 31, Article ID 101895, 2020.

[39] A. García-Ben, I. Garcia-Basterra, A. González-Gómez et al., "Comparison of long-term clinical evolution in highly myopic eyes with vertical oval-shaped dome with or without untreated serous retinal detachment," *British Journal of Ophthalmology*, vol. 103, no. 3, pp. 385–389, 2019.

[40] F. Viola, G. Leone, E. Garoli et al., "Long-term natural history of highly myopic eyes with a dome-shaped macula with or without untreated serous retinal detachment: a 4-year follow-up study," *British Journal of Ophthalmology*, 2020.

Research Article

Novel Optical Coherence Tomography Parameters as Prognostic Factors for Stage 3 Epiretinal Membranes

Young Gun Park [ID],[1] **Seo Yeon Hong,**[1] **and Young-Jung Roh**[2]

[1]*Department of Ophthalmology and Visual Science, Seoul St. Mary's Hospital, College of Medicine,*
 The Catholic University of Korea, Seoul, Republic of Korea
[2]*Department of Ophthalmology and Visual Science, Yeoido St. Mary's Hospital, College of Medicine,*
 The Catholic University of Korea, Seoul, Republic of Korea

Correspondence should be addressed to Young Gun Park; cuteyg2000@catholic.ac.kr

Purpose. We aimed to describe the visual prognosis of eyes with ectopic inner foveal layers (EIFLs) after epiretinal membrane (ERM) surgery. *Methods*. This retrospective study enrolled patients diagnosed with stage 3 ERM based on the EIFL staging scheme who underwent ERM surgery with a minimum follow-up period of 12 months. Central foveal thickness (CFT), EIFL thickness, and the length of the ellipsoid zone defect were evaluated at baseline and at 1 month, 6 months, and 12 months after surgery based on pre- and postoperative swept-source optical coherence tomography (OCT) images. The association of EIFL thickness and other OCT parameters with pre- and postoperative best-corrected visual acuity (BCVA) was analyzed. *Results*. Sixty-nine eyes with stage 3 ERMs were analyzed. Preoperative BCVA was correlated with preoperative CFT ($r = 0.517$, $p < 0.001$) and preoperative EIFL thickness ($r = 0.652$, $p < 0.001$). At 12 months, postoperative BCVA was correlated negatively with preoperative CFT ($r = 0.470$, $p = 0.016$) and preoperative EIFL thickness ($r = 0.582$, $p = 0.004$). The improvement in BCVA was not associated with postoperative reduction in CFT ($p = 0.06$), although it was significantly associated with postoperative reduction in EIFL thickness ($r = 0.635$, $p = 0.007$). *Conclusions*. EIFL thickness should be considered a negative prognostic factor for postoperative anatomical and functional recovery in patients with stage 3 ERMs.

1. Introduction

The epiretinal membrane (ERM) is a common macular disorder characterized by fibrocellular proliferation on the inner retinal surface, which causes morphologic distortion and affects central vision [1]. ERM cases that involve decreased or distorted central vision require treatment with surgical procedures such as pars plana vitrectomy with ERM peeling. Microincision vitrectomy has been widely used recently and has shown higher rates of anatomical success [2, 3]. However, these anatomical outcomes do not correspond with better visual prognosis. Visual prognostic factors for ERM surgery, using spectral-domain optical coherence tomography (OCT), have consequently been published [4–7].

Previously published visual prognostic spectral-domain OCT findings regarding ERM surgery may be divided into inner and outer segment factors. The inner segment factor associated with poor visual prognosis after ERM surgery is foveal inner retinal layer thickness [8, 9]; outer segment factors associated with poor visual prognosis include an outer nuclear complex, cone outer segment tip defect length, and ellipsoid zone (EZ) defect length [10, 11].

Govetto et al. [12] recently suggested a new OCT-based grading system to classify ERMs based on the presence of a continuous ectopic inner foveal layer (EIFL) as a new finding in advanced stages (i.e., stages 3 and 4). They also suggested the presence of the "central bouquet" on OCT images that refers to a foveal bulge at the level of the outer retina. Stage 3 was defined as the presence of an ERM with a continuous

EIFL, whereas stage 4 was defined as significant retinal thickening with anatomical disruptions in the macula (Figure 1).

Previous reports have described relative associations between inner retinal thickness, EIFL thickness, and postoperative visual acuity in idiopathic ERMs [13, 14]. However, EIFL thickness measurements in patients with stage 4 ERMs are unreliable because of the remarkable preoperative disruption of the retinal layers. Therefore, we excluded patients with stage 4 ERMs. The aim of the current study was to investigate the relationship between OCT parameters and visual prognosis in stage 3 ERM patients who underwent 25-gauge vitrectomy.

2. Materials and Methods

2.1. Study Design. In this study, we retrospectively reviewed data of consecutive patients who presented to the Department of Ophthalmology of Seoul St. Mary's Hospital, Korea, between January 2018 and January 2019 with a confirmed diagnosis of primary idiopathic stage 3 ERM and were treated with 25-gauge vitrectomy for ERM with indocyanine green- (ICG-) assisted internal limiting membrane peeling by a single surgeon (YGP).

All procedures were conducted according to the tenets of the Declaration of Helsinki and its later amendments. The study was approved by the ethics committee of Seoul St. Mary's Hospital and the Catholic University of Korea. The need to obtain informed patient consent was waived because of the retrospective study design.

Patients who underwent ERM removal surgery for unilateral idiopathic stage 3 ERM and have been followed at least 12 months after surgery were included. Those with stage 4 ERM, secondary or bilateral ERM, and any other ocular disease that could affect visual function (e.g., glaucoma, age-related macular degeneration, and refractive error >5 diopters), severe media opacity (e.g., lens opacity owing to cataract or thick asteroid hyalosis), or those lost to the follow-up after ERM surgery were excluded.

All patients and controls initially underwent measurement of their best-corrected visual acuity (BCVA) using the standard Snellen chart. The results were converted to the logarithm of the minimal angle of resolution (logMAR) values for statistical analysis. The patients then underwent standardized fundus examination, which included measurements using swept-source OCT (DRI OCT Triton; Topcon, Tokyo, Japan). SS-OCT was performed before and at 1, 6, and 12 months after surgery.

2.2. Swept-Source OCT Imaging and OCT Parameters. Swept-source OCT utilizes a wavelength of 1,050 nm and reaches a scanning speed of 100,000 A-scans per second, with 8 μm and 20 μm axial and transverse resolution in tissue [15]. The devices produce OCT B-scan images derived from 512×256 axial scans over a scan area of $12 \times 9 \, \text{mm}^2$. This high-quality fundus imaging technique relies on active eye tracking. Only images with a quality score of more than 60 were included. We used image viewer software (IMAGEnet
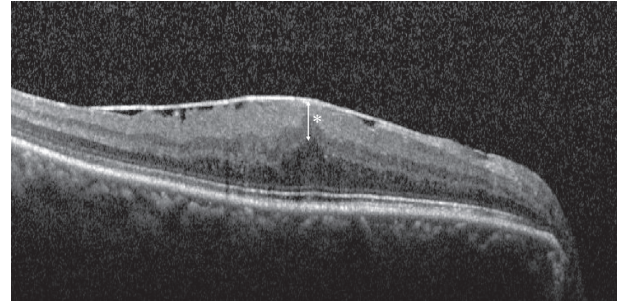

FIGURE 1: An ectopic inner foveal layer (EILF). The EIFL (asterisk) on the optical coherence tomography image indicates the presence of continuous hyporeflective and hyperreflective bands extending from the inner nuclear layer and inner plexiform layer across the foveal region.

6, version 1.24; Topcon), and the thickness was determined by consensus between two observers (YGP and YJR) who were blinded to all clinical information.

OCT parameters included central foveal thickness (CFT), outer nuclear layer thickness (ONL), EIFL thickness, and length of the EZ defect. When the foveal depression was absent, the foveal center was identified by the point of the greatest outer nuclear layer thickness and the bulge-like structure of the IS/OS junction at the fovea. The ONL thickness measured from the inner border of the retinal pigment epithelium to the border of the ONL, and the EIFL thickness, defined as the distance between the inner border of the ONL and the ILM at the foveal center [16]. The EZ defect was considered to be the extent with the loss of the hyperreflective signal that characterizes the layer at the horizontal one passing through the fovea [17]. Previous reports have demonstrated a relationship between vision loss associated with ERM and disruption of the EZ and outer photoreceptor segments [9, 18]. Disruption of the EZ has been widely recognized to be related with visual prognosis in various macular diseases, such as macular holes and edema [19–21]. We therefore measured the length of EZ disruption.

2.3. Surgical Treatment. All surgeries were performed by a single surgeon (YGP). A three-port 25-gauge transconjunctival sutureless vitrectomy was performed to remove the ERM. After vitrectomy, the ERM was removed using end-gripping forceps (Alcon, Fort Worth, TX, USA). After removing the ERM, internal limiting membrane peeling was performed with 0.25% indocyanine green dye. ERM and internal limiting membrane peeling were started at the outer region around the fovea, particularly in the parafoveal area.

2.4. Statistical Analysis. The normal distribution of data was assessed using the Shapiro–Wilk test. For normally distributed data, Pearson's correlation and regression tests were performed. The analysis of variance was performed for each parameter. For nonparametric data, Spearman's rank correlation test was used. All analyses were conducted using SPSS (IBM SPSS Statistics, version 24.0; IBM Corporation, New York, NY, USA). A p value < 0.05 was statistically significant.

TABLE 1: Baseline demographics.

Characteristic	
Number of patients (n)	69
Sex (male : female)	25 : 44
Age (y)	67.78 ± 6.69
Combined cataract surgery	52 (75.4%)
BCVA (logMAR)	0.47 ± 0.16
CFT (μm)	480.08 ± 60.47
ONL thickness (μm)	163.04 ± 46.3
EIFL thickness (μm)	183.41 ± 89.50
Length of the EZ defect (μm)	480.3 ± 162.1
Cotton ball sign	18 (26.1%)

BCVA, best-corrected visual acuity; CFT, central foveal thickness; ONL, outer nuclear layer thickness; EIFL, ectopic inner foveal layer; EZ, ellipsoid zone.

3. Results

We reviewed clinical records of 69 patients diagnosed with stage 3 ERMs; the patients comprised 25 (36.2%) men and 44 (63.8%) women. The mean age of the patients was 67.78 ± 6.69 years; 52 of 69 eyes (75.4%) exhibited mild cataract (2.06 ± 0.64 using the lens opacity classification (LOCS III) scale) [22] and underwent combined phacoemulsification. The mean preoperative BCVA was 0.47 ± 0.16 logMAR, and the mean CFT was $480.08 \pm 60.47\,\mu$m. The mean EIFL thickness was $183.41 \pm 89.50\,\mu$m, and the mean ONL was $163.04 \pm 46.3\,\mu$m; the mean EZ defect length was $480.3 \pm 162.1\,\mu$m. Baseline characteristics of the patients at presentation are summarized in Table 1.

3.1. Preoperative Visual Acuity and OCT Parameters.

The preoperative BCVA correlated with preoperative CFT ($r = 0.517$, $p < 0.001$) and preoperative EIFL thickness ($r = 0.652$, $p < 0.001$). The preoperative CFT was relatively strongly correlated with preoperative EIFL thickness ($r = 0.54$, $p = 0.001$). Thus, these variables shared an effect on BCVA. On multiple regression analysis, only EIFL thickness ($p < 0.001$) was significantly associated with worse preoperative BCVA.

3.2. Postoperative Visual Acuity and OCT Parameters.

The mean preoperative and postoperative BCVA at 1, 6, and 12 months are listed in Table 2. The CFT and EIFL thickness also significantly decreased at 1, 6, and 12 months postoperatively, as shown in Table 2. However, the ONL thickness and length of the EZ defect did not show a significant difference (all, $p > 0.05$).

Postoperative changes in EIFL thickness and CFT were greatest in the first month after surgery, and the postoperative BCVA continued to improve slightly until 12 months postoperatively (Figure 2). The postoperative BCVA improved gradually until the end of the follow-up period (Figures 3 and 4). At 12 months, the postoperative BCVA correlated negatively with the preoperative CFT ($r = 0.470$, $p = 0.016$) and preoperative EIFL thickness ($r = 0.582$, $p = 0.004$). However, the ONL thickness and length of the

EZ defect showed no significant difference (all, $p > 0.05$) (Figure 4).

To identify OCT parameters whose improvement after ERM surgery was associated with visual improvement, a correlation analysis was conducted between the amount of postoperative BCVA improvement and changes in OCT parameters. BCVA improvement was not associated with postoperative CFT reduction ($p = 0.06$), although it was significantly associated with a postoperative decrease in EIFL thickness ($r = 0.635$, $p = 0.007$).

At 12 months after surgery, the EIFL persisted postoperatively in most patients and was present in 54 (78.3%) of 69 eyes. Cotton ball signs existed in 18 (26.1%) of 69 eyes at baseline; however, all of these signs disappeared during the postoperative follow-up period. No serious intra- or postoperative complications were recorded during the follow-up period.

4. Discussion

ERM is one of the most common macular diseases, and its prevalence tends to increase with age [23, 24]. Patients with ERM may experience problems such as metamorphopsia and decreased visual acuity. To resolve these symptoms, surgical removal of ERM is recommended as standard treatment [25]. However, the desired visual outcomes are not always achieved, even with apparently successful ERM removal. Clinicians need to measure the severity of ERM and predict parameters for visual prognosis.

Recent advancements in OCT have led to a greater interest in assessing retinal microstructures using this technology. Therefore, the identification of reliable prognostic biomarkers with OCT is important for improving prediction of postoperative outcomes in patients with idiopathic ERMs. Many published spectral-domain OCT studies have demonstrated a relationship between retinal microstructural alterations such as the disruption of EZ or outer photoreceptor segments and vision loss in ERMs [13, 26–28].

The role of the inner retina in visual acuity loss has been studied more closely. Govetto et al. [12] suggested a new OCT-based grading system to classify ERMs, with advanced ERMs showing the presence of a preoperative continuous EIFL. As the ERM stage increases, the progression of this anatomical finding correlates with decreased visual acuity [29]. This factor may also be associated with visual acuity in patients with idiopathic ERM formation. Our study focused on stage 3 ERM to ascertain the influence of EIFL. Patients with stage 4 ERM had an extensive EIFL that covered the entire foveal area. Their retinal layers were noted to be significantly distorted and disorganized and were not clearly identified with OCT. Therefore, we excluded patients with stage 4 ERM and only included cases with stage 3 severity.

Preoperative BCVA correlated with preoperative CFT and preoperative EIFL thickness. However, the preoperative CFT was relatively strongly correlated with preoperative EIFL thickness. These variables shared an effect on BCVA; it may be explained by the fact that the EIFL is a key factor underlying increased CFT. The primary finding of this study

TABLE 2: Comparison of preoperative and postoperative BCVA, CFT, and the thickness of EIFL in patients with idiopathic epiretinal membranes.

Time point	BCVA (logMAR)		CFT (μm)		The thickness of EIFL (μm)	
	Mean ± SD	p value[a]	Mean ± SD	p value[a]	Mean ± SD	$p$value[a]
Preoperative	0.47 ± 0.16		480.08 ± 60.47		183.41 ± 89.5	
Post-1M	0.38 ± 0.18	0.008*	384.03 ± 41.55	<0.001*	104.18 ± 46.13	0.012*
Post-6M	0.25 ± 0.14	0.001*	360.03 ± 44.84	<0.001*	93.25 ± 27.1	0.028*
Post-12M	0.20 ± 0.13	<0.001*	342.63 ± 42.46	<0.001*	80.5 ± 37.3	0.003*

[a]P value vs. preoperative; BCVA, best-corrected visual acuity; CFT, central foveal thickness; EIFL, ectopic inner foveal layer.

(a)

(b)

(c)
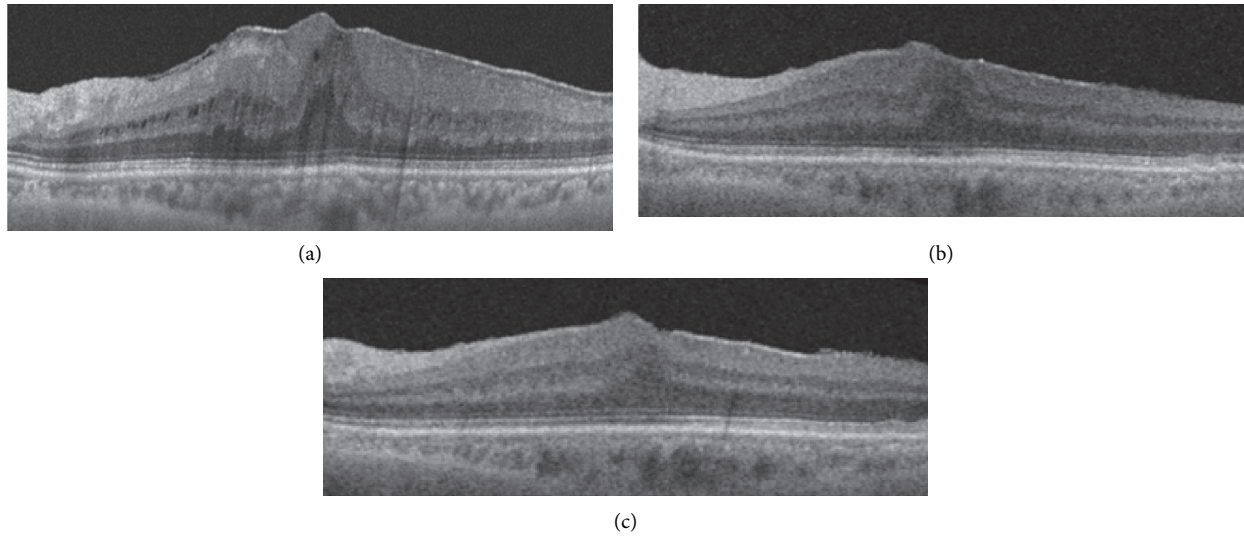
FIGURE 2: Optical coherence tomography images from a patient diagnosed with an epiretinal membrane (ERM). (a) Stage 3 ERM was diagnosed based on swept-source optical coherence tomography findings: the central fovea contains continuous ectopic inner foveal layers (EIFLs). (b) At 1 month after surgery, a thick EIFL persists over the outer nuclear layer. (c) At 12 months after surgery, the EIFL persists, although significant thinning has occurred. Visual acuity changed from 0.39 logMAR to 0.1 logMAR at 12 months after ERM surgery.

(a)

(b)

(c)
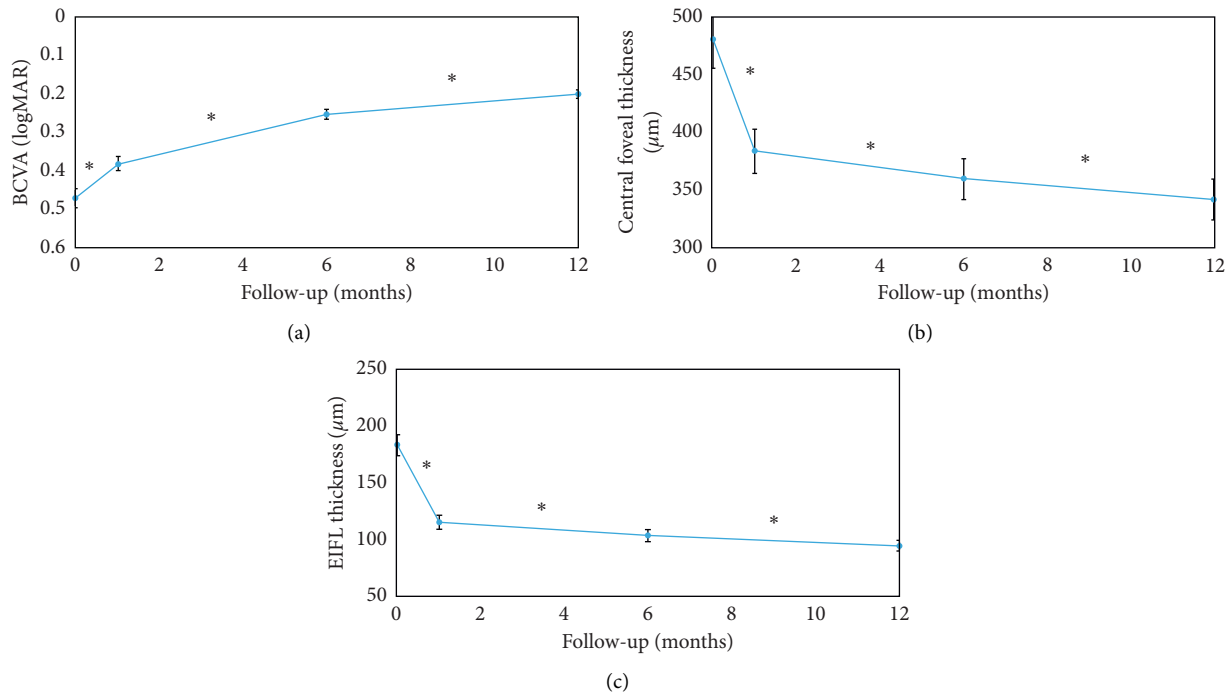
FIGURE 3: Functional and anatomical changes occurring from baseline to the 12 months postoperatively. (a) The best-corrected visual acuity (BCVA) significantly improved in the postoperative follow-up period ($p < 0.001$). (b) In the follow-up period, the central foveal thickness (CFT) decreased significantly with a noticeable effect at 1 month after surgery ($p = 0.001$). (c) Similar to the CFT, the thickness of the ectopic inner foveal layers (EIFLs) decreased significantly with a prominent effect in the first month after surgery ($p = 0.003$).

(a)

(b)
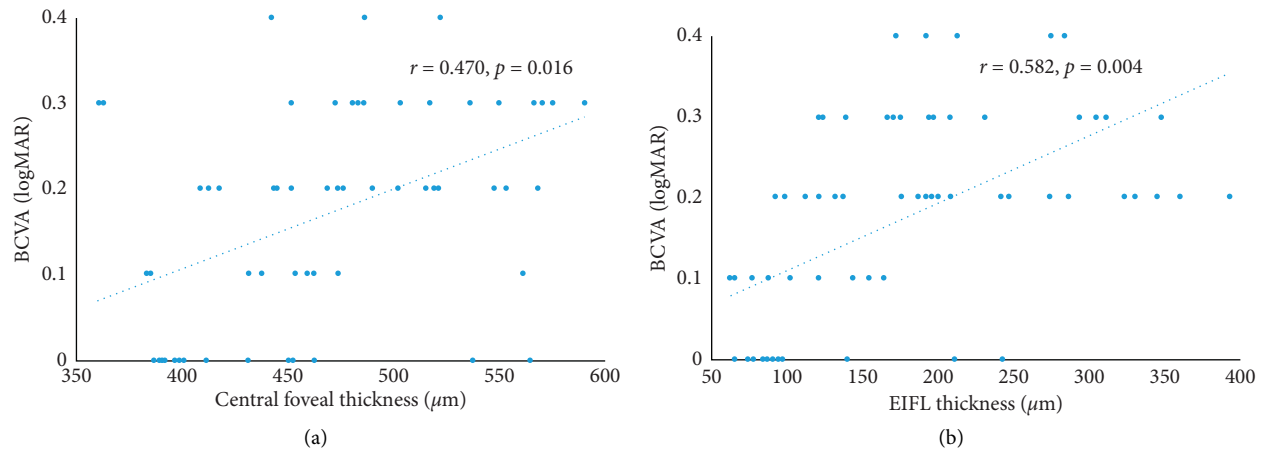
FIGURE 4: a, b Correlation analysis between postoperative best-corrected visual acuity (BCVA) and the central foveal thickness (CFT) and ectopic inner foveal layer (EIFL) thickness at 12 months after surgery. Optical coherence tomography parameters are significantly associated with postoperative BCVA (CFT: r = 0.470 and $p = 0.016$; EIFL: r = 0.582 and $p = 0.004$). logMAR, logarithm of the minimum angle of resolution.

was that preoperative CFT thickness and EIFL thickness were significantly associated with poor postoperative visual prognosis in patients with stage 3 ERM. In addition, only preoperative EIFL thickness was significantly associated with BCVA improvement. Thus, inner retinal OCT findings associated with EIFL thickness were more significantly associated with visual prognosis after ERM surgery.

Alkabes et al. [30] demonstrated that EIFL thickness and CFT correlated significantly with metamorphopsia, demonstrated by M-CHARTS in the advanced stages of ERM (stages 3 and 4) based on the OCT-based grading scheme [12] which included a new OCT parameter such as EIFL (both $p < 0.0001$). They only included 37 eyes with advanced ERMs; however, the results indicated that EIFL thickness could be a good indicator for metamorphopsia. Gonzalez-Saldivar et al. [16] used the EIFL staging scheme as a visual prognostic factor and assessed final BCVA based on the stages. They found that earlier stages were associated with better visual outcomes preoperatively and postoperatively in patients undergoing ERM surgery (stage 2 > stage 3 > stage 4, $p < 0.001$). They also noted that surgery in patients with stage 2 ERM results in significantly better visual outcomes. In our study, we also noted that the thickness of the preoperative EIFL was negatively associated with postoperative BCVA.

ERM is an inner retinal disease, and OCT findings showing improvement after surgery are mostly observed in the inner retina. Several recent studies have evaluated inner rather than external retinal biomarkers as prognostic factors for ERM surgery [8, 31–33]. In our study, as an outer biomarker, EZ disruption was not significantly correlated with poor visual prognostic factors. Conversely, the EIFL thickness of the inner retinal OCT parameters was more significantly associated with the visual prognosis of ERM surgery in patients with advanced ERM stages. The EIFL thickness, which is based on OCT images, is a more practical and reproducible tool for obtaining visual prognosis in patients with ERM. Therefore, it is essential that EIFL formation is taken into consideration during decision-making for ERM surgery.

This study had some limitations. First, data collection was performed retrospectively by reviewing medical records. Second, we used a relatively small sample and included patients with and without a history of cataract surgery. Third, VA values may be affected by different degrees of lens opacity. Fourth, OCT images were analyzed by a skilled retinal specialist; however, the use of manual measurements instead of automatically provided absolute values, which could have introduced bias. Finally, we used ICG dye for staining during internal limiting membrane peeling. ICG dye is associated with retinal toxicity; therefore, we attempted to reduce the exposure time to a relatively short duration.

5. Conclusions

We observed that the postoperative visual outcome of eyes with stage 3 ERM significantly correlated with preoperative EIFL thickness and CFT at baseline. Moreover, the length of the EZ defect at baseline did not significantly correlate with postoperative visual acuity. These findings may help retinal surgeons determine the surgical indications and optimal timing for surgical treatments. Further clinical studies are required to validate the findings of this study.

Data Availability

The data used to support the findings of this study are available from the corresponding author upon request.

Conflicts of Interest

The authors declare that they have no conflicts of interest.

Acknowledgments

References

[1] Y. Nishi, H. Shinoda, A. Uchida et al., "Detection of early visual impairment in patients with epiretinal membrane," *Acta Ophthalmologica*, vol. 91, no. 5, pp. e353–e357, 2013.

[2] E. Moisseiev, M. Kinori, I. Moroz, E. Priel, and J. Moisseiev, "25-Gauge vitrectomy with epiretinal membrane and internal limiting membrane peeling in eyes with very good visual acuity," *Current Eye Research*, vol. 41, no. 10, pp. 1387–1392, 2016.

[3] S. Naruse, H. Shimada, and R. Mori, "27-gauge and 25-gauge vitrectomy day surgery for idiopathic epiretinal membrane," *BMC Ophthalmol*, vol. 17, no. 1, p. 188, 2017.

[4] K. G. Laban, L. M. E. Scheerlinck, and R. Van Leeuwen, "Prognostic factors associated with visual outcome after pars plana vitrectomy with internal limiting membrane peeling for idiopathic epiretinal membrane," *Ophthalmologica*, vol. 234, no. 3, pp. 119–126, 2015.

[5] H. M. Kang, H. J. Koh, and S. C. Lee, "Visual outcome and prognostic factors after surgery for a secondary epiretinal membrane associated with branch retinal vein occlusion," *Graefe's Archive for Clinical and Experimental Ophthalmology*, vol. 253, no. 4, pp. 543–550, 2015.

[6] S. J. Song, A. E. Kuriyan, and W. E. Smiddy, "Results and prognostic factors for visual improvement after pars plana vitrectomy for idiopathic epiretinal membrane," *Retina*, vol. 35, no. 5, pp. 866–872, 2015.

[7] M. Takabatake, T. Higashide, S. Udagawa, and K. Sugiyama, "Postoperative changes and prognostic factors of visual acuity, metamorphopsia, and aniseikonia after vitrectomy for epiretinal membrane," *Retina*, vol. 38, no. 11, pp. 2118–2127, 2018.

[8] S. G. Joe, K. S. Lee, J. Y. Lee, J.-U. Hwang, J.-G. Kim, and Y. H. Yoon, "Inner retinal layer thickness is the major determinant of visual acuity in patients with idiopathic epiretinal membrane," *Acta Ophthalmologica*, vol. 91, no. 3, pp. e242–e243, 2013.

[9] H. S. Yang, J. T. Kim, S. G. Joe, J. Y. Lee, and Y. H. Yoon, "Postoperative restoration of foveal inner retinal configuration in patients with epiretinal membrane and abnormally thick inner retina," *Retina*, vol. 35, no. 1, pp. 111–119, 2015.

[10] M. Inoue, S. Morita, Y. Watanabe et al., "Inner segment/outer segment junction assessed by spectral-domain optical coherence tomography in patients with idiopathic epiretinal membrane," *American Journal of Ophthalmology*, vol. 150, no. 6, pp. 834–839, 2010.

[11] M. Shimozono, A. Oishi, M. Hata et al., "The significance of cone outer segment tips as a prognostic factor in epiretinal membrane surgery," *American Journal of Ophthalmology*, vol. 153, no. 4, pp. 698–704.e691, 2012.

[12] A. Govetto, R. A. Lalane, D. Sarraf, M. S. Figueroa, and J. P. Hubschman, "Insights into epiretinal membranes: presence of ectopic inner foveal layers and a new optical coherence tomography staging scheme," *American Journal of Ophthalmology*, vol. 175, pp. 99–113, 2017.

[13] E. K. Lee and H. G. Yu, "Ganglion cell-inner plexiform layer thickness after epiretinal membrane surgery," *Ophthalmology*, vol. 121, no. 8, pp. 1579–1587, 2014.

[14] A. Govetto, G. Virgili, F. J. Rodriguez, M. S. Figueroa, D. Sarraf, and J. P. Hubschman, "Functional and anatomical significance of the ectopic inner foveal layers in eyes with idiopathic epiretinal membranes," *Retina*, vol. 39, no. 2, pp. 347–357, 2019.

[15] S. Copete, I. Flores-Moreno, J. A. Montero, J. S. Duker, and J. M. Ruiz-Moreno, "Direct comparison of spectral-domain and swept-source OCT in the measurement of choroidal thickness in normal eyes," *British Journal of Ophthalmology*, vol. 98, no. 3, pp. 334–338, 2014.

[16] G. González-Saldivar, A. Berger, D. Wong, V. Juncal, and D. R. Chow, "Ectopic inner foveal layer classification scheme predicts visual outcomes after epiretinal membrane surgery," *Retina*, vol. 40, no. 4, pp. 710–717, 2020.

[17] W. J. Mayer, C. Fazekas, R. Schumann et al., "Functional and morphological correlations before and after video-documented 23-gauge pars plana vitrectomy with membrane and ILM peeling in patients with macular pucker," *Journal of Ophthalmol*, vol. 2015, Article ID 297239, 7 pages, 2015.

[18] S. Ozdek, E. Ozdemir Zeydanli, L. Karabas et al., "Relation of anatomy with function following the surgical treatment of idiopathic epiretinal membrane: a multicenter retrospective study," *Graefe's Archive Clinical Experimental Ophthalmology*, 2020.

[19] Y.-C. Chang, W.-N. Lin, K.-J. Chen et al., "Correlation between the dynamic postoperative visual outcome and the restoration of foveal microstructures after macular hole surgery," *American Journal of Ophthalmology*, vol. 160, no. 1, pp. 100–106, 2015.

[20] N. M. Samy El Gendy, "Outer retinal healing after internal limiting membrane peeling in diabetic macular oedema with vitreomacular interface abnormality using three different dyes," *Semin in Ophthalmology*, vol. 34, no. 7-8, pp. 504–510, 2019.

[21] E. W. Chan, M. Eldeeb, V. Sun et al., "Disorganization of retinal inner layers and ellipsoid zone disruption predict visual outcomes in central retinal vein occlusion," *Ophthalmology Retina*, vol. 3, no. 1, pp. 83–92, 2019.

[22] L. T. Chylack Jr, J. K. Wolfe, D. M. Singer et al., "The lens opacities classification system III," *Archives of Ophthalmology*, vol. 111, no. 6, pp. 831–836, 1993.

[23] J. H. Kim, Y. M. Kim, E. J. Chung, S. Y. Lee, and H. J. Koh, "Structural and functional predictors of visual outcome of epiretinal membrane surgery," *American Journal of Ophthalmology*, vol. 153, no. 1, pp. 103–110, 2012.

[24] M. Rispoli, J.-F. Le Rouic, G. Lesnoni, L. Colecchio, S. Catalano, and B. Lumbroso, "Retinal surface en face optical coherence tomography," *Retina*, vol. 32, no. 10, pp. 2070–2076, 2012.

[25] E. Moisseiev, Z. Davidovitch, M. Kinori, A. Loewenstein, J. Moisseiev, and A. Barak, "Vitrectomy for idiopathic epiretinal membrane in elderly patients: surgical outcomes and visual prognosis," *Current Eye Research*, vol. 37, no. 1, pp. 50–54, 2012.

[26] G. Mylonas, M. Schranz, M. Georgopoulos et al., "Are there funduscopic and optical coherence tomography preoperative characteristics to predict surgical difficulty of epiretinal membrane removal?" *Current Eye Research*, vol. 45, pp. 1012–1016, 2020.

[27] Ü. Yolcu and F. C. Gundogan, "Is it possible to predict the postoperative visual outcome before epiretinal membrane removal?" *Canadian Journal of Ophthalmology*, vol. 50, no. 2, p. 180, 2015.

[28] S. W. Park, I. S. Byon, H. Y. Kim, J. E. Lee, and B. S. Oum, "Analysis of the ganglion cell layer and photoreceptor layer using optical coherence tomography after idiopathic epiretinal membrane surgery," *Graefe's Archive for Clinical and Experimental Ophthalmology*, vol. 253, no. 2, pp. 207–214, 2015.

[29] S. Doguizi, M. A. Sekeroglu, D. Ozkoyuncu, A. E. Omay, and P. Yilmazbas, "Clinical significance of ectopic inner foveal layers in patients with idiopathic epiretinal membranes," *Eye*, vol. 32, no. 10, pp. 1652–1660, 2018.

[30] M. Alkabes, P. Fogagnolo, S. Vujosevic, L. Rossetti, G. Casini, and S. De Cilla, "Correlation between new OCT parameters and metamorphopsia in advanced stages of epiretinal membranes," *Acta Ophthalmologica*, vol. 98, no. 8, pp. 780–786, 2020.

[31] K. H. Cho, S. J. Park, J. H. Cho, S. J. Woo, and K. H. Park, "Inner-retinal irregularity index predicts postoperative visual prognosis in idiopathic epiretinal membrane," *American Journal of Ophthalmology*, vol. 168, pp. 139–149, 2016.

[32] J.-U. Hwang, J. Sohn, B. G. Moon et al., "Assessment of macular function for idiopathic epiretinal membranes classified by spectral-domain optical coherence tomography," *Investigative Opthalmology & Visual Science*, vol. 53, no. 7, pp. 3562–3569, 2012.

[33] S. Jeon, B. Jung, and W. K. Lee, "Long-term prognostic factors for visual improvement after epiretinal membrane removal," *Retina*, vol. 39, no. 9, pp. 1786–1793, 2019.

Research Article

Choroidal Structural Changes Assessed with Swept-Source Optical Coherence Tomography after Cataract Surgery in Eyes with Diabetic Retinopathy

Huiping Yao [ID],[1,2] **Sha Gao,**[1,2] **Xiaoqing Liu,**[1,2] **Yufeng Zhou,**[1] **Yu Cheng** [ID],[1,2] **and Xi Shen** [ID][1]

[1]*Department of Ophthalmology, Ruijin Hospital, Shanghai Jiao Tong University School of Medicine, Shanghai 200025, China*
[2]*Department of Ophthalmology, Ruijin Hospital North, Shanghai Jiao Tong University School of Medicine,*
Shanghai 201801, China

Correspondence should be addressed to Yu Cheng; wangchengyuyi@hotmail.com
and Xi Shen; carl_shen2005@126.com

Objective. To determine the influence of phacoemulsification on choroidal vasculature in patients with diabetic retinopathy (DR) undergoing cataract surgery using swept-source optical coherence tomography (SS-OCT). *Methods.* The study was conducted in 23 eyes of 23 cataract patients with mild/moderate nonproliferative diabetic retinopathy (NPDR) without diabetic macular edema (DME) and 23 age-matched controls. Choroidal thickness (CT) and choroidal vascularity index (CVI) were measured at baseline and 1 week, 1 month, and 3 months after surgery. *Results.* The baseline CVI in the DR group was significantly lower than that in the control group ($P = 0.001$). CVI in DR patients after surgery significantly increased compared with preoperative values (all $P < 0.001$ for 1 week, 1 month, and 3 months after surgery). Postoperative increase of CVI and CT in the DR group was more than in the control group, and the difference was significant 1 month and 3 months after surgery (all $P < 0.05$). *Conclusion.* Patients with mild/moderate NPDR have reduced CVI compared with nondiabetic patients at baseline; diabetic cataract surgery tended to induce more increase in CVI and CT as compared with nondiabetic patients. This trial is registered with NCT04499768.

1. Introduction

Diabetes is considered to be a risk factor of cataract incidence and development; diabetic patients usually develop cataracts earlier [1]. Cataract extraction using phacoemulsification usually results in remarkable visual acuity outcomes and is one of the most common and safe ophthalmic surgical procedures. However, diabetic cataract surgery sometimes could be complicated by macular edema, and progression of diabetic retinopathy [2, 3], and these complications also lead to poor visual acuity recovery, so the right timing of cataract surgery of diabetic patients should be considered.

The choroid is one region with high blood circulation ratio, predominantly composed of blood vessels and surrounding stromal tissue. Choroid is the major blood supply to the retina, supplying nutrients and oxygen to the retina. Thus, choroid with normal structure and function is important for maintaining normal retinal physiology [4, 5]. Diabetic choroidopathy (DC) was firstly reported by Hidayat and Fine, and it was reported that there existed arteriosclerotic choroidal arteries, luminal narrowing, basement membranes thickening, and choriocapillaris dropout in DC [6]. It was pointed out that DC may play a role in the pathology of DR [6, 7].

With the advent of optical coherence tomography (OCT) technology, choroidal thickness (CT) was widely measured and it was noted that most patients with senile cataract were expected to maintain increased choroid

thickness at least for several months after cataract surgery [8–10]. Recently, CVI is used to distinguish lumens of choroidal vasculature from surrounding stroma and has been proposed as a marker for vascular health of choroid [11–15]. Choroidal vasculature might be involved in the diabetic eyes and change with duration of diabetes, and a reduced CVI has been recently noted in DR [13, 16]. But the influence of the cataract surgery on the choroidal vascular structures in DR patients is not clear.

The new generation swept-source optical coherence tomography (SS-OCT) system penetrates deeper into the tissue and provides high-resolution images, so it is thought to have advantages for the assessment of the choroid [17, 18]. In this study, we aimed to determine the influence of phacoemulsification on choroidal vascular structures in patients with DR undergoing cataract surgery through the follow-up values of CT and CVI using this SS-OCT system.

2. Methods

2.1. Study Subjects. This study included 23 eyes of 23 cataract patients with mild/moderate NPDR without DME, and 23 age-matched nondiabetic patients were also enrolled in this study. All individuals underwent comprehensive ophthalmologic examination, including a dilated fundal examination, measurements of IOP, best-corrected visual acuity (BCVA), axial length (AL), and SS-OCT. IOP was measured using noncontact tonometry (TX-20, Canon, Japan) at all visits; BCVA was measured using a standard logarithmic visual acuity chart to calculate the logarithm of reciprocal decimal visual acuity (logMAR VA) at baseline and 3 months after surgery; AL was measured using ocular biometry (LenStar LS-900, Haag-Streit AG, Switzerland) at baseline; and SS-OCT was measured at all visits. The stage of NPDR was graded based on the international clinical disease severity scale for DR [19]. All cataract patients undergoing uncomplicated phacoemulsification surgery were recruited consecutively (from June 2018 to June 2019) from the Ophthalmology Department of Ruijin Hospital North and signed the consent forms. The study was adhered to the provisions of the Declaration of Helsinki and was approved by the Ethical Review Committee of Ruijin Hospital North. If both eyes of one patient were operated, only the eye which was operated on first was enrolled.

The inclusion criteria were as follows: aged >40 years, intraocular pressure (IOP) < 21 mmHg in both eyes, and spherical refractive error <6 diopters spherical equivalent. The exclusion criteria were as follows: previous retinal surgery, glaucoma, uveitis, age-related macular degeneration, arterial or vein occlusions, macular hole, or other ocular diseases that could interfere the CT and/or CVI measurement, severe systemic diseases, such as leukemia, rheumatic disease, malignant tumors, uncontrolled hypertension, obstructive sleep apnea, etc., and decreased media transparency precluding appropriate OCT imaging.

2.2. Cataract Surgery. The phacoemulsification cataract surgeries were performed by the same skilled surgeon using the Infinity Vision System (Alcon Laboratories, Inc.). None of the patients had operative complications. All patients had hydrophilic acrylic intraocular lens (Softec HD, Lenstec, Inc. USA) implanted into their capsular bags and had one month of topical steroids. The cumulative dissipated energy (CDE) was documented. Postoperative treatment consisted of tobramycin dexamethasone eyedrops administered 4 times a day for 1 week and then prednisolone acetate 1.0% and levofloxacin 0.5% eyedrops administered 3 times a day for 3 weeks.

2.3. SS-OCT Data Acquisition. All study subjects were imaged using the SS-OCT (Triton DRI-OCT, Topcon, Inc, Tokyo, Japan) preoperatively and at 1 week (W1), 1 month (M1), and 3 months (M3) postoperatively, and the OCT scans were tracked at all follow-up visits. All images were acquired in the morning considering the diurnal variation of choroid vasculature. Images with a signal strength index of more than 40 and no residual motion artifacts were saved for further analysis. CT was defined as the distance between the outer boundary of retinal pigment epithelium/Bruch's membrane and the chorioscleral interface, and the CT values were obtained with the built-in software of the SS-OCT device (Topcon FastMap, version 10.13.003.06). The foveal CT was defined as the CT value in the center circle in the standard ETDRS grid; the parafoveal CT was defined as the arithmetic average value of CT in subregions in the annulus with an outer diameter of 3.0 mm and an inner diameter of 1.0 mm in the standard ETDRS grid; the perifoveal CT was defined as the arithmetic average value of CT in subregions in the annulus with an outer diameter of 6.0 mm and an inner diameter of 3.0 mm in the standard ETDRS grid.

2.4. Procedures of Image Binarization. CVI was acquired through the method described as follows. Images were analyzed by one public domain software, Image J (version 1.52a, provided in the public domain by the National Institutes of Health, Bethesda, MD, USA; http://imagej.nih.gov/ij/), using the protocol as previously described with modifications [11, 12, 20]. Briefly, 9 mm scan images passing through the fovea horizontally were chosen. The region of interest (ROI) was manually selected using the polygon tool and added to the ROI manager. The images were adjusted by the Niblack auto local threshold. The binarized image was converted to the RGB image, and the luminal area was determined using the threshold tool. The dark pixels represented the luminal or vascular area, and the light pixels were defined as stromal or interstitial area (Figure 1). CVI was defined as the proportion of vascular area to total circumscribed area.

2.5. Inter-Rater and Intra-Rater Agreement. Two independent graders masked from patient information initially segmented 46 images from all the subjects. The same images were segmented by one of the above two graders after an interval of one week to determine intra-rater reliability. The inter-rater reliability and intra-rater reliability for image
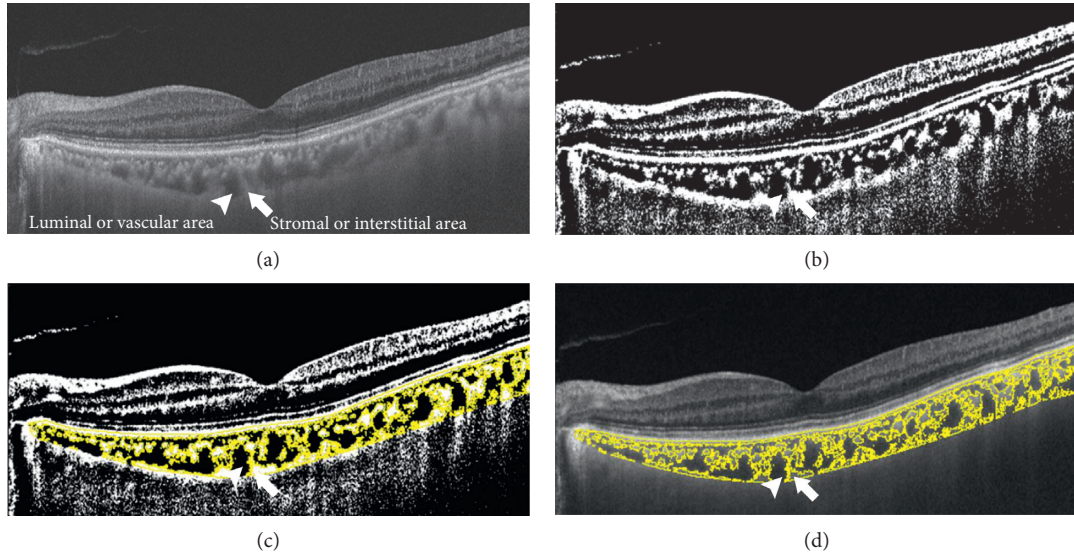
(a)

(b)

(c)

(d)

FIGURE 1: The dark pixels (arrow head) represented the luminal or vascular area and the light pixels (arrow) were defined as stromal or interstitial area. (a) SS-OCT scan image. (b) Image was converted with the auto local threshold tool. (c) The dark pixels were selected using the threshold tool. (d) An overlay image of ROI of the binarized segment of the choroid on SS-OCT scan.

TABLE 1: Demographic and clinical characteristics of the eyes included for analysis.

		Control ($n = 23$)	DR ($n = 23$)	P value
Age, years (mean ± SD)		67.0 ± 9.5	66.2 ± 7.6	0.758
Gender, n (%)	Male	13 (56.5)	12 (52.2)	0.767
	Female	10 (43.5)	11 (47.8)	
BCVA, log MAR (mean ± Sd)	B	0.56 ± 0.17	0.54 ± 0.14	0.58
	M3	0.04 ± 0.09	0.03 ± 0.1	0.665
IOP, mmHg (mean ± SD)	B	15.6 ± 2.8	16.1 ± 2.7	0.574
	W1	13.8 ± 3.8	14.2 ± 2.7	0.672
	M1	13.7 ± 2.8	13.8 ± 2.5	0.974
	M3	13.5 ± 2.5	13.7 ± 2.6	0.763
AL, mm (mean ± SD)		23.3 ± 1.0	23.2 ± 1.0	0.794
CDE (mean ± SD)		6.4 ± 4.6	5.7 ± 4.4	0.616
FBS, mmol/L (mean ± SD)		NA	7.48 ± 1.00	NA
HbA1c, % (mean ± SD)		NA	7.36 ± 0.78	NA
Cr, μmol/L (mean ± SD)		NA	80.39 ± 15.99	NA

B: baseline; W1: 1 wk postop; M1: 1 mo postop; M3: 3 mo postop; CDE: cumulative dissipated energy; AL: axial length; SD: standard deviation; FBS: fasting blood sugar; HbA1c: glycated hemoglobin A1c; Cr: creatinine.

binarization were indicated by the absolute agreement model of the intraclass correlation coefficient (ICC), performed using IBM SPSS statistics version 21.0. The ICC value of 0.81–1.00 indicates good agreement.

2.6. Statistical Analysis. Statistical analyses were performed using GraphPad Prism 7.0 (GraphPad Software, CA). Normally distributed data were expressed as mean ± standard deviation (SD). The preoperative and postoperative measurements were compared by the paired t-test. The difference between two groups was compared by the unpaired t-test. Pearson correlation analyses were performed to determine the relationships between CVI/CT and related factors. $P < 0.05$ was considered to be statistically significant.

3. Results

A total of 46 eyes of 46 subjects were recruited in the study; the DR group included 23 mild/moderate NPDR patients (12 males and 11 females) and the control group included 23 nondiabetic patients (13 males and 10 females). Table 1 shows patients' demographic and clinical characteristics, and the DR group included 14 moderate NPDR patients and 9 mild NPDR patients; 3 patients had coronary heart disease and 7 patients had well-controlled hypertension in the DR

TABLE 2: CVI of the patients with mild/moderate NPDR (DR) and nondiabetic patients (control) at four visits (mean ± SD).

| | Baseline | Postop | | | | | |
| | | 1 wk postop | | 1 mo postop | | 3 mo postop | |
	CVI	CVI	P value	CVI	P value	CVI	P value
Control (%)	62.77 ± 1.73	63.64 ± 1.97	0.136	64.25 ± 2.61	0.044*	63.74 ± 1.86	0.044*
DR (%)	60.76 ± 1.85	62.5 ± 1.8	<0.001*	63.82 ± 1.3	<0.001*	63.03 ± 1.54	<0.001*

*$P < 0.05$. SD: standard deviation.
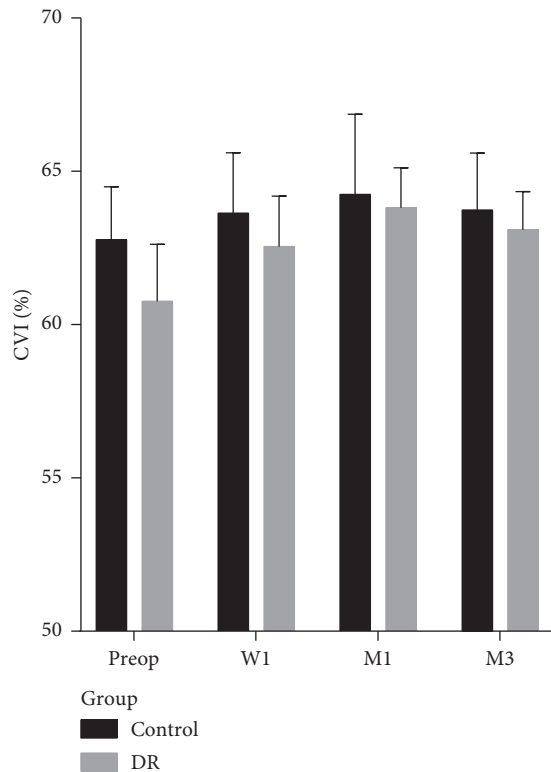

FIGURE 2: The choroidal vascularity index for patients with mild/moderate NPDR (DR) and nondiabetic patients (control) at the four visits (mean ± SEM). W1: 1 wk postop; M1: 1 mo postop; M3: 3 mo postop.

group. There was no significant difference in age, gender, BCVA, IOP, AL, or CDE between the DR group and the control group.

After the cataract surgery, the BCVA was significantly improved and IOP significantly decreased. The baseline IOP in DR and control groups was 16.1 ± 0.6 mmHg and 15.6 ± 0.6 mmHg, respectively. After surgery, the IOP of the control group significantly decreased ($P = 0.019$, <0.001, and <0.001 for 1 week, 1 month, and 3 months after surgery compared with the preoperative values). After surgery, the IOP of the DR group also significantly decreased ($P = 0.002$, <0.001, and <0.001 for 1 week, 1 month, and 3 months after surgery compared with the preoperative values).

3.1. Inter-Rater and Intra-Rater Agreement for CVI. The inter-rater agreement for CVI was 0.932 (95% confidence interval (CI): 0.877–0.962) for average measure and 0.872

(95% CI: 0.781–0.927) for single measure; the intra-rater agreement for CVI was 0.951 (95% CI: 0.911–0.973) for average measure and 0.906 (95% CI: 0.837–0.947) for single measure. These ICC values above indicated a significantly high agreement for the image segment.

3.2. CVI. The baseline CVI in the DR group was significantly lower than that in the control group; there was a significant difference between the two groups (mean difference = 2.00% and 95% CI: 0.94%–3.07%). After surgery, the CVI of the control group was significantly increased at 1 month and 3 months postoperatively. The CVI of the DR group significantly increased at 1 week, 1 month, and 3 months postoperatively (Table 2 and Figure 2). CVI at any visit did not correlate with age, AL, CDE, or IOP in the DR group and control group (Supplementary Table 1).

After surgery, increase of CVI in DR group was more than that in the control group, and the difference was significant at 1 month and 3 months after surgery (mean difference = 1.57%; 95% CI: 0.04–3.09% for 1 month after surgery; mean difference = 1.29%; 95% CI: 0.12%–2.46% for 3 months after surgery) (Table 3 and Figure 3).

3.3. CT. The baseline CT of the fovea, parafovea, and perifovea of the DR group was not significantly thinner than that of the control group ($P = 0.423$, 0.254, and 0.133 for fovea, parafovea, and perifovea, respectively).

A significant increase in CT was found after surgery in the DR group. The CT of the DR group significantly increased at 1 week, 1 month, and 3 months postoperatively in all regions (Figure 4 and Table 4).

In the control group, CT was found to increase in some parts of the macula. The CT of fovea at 3 months postoperatively, the CT of parafovea at 1 week, 1 month and 3 months postoperatively, and the CT of perifovea at 1 month and 3 months postoperatively were found significantly thicker than the baseline CT (Figure 4 and Table 4). CT did not correlate with AL, CDE, or IOP at any region in the control group and DR group (Supplementary Tables 2 and 3).

After surgery, increase of CT in the DR group was more than that in the control group, 1 month, and 3 months after surgery in all regions of macula (Table 3 and Figure 3). The difference between the two groups was significant for 1 month and 3 months after surgery at fovea (mean difference = 15.86; 95% CI: 3.46–28.26 for 1 month after surgery; mean difference = 12.39; 95% CI: 3.77–21.01 for 3

TABLE 3: Changes of CVI and CT after cataract surgery (mean ± SD).

		W1			M1			M3		
		Control	DR	P value	Control	DR	P value	Control	DR	P value
CVI (%)		0.871 ± 2.697	1.736 ± 1.495	0.204	1.486 ± 3.331	3.051 ± 1.436	0.044*	0.974 ± 2.19	2.267 ± 1.72	0.035*
CT (μm)	Fovea	7.174 ± 18.85	14.00 ± 18.48	0.222	6.587 ± 26.36	22.45 ± 13.27	0.013*	7.435 ± 14.95	19.83 ± 14.05	0.006*
	Parafovea	6.609 ± 13.11	14.37 ± 18.52	0.108	9.935 ± 16.25	21.26 ± 15.76	0.021*	7.641 ± 12.36	17.86 ± 13.84	0.011*
	Perifovea	4.065 ± 14.66	11.46 ± 14.82	0.096	6.978 ± 15.66	18.08 ± 12.89	0.012*	7.848 ± 14.33	17.02 ± 11.92	0.023*

W1: 1 wk postop; M1: 1 mo postop; M3: 3 mo postop. $*P < 0.05$. SD: standard deviation.

months after surgery); the difference was also significant for 1 month and 3 months after surgery at parafovea (mean difference = 11.33; 95% CI: 1.81–20.84 for 1 month after surgery; mean difference = 10.22; 95% CI: 2.42–18.02 for 3 months after surgery) and was significant for 1 month and 3 months after surgery at perifovea (mean difference = 11.1; 95% CI: 2.57–19.62 for 1 month after surgery; mean difference = 9.17; 95% CI: 1.34–17.01 for 3 months after surgery).

4. Discussion

Cataract extraction has been identified as a risk factor for DR progression [21, 22]. However, less DR progression was reported in patients undergoing phacoemulsification as compared with intracapsular cataract extraction and extracapsular cataract extraction [23], and Squirrell et al. even concluded that uncomplicated phacoemulsification cataract surgery does not cause acceleration of diabetic retinopathy postoperatively [24]. There seems to exist some controversies.

In the present study, we focused on quantitatively evaluating changes of the choroidal structures through SS-OCT-based CT and CVI measurements in patients with DR and controls undergoing phacoemulsification, aiming to make clear the possible influence of cataract surgery on changes of choroidal structure in patients with DR, which might play an important role in the pathogenesis of DR.

CVI has been found to be a relatively stable index to monitor the progression of choroidal diseases [13, 25, 26] and provide us more information on the proportion of vascularity in the choroid [11]. The significantly low CVI might reflect the narrowing and/or closure of choroidal vessels. In this study, baseline CVI was found to be significantly lower in patients with mild/moderate NPDR as compared with the controls, which seemed to be a hint of the existence of diabetic vasculopathy in DR patients, despite the result that no significant difference had been found between DR patients and controls in the baseline CT in this study. These results were similar to the previous studies [13, 16]. Tan et al. have reported a significantly lower CVI in diabetic patients with DR and without DR as compared with controls, but they found no significant differences in the CT between patients with DM and controls [13]. CVI seems to provide us more information on diabetic vasculopathy in DR and be more sensitive in monitoring the changes of choroidal vascularity in DR.

The influence of surgery on the choroidal structure is uncertain in the diabetics in previous studies. A number of publications have reported that phacoemulsification may cause a significant increase in choroid thickness [27–29]. However, some studies found no CT variation after cataract surgery in diabetics [30, 31].

In our study, CVI of the patients with mild/moderate NPDR was found to increase significantly at all visits after surgery; in contrast, the CVI of the control group had no significant increase 1 week after surgery, but it was found to increase 1 month and 3 months after surgery; therefore, the increase of CVI seemed to occur earlier in the patients with mild/moderate NPDR than in the controls. In addition, we also found that the variation in CVI and CT before and after surgery in patients with mild/moderate NPDR was more than that in the controls 1 month and 3 months after surgery. Obviously, for the first time, our present study showed that diabetic cataract surgery tended to induce more increase in the CVI and CT as compared with the controls. All the results above implied that cataract surgery seemed to have more influence on the choroidal vascularity in mild/moderate DR patients than in nondiabetic patients.

It has been experimentally verified that cataract surgery induces the expression of some proinflammatory cytokine in the choroid; it was detected that IL-1β and CCL2 gene expression and protein expression were upregulated in the choroid [32]. In addition, the upregulation of vascular endothelial growth factor (VEGF) was observed in the diabetic choroid, and VEGF may contribute to increased vascular permeability and angiogenesis during retinopathy [33]. The high levels of proinflammatory cytokines and VEGF in the preoperative choroid of patients with DR may be one of the underlying mechanisms of the upregulating expression postoperatively, which is likely to induce more increase in CT and CVI in mild/moderate NPDR patients than in nondiabetic patients.

In addition, the increased ocular perfusion pressure caused by reduced IOP may induce increased CT in the early period after phacoemulsification [28]. In our study, the IOP of patients with mild/moderate NPDR and controls both significantly decreased after surgery and no significant difference existed between the two groups. The reduced IOP might not be one of the underlying causes of the difference in the variation of CT and CVI following cataract surgery between the patients with mild/moderate NPDR and nondiabetic patients.
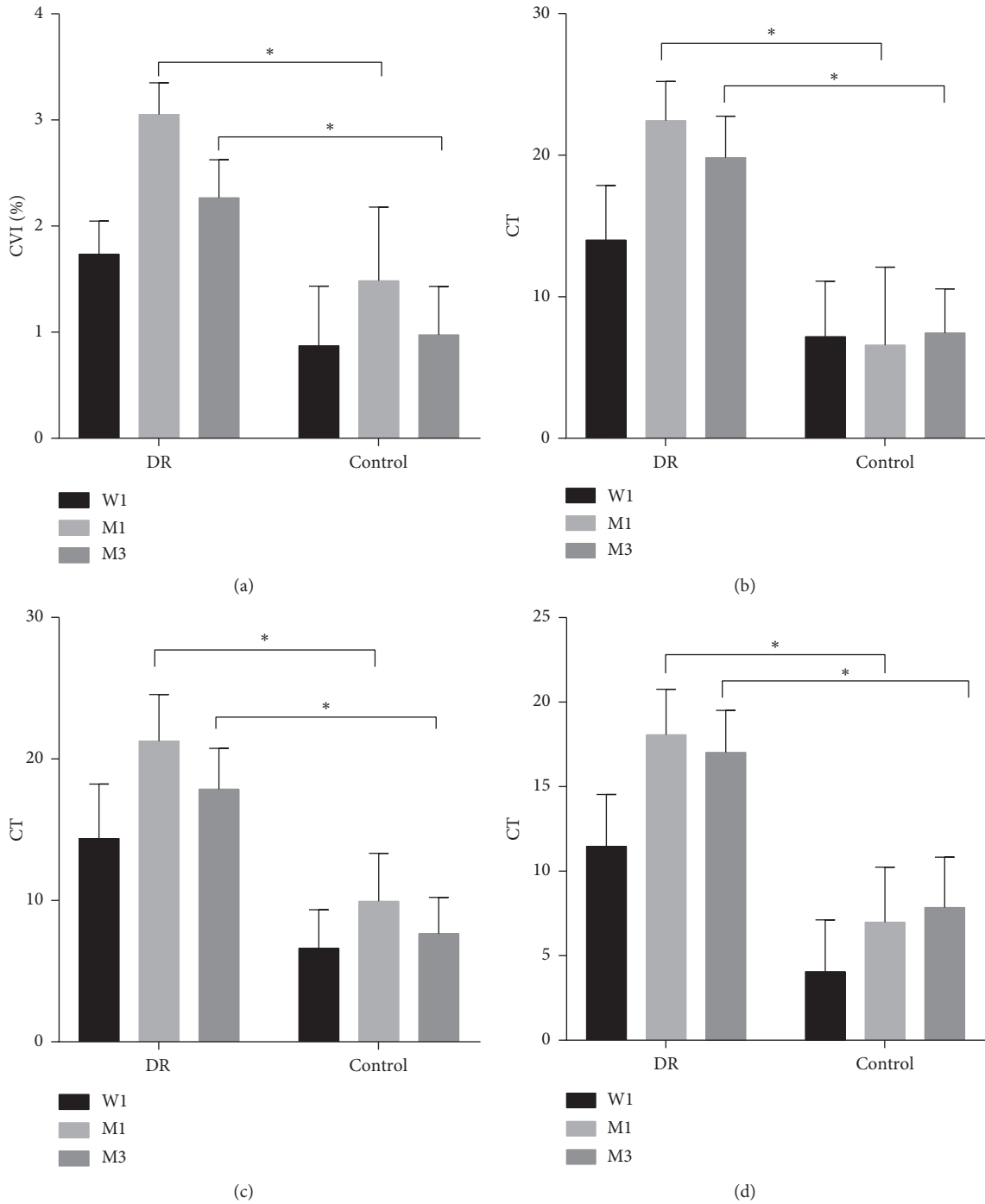
(a)

(b)

(c)

(d)

Figure 3: (a) Changes of CVI, (b) changes of foveal CT, (c) changes of parafoveal CT, and (d) changes of perifoveal CT for patients with mild/moderate NPDR (DR) and nondiabetic patients (control) at 1 week, 1 month, and 3 months postoperatively (mean ± SEM). W1: 1 wk postop; M1: 1 mo postop; M3: 3 mo postop. $^*P < 0.05$.

One limitation of our study is the relatively small sample size, but the individuals enrolled in had homogeneous ethnicity and similar gender distribution, which reduced some confounding effects. Another limitation is that the follow-up time is short, so the long period influence on choroid could not be observed in this study. A long-time follow-up should
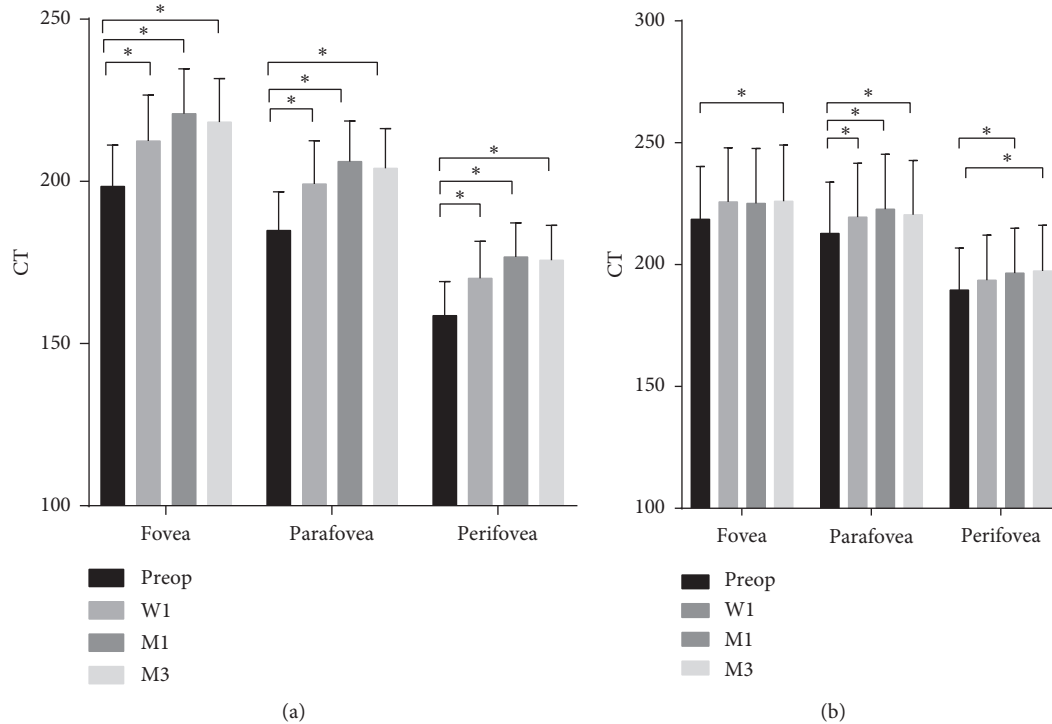
(a)　　　　　　　　　　　　(b)

FIGURE 4: The choroidal thickness of fovea, parafovea, and perifovea for patients with mild/moderate NPDR (a) and nondiabetic patients (b) at four visits (mean ± SEM) W1: 1 wk postop; M1: 1 mo postop; M3: 3 mo postop. $^{*}P < 0.05$.

TABLE 4: The choroid thickness of the patients with mild/moderate NPDR (DR) and nondiabetic patients (control) at four visits (mean ± SD).

		Baseline	Postop					
			1 wk postop		1 mo postop		3 mo postop	
		CT	CT	P value	CT	P value	CT	P value
Control (μm)	Fovea	217.6 ± 105.2	223.3 ± 108.1	0.106	223.8 ± 109.2	0.269	224.7 ± 112	0.031*
	Parafovea	213.8 ± 99.9	221.9 ± 104.4	0.025*	224.2 ± 106.6	0.006*	221.8 ± 105.7	0.006*
	Perifovea	189.6 ± 82.9	193.6 ± 88.5	0.2	196.5 ± 88.2	0.044*	197.4 ± 90	0.015*
DR (μm)	Fovea	198.4 ± 61.2	212.4 ± 68.2	0.002*	220.9 ± 66.4	<0.001*	218.3 ± 64.3	<0.001*
	Parafovea	184.9 ± 57.3	199.2 ± 63.7	0.001*	206.1 ± 60.1	<0.001*	204.1 ± 58.7	<0.001*
	Perifovea	158.7 ± 50.1	170.1 ± 54.6	0.001*	176.7 ± 50.1	<0.001*	175.7 ± 51.6	<0.001*

$^{*}P < 0.05$. SD: standard deviation.

be needed in future studies to make clear how long the increase in CVI and CT following cataract surgery would last. Therefore, a large population sample with a longer follow-up should be recommended in future studies.

5. Conclusion

For the first time, the present study showed that cataract surgery tended to induce more increase of CVI and CT in patients with mild/moderate NPDR as compared with nondiabetic patients. Therefore, the cataract surgery seemed to have more influence on the choroid vasculature in DR patients than in nondiabetic patients, which might imply the underlying impact of cataract surgery on the progression of the choroidopathy in DR patients. Meanwhile, baseline CVI was found to be significantly lower in DR patients as compared with the nondiabetic patients. Therefore, CVI could be reckoned as a biomarker for vascular health of choroid in DR patients and might have the potential to be a predictor of progression of DC following cataract surgery. Furthermore, whether changes of CVI and/or CT could be the predictors of progression of DR following cataract surgery at subclinical stages should be focused on in future studies.

Data Availability

All the relevant data of this study are available from the corresponding author upon request.

Conflicts of Interest

The authors declare that they have no conflicts of interest.

Authors' Contributions

Huiping Yao and Sha Gao contributed equally to the work.

Acknowledgments

Supplementary Materials

Supplementary Table 1: correlations of CVI with AL, CDE, and IOP for patients with mild/moderate NPDR (DR) and nondiabetic patients (control) at four visits. Supplementary Table 2: correlations of CT with AL, CDE, and IOP for patients with mild/moderate NPDR at four visits in fovea, parafovea, and perifovea. Supplementary Table 3: correlations of CT with AL, CDE, and IOP for nondiabetic patients at four visits in fovea, parafovea, and perifovea. (*Supplementary Materials*)

References

[1] B. E. K. Klein, R. Klein, and K. E. Lee, "Diabetes, cardiovascular disease, selected cardiovascular disease risk factors, and the 5-year incidence of age-related cataract and progression of lens opacities: the Beaver dam eye study," *American Journal of Ophthalmology*, vol. 126, no. 6, pp. 782–790, 1998.

[2] I. A. Cunliffe, D. W. Flanagan, N. D. George, R. J. Aggarwaal, and A. T. Moore, "Extracapsular cataract surgery with lens implantation in diabetics with and without proliferative retinopathy," *British Journal of Ophthalmology*, vol. 75, no. 1, pp. 9–12, 1991.

[3] H. Schatz, D. Atienza, H. R. McDonald, and R. N. Johnson, "Severe diabetic retinopathy after cataract surgery," *American Journal of Ophthalmology*, vol. 117, no. 3, pp. 314–321, 1994.

[4] A. Campos, E. J. Campos, J. Martins, A. F. Ambrósio, and R. Silva, "Viewing the choroid: where we stand, challenges and contradictions in diabetic retinopathy and diabetic macular oedema," *Acta Ophthalmologica*, vol. 95, no. 5, pp. 446–459, 2017.

[5] D. L. Nickla and J. Wallman, "The multifunctional choroid," *Progress in Retinal and Eye Research*, vol. 29, no. 2, pp. 144–168, 2010.

[6] A. A. Hidayat and B. S. Fine, "Diabetic choroidopathy," *Ophthalmology*, vol. 92, no. 4, pp. 512–522, 1985.

[7] G. A. Lutty, "Diabetic choroidopathy," *Vision Research*, vol. 139, pp. 161–167, 2017.

[8] A. Pierru, M. Carles, P. Gastaud, and S. Baillif, "Measurement of subfoveal choroidal thickness after cataract surgery in enhanced depth imaging optical coherence tomography," *Investigative Opthalmology & Visual Science*, vol. 55, no. 8, pp. 4967–4974, 2014.

[9] R. Shahzad, M. A. R. Siddiqui, S. Zafar, F. Kausar, and M. H. Shahzad, "Choroidal thickness changes following cataract surgery using swept source optical coherence tomography," *Canadian Journal of Ophthalmology*, vol. 53, no. 1, pp. 60–64, 2018.

[10] H. Jiang, Z. Li, R. Sun, D. Liu, and N. Liu, "Subfoveal choroidal and macular thickness changes after phacoemulsification using enhanced depth imaging optical coherence tomography," *Ophthalmic Research*, vol. 60, no. 4, pp. 243–249, 2018.

[11] R. Agrawal, P. Gupta, K. A. Tan, C. M. Cheung, T. Y. Wong, and C. Y. Cheng, "Choroidal vascularity index as a measure of vascular status of the choroid: measurements in healthy eyes from a population-based study," *Scientific Reports*, vol. 6, 2016.

[12] R. Agrawal, M. Salman, K. A. Tan et al., "Choroidal vascularity index (CVI)--A novel optical coherence tomography parameter for monitoring patients with panuveitis?" *PLoS One*, vol. 11, 2016.

[13] K.-A. Tan, A. Laude, V. Yip, E. Loo, E. P. Wong, and R. Agrawal, "Choroidal vascularity index - a novel optical coherence tomography parameter for disease monitoring in diabetes mellitus?" *Acta Ophthalmologica*, vol. 94, no. 7, pp. e612–e616, 2016.

[14] R. Agrawal, J. Ding, P. Sen et al., "Exploring choroidal angioarchitecture in health and disease using choroidal vascularity index," *Progress in Retinal and Eye Research*, vol. 77, 2020.

[15] C. Iovino, M. Pellegrini, F. Bernabei et al., "Choroidal vascularity index: an in-depth analysis of this novel optical coherence tomography parameter," *Journal of Clinical Medicine*, vol. 9, 2020.

[16] H. Endo, S. Kase, Y. Ito et al., "Relationship between choroidal structure and duration of diabetes," *Graefe's Archive for Clinical and Experimental Ophthalmology*, vol. 257, no. 6, pp. 1133–1140, 2019.

[17] A. Miki, Y. Ikuno, Y. Jo, and K. Nishida, "Comparison of enhanced depth imaging and high-penetration optical coherence tomography for imaging deep optic nerve head and parapapillary structures," *Clinical Ophthalmology*, vol. 7, pp. 1995–2001, 2013.

[18] H.-Y. L. Park, H.-Y. Shin, and C. K. Park, "Imaging the posterior segment of the eye using swept-source optical coherence tomography in myopic glaucoma eyes: comparison with enhanced-depth imaging," *American Journal of Ophthalmology*, vol. 157, no. 3, pp. 550–557, 2014.

[19] C. P. Wilkinson, F. L. Ferris, R. E. Klein et al., "Proposed international clinical diabetic retinopathy and diabetic macular edema disease severity scales," *Ophthalmology*, vol. 110, no. 9, pp. 1677–1682, 2003.

[20] H. Chen, Z. Wu, Y. Chen, M. He, and J. Wang, "Short-term changes of choroidal vascular structures after phacoemulsification surgery," *BMC Ophthalmology*, vol. 18, 2018.

[21] J. J. Alpar, "Cataract extraction and diabetic retinopathy," *American Intra-ocular Implant Society Journal*, vol. 10, no. 4, pp. 433–437, 1984.

[22] G. J. Jaffe and T. C. Burton, "Progression of nonproliferative diabetic retinopathy following cataract extraction," *Archives of Ophthalmology*, vol. 106, no. 6, pp. 745–749, 1988.

[23] T. Hong, P. Mitchell, T. de Loryn, E. Rochtchina, S. Cugati, and J. J. Wang, "Development and progression of diabetic retinopathy 12 months after phacoemulsification cataract surgery," *Ophthalmology*, vol. 116, no. 8, pp. 1510–1514, 2009.

[24] D. Squirrell, R. Bhola, J. Bush, S. Winder, and J. F. Talbot, "A prospective, case controlled study of the natural history of diabetic retinopathy and maculopathy after uncomplicated phacoemulsification cataract surgery in patients with type 2 diabetes," *British Journal of Ophthalmology*, vol. 86, no. 5, pp. 565–571, 2002.

[25] L. H. L. Koh, R. Agrawal, N. Khandelwal, L. Sai Charan, and J. Chhablani, "Choroidal vascular changes in age-related macular degeneration," *Acta Ophthalmologica*, vol. 95, no. 7, pp. e597–e601, 2017.

[26] W. Y. Ng, D. S. W. Ting, R. Agrawal et al., "Choroidal structural changes in myopic choroidal neovascularization after treatment with antivascular endothelial growth factor over 1 year," *Investigative Opthalmology & Visual Science*, vol. 57, no. 11, pp. 4933–4939, 2016.

[27] S. A. Bayhan, H. A. Bayhan, E. Muhafiz, K. Kırboğa, and C. Gurdal, "Evaluation of choroidal thickness changes after phacoemulsification surgery," *Clinical Ophthalmology*, vol. 10, pp. 961–967, 2016.

[28] H. Ohsugi, Y. Ikuno, Z. Ohara et al., "Changes in choroidal thickness after cataract surgery," *Journal of Cataract & Refractive Surgery*, vol. 40, no. 2, pp. 184–191, 2014.

[29] T. Yilmaz, A. A. Karci, I. Yilmaz et al., "Long-Term changes in subfoveal choroidal thickness after cataract surgery," *Medical Science Monitor*, vol. 22, pp. 1566–1570, 2016.

[30] P. N. Brito, V. M. Rosas, L. M. Coentrão et al., "Evaluation of visual acuity, macular status, and subfoveal choroidal thickness changes after cataract surgery in eyes with diabetic retinopathy," *Retina*, vol. 35, no. 2, pp. 294–302, 2015.

[31] V. C.-H. Yip, A. Laude, K. A. Tan, J. Ding, E. Wong, and R. Agrawal, "A longitudinal study of choroidal changes following cataract surgery in patients with diabetes," *Diabetes and Vascular Disease Research*, vol. 16, no. 4, pp. 369–377, 2019.

[32] H. Xu, M. Chen, J. V. Forrester, and N. Lois, "Cataract surgery induces retinal pro-inflammatory gene expression and protein secretion," *Investigative Opthalmology & Visual Science*, vol. 52, no. 1, pp. 249–255, 2011.

[33] G. A. Lutty, D. S. McLeod, C. Merges, A. Diggs, and J. Plouet, "Localization of vascular endothelial growth factor in human retina and choroid," *Archives of Ophthalmology*, vol. 114, no. 8, pp. 971–977, 1996.

Research Article

Early Detection of Incipient Retinal Pigment Epithelium Atrophy Overlying Drusen with Fundus Autofluorescence *vs.* Spectral Domain Optical Coherence Tomography

Anabel Rodríguez,[1,2] **Marc Biarnés,**[1,2] **Rosa M. Coco-Martin** ⓘ **,**[3,4] **Anna Sala-Puigdollers,**[1,5] **and Jordi Monés**[1,2]

[1]*Institut de la Màcula Centro Médico Teknon, Barcelona, Spain*
[2]*Barcelona Macula Foundation, Barcelona, Spain*
[3]*Instituto de Oftalmobiología Aplicada (IOBA), Universidad de Valladolid, Valladolid, Spain*
[4]*Red Temática de Investigación Cooperativa en Salud de Oftalmologia (Oftared), Instituto de Salud Carlos III, Madrid, Spain*
[5]*Institut Clínic d'Oftalmologia (ICOF), Hospital Clínic, Barcelona, Spain*

Correspondence should be addressed to Rosa M. Coco-Martin; rosa@ioba.med.uva.es

Purpose. This study aims to find out which tool, fundus autofluorescence (FAF) or spectral domain optical coherence tomography (SD-OCT), is more sensitive in detecting retinal pigment epithelium (RPE) demise overlying drusen and can, therefore, help predict geographic atrophy (GA) appearance in Age-Related Macular Degeneration (AMD). *Methods.* A single-site, retrospective, observational, longitudinal study was conducted. Patients with intermediate AMD (iAMD) (large (>125 μm) or intermediate (63–125 μm) drusen with hyper/hypopigmentation) with a minimum follow-up of 18 months were included. Drusen with overlying incipient RPE atrophy were identified on SD-OCT defined as choroidal hypertransmission or nascent geographic atrophy (nGA). These selected drusen were, then, traced backwards in time to determine if incipient RPE atrophy overlying drusen was observed on FAF (well-demarcated region of absence of autofluorescence) before, simultaneously, or after having detected the first signs of incipient RPE atrophy on SD-OCT. The number of drusen in which signs of incipient RPE atrophy was detected earlier using FAF or SD-OCT was compared. The time elapsed from the identification with the more sensitive method to the other was recorded and analyzed. *Results.* One hundred and thirty-three drusen in 22 eyes of 22 patients were included. Of these, 112 (84.2%) drusen showed choroidal hypertransmission and 21(15.8%) nGA. Early signs of atrophy overlying drusen were found simultaneously on SD-OCT and FAF in 52 cases (39.1%, 95% CI 30.8–47.9%), earliest on FAF in 51 (38.3%, 95% CI 30.0–47.2%) and first on SD-OCT in 30 (22.6%, 95% CI 15.8–30.6%; $p < 0.05$). Statistically significant differences were found between both techniques ($p = 0.005$), with FAF detecting it earlier than SD-OCT. When RPE atrophy was found first on FAF, the median time to diagnosis with SD-OCT was 6.6 months (95% CI 5.5 to 8.6), while if detection occurred earlier on SD-OCT, the median time until identification with FAF was 12.6 months (95% CI 6.0 to 23.4; $p = 0.0003$). *Conclusions.* In iAMD cases in which early atrophy overlying drusen is not detected simultaneously in FAF and SD-OCT, FAF was significantly more sensitive. Nevertheless, a multimodal approach is recommended and required to evaluate these patients.

1. Introduction

The hallmark of the intermediate stage of age-related macular degeneration (AMD) is the presence of drusen [1]. Drusen are deposits of extracellular material located between the basement membrane of the retinal pigment epithelium (RPE) and the inner collagenous layer of Bruch's membrane [2]. They can cause mild metamorphopsia and decreased sensitivity in microperimetry or dark adaptation, among other clinical symptoms. As drusen increase in number or

size, the disease progresses and the risk of vision loss increases. In the late stages of AMD, the disease advances towards neovascular AMD and/or geographic atrophy (GA) usually inducing great vision worsening [3, 4].

In the last two decades, new imaging techniques have been incorporated to study AMD, and one of such techniques is fundus autofluorescence imaging (FAF), which provides information about RPE integrity in a noninvasive way [5]. Different studies have shown that, in early or intermediate stages of the disease, the FAF image has the capacity to show RPE alterations in normal-appearing fundus regions [5–8]. On FAF, GA appears as a well-demarcated region of marked hypoautofluorescence due to the absence of the fluorophore lipofuscin contained within the RPE [7–11]. GA usually appears in the central or parafoveal macula and spreads centrifugally [8, 12]. New areas of atrophy may show a relatively lower intensity of hypoautofluorescence. FAF imaging is especially valuable in GA because it better delineates the areas of discrete or small GA in comparison with other imaging modalities [11, 13].

On the other hand, spectral domain optical coherence tomography (SD-OCT) facilitates *in vivo* high-resolution evaluation of the retina [14]. GA has been extensively studied with SD-OCT, and alterations within the atrophic area and its borders have been described in detail, hypertransmission of OCT signal below Bruch's membrane being one of the best recognized findings [14–18]. Besides, Guymer et al. used SD-OCT to describe precursors of GA. They defined nascent geographic atrophy (nGA) by the presence of either the subsidence of the outer plexiform layer (OPL) and the inner nuclear layer (INL) and/or a wedge-shaped band within the boundaries of the OPL [18–20].

Additionally, Wu et al. investigated FAF in areas of nGA and areas of drusen-associated atrophy and concluded that areas of nGA can present as both hyper- and hypoautofluorescent changes, while in drusen-associated atrophy, most often appeared as hypoautofluorescent areas [19].

Currently, GA has no treatment, but detecting its earliest signs can help understand its natural course and assist in the characterization of the disease spectrum. This would also improve the design of clinical trials to develop preventive or therapeutic strategies. Therefore, knowing which one of two commonly used imaging methods for monitoring GA, FAF, and SD-OCT is more sensitive for detecting the earliest signs of the disease is relevant for future advances in this field.

In the present study, we aim to compare two imaging techniques, SD-OCT and FAF, to determine which one is more sensitive to detect incipient RPE atrophy overlying drusen in patients with iAMD.

2. Materials and Methods

2.1. Design and Participants. This is a retrospective, observational, longitudinal study conducted at the Institut de la Màcula (Hospital Quirón Teknon; Barcelona, Spain). The study adhered to the tenets of the Declaration of Helsinki and was approved by the Fundación Quirón Salud Ethics Committee. All patients signed informed consent.

Charts of patients with a diagnosis of iAMD visited between January 2010 and October 2014 were reviewed, and the last date of follow-up was July 2017. The drusen type of interest was soft drusen.

All patients met the following inclusion criteria: male or female patients, over 50 years of age, diagnosed with iAMD (AREDS stage 2 or 3: large (>125 μm) or intermediate (63–125 μm) drusen and associated hyper-/hypopigmentation), with a minimum follow-up of 18 months after diagnosis. Patients were excluded if the studied eye included any prior history of neovascular AMD, >0.5 disc areas of RPE atrophy (1.27 mm^2), other concomitant macular diseases (macular edema and retinal dystrophies), spherical equivalent greater than ± 6′00 D, previous history of intraocular treatment (laser photocoagulation and intravitreal injections) or surgery (with the exception of phacoemulsification), concomitant use of medications known to be toxic to the retina (chloroquine, hydroxychloroquine, and tamoxifen), or SD-OCT image quality < 20. The presence of reticular drusen in the studied eye was not considered a reason for exclusion.

2.2. Procedures. All patients received a complete ophthalmic examination by an experienced retina specialist. The checkup included medical history, best-corrected visual acuity (BCVA) measured in logMAR, and intraocular pressure measured with Goldmann applanation tonometry and indirect fundus ophthalmoscopy. Imaging exam entailed FAF (excitation 488 nm, absorption >500 nm) and SD-OCT imaging (Heidelberg Spectralis™ HRA + OCT, Heidelberg Engineering, Heidelberg, Germany), alongside fovea-centered nonstereoscopic 30° color fundus retinography (TRC-50DX, Topcon Medical Systems, Tokyo, Japan). The SD-OCT exam was performed using a high-resolution volumetric scanning protocol centered on the fovea (19 or 37 horizontal B-scans). Alongside, a high-resolution (1536 × 1536 pixels) infrared FAF image covering a 30° angle of the fundus and centered on the fovea was recorded.

Upon review of the Heidelberg Spectralis database of the Institut de la Màcula, an experienced observer (AR) selected and classified the patients with iAMD who met the aforementioned eligibility criteria. Then, individual soft drusen showing early signs of RPE atrophy overlying them were identified. This was defined by the presence of any of the following:

(1) Hypertransmission: drusen that show increased hypertransmission signal below Bruch's membrane on SD-OCT, which indicates a loss of overlying RPE (Figure 1(a))

(2) Nascent GA (nGA): subsidence of the outer plexiform layer (OPL)/inner nuclear layer (INL) and/or a hyporeflective wedge-shaped band within the boundaries of the OPL (Figure 1(b))

RPE atrophy on FAF was defined as a well-demarcated region of absence of autofluorescence (Figure 2).

The color fundus retinography was used to verify that the absence of autofluorescence was not caused by pigment
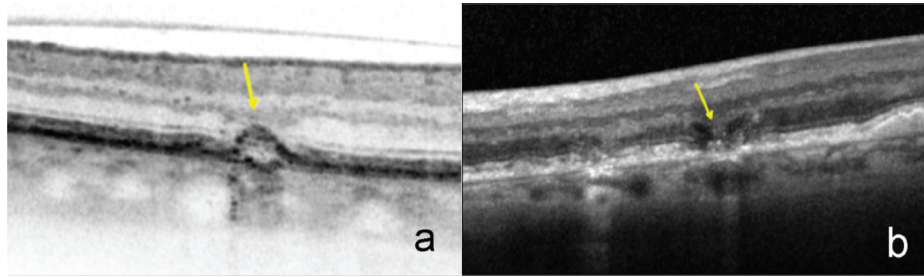
FIGURE 1: SD-OCT features. (a) B-scan of SD-OCT where drusen with hypertransmission are observed; (b) B-scan of SD-OCT showing nascent geographic atrophy.
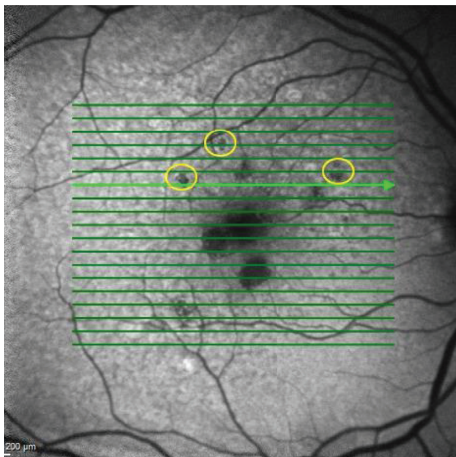

FIGURE 2: An example of retinal pigment epithelium atrophy by fundus autofluorescence. The yellow circle shows a region of absence of autofluorescence.

clumping over drusen. Drusenoid pigment epithelium detachments (defined in the AREDS studies as a well-defined, pale yellow or white, large mound consisting of many large drusen or confluent drusen with $\geq 350 \mu m$ in the narrowest diameter) [21] were excluded.

When a drusen presented hypertransmission or nGA, previous and subsequent SD-OCT and FAF images were reviewed. The first data in which the absence of autofluorescence on FAF was observed was, then, recorded. There were three possible scenarios:

(i) The first time that the absence of autofluorescence on FAF was observed coincided with the date in which atrophy of the RPE was first detected by SD-OCT. Thus, the diagnosis of incipient RPE atrophy overlying drusen was simultaneous with both imaging methods.

(ii) The absence of autofluorescence on FAF was present before RPE atrophy was detected by SD-OCT. Thus, FAF identified incipient RPE atrophy overlying drusen earlier than SD-OCT.

(iii) The absence of autofluorescence on FAF was appreciated after RPE atrophy detection by SD-OCT. Thus, SD-OCT identified incipient RPE atrophy overlying drusen earlier than FAF.

When in doubt, a second experienced observer (AS) reevaluated the case and the decision of the second evaluator was taken as the outcome for the analysis.

2.3. Main Outcome Measures. The primary endpoint was the comparison of the number of drusen in which there was incipient RPE atrophy overlying drusen detected earlier by FAF than by SD-OCT *vs.* the number of drusen in which this occurred earlier on SD-OCT than on FAF. The number of drusen in which RPE atrophy was detected simultaneously on both imaging modalities was also recorded.

The secondary endpoint included the time elapsed from the identification with the more sensitive method to identification with the other in cases of nonsimultaneous identification of early atrophy overlying drusen.

2.4. Statistical Analysis. Univariate statistics were used to describe the sample using mean and standard deviation (SD) for quantitative and number and percentage for categorical variables. The unit of analysis was each soft drusen contained in the $20° \times 30°$, fovea-centered SD-OCT macular grid. The percentage of time in which RPE atrophy overlying drusen was detected earlier by SD-OCT or by FAF was determined and compared using Fisher's exact test.

2.5. Secondary Endpoints. When one imaging method detected incipient RPE atrophy overlying drusen earlier than the other, the Kaplan–Meyer plots were used to estimate the median time to detection with the second, less-sensitive tool. The time when one method detected RPE atrophy for the first time (either FAF or SD-OCT) was considered time 0. The logrank test was used to compare both curves.

In cases where FAF detected RPE atrophy earlier than SD-OCT, the time to detection of RPE atrophy with SD-OCT, using either the definition of hypertransmission or nGA, was determined. The results were again compared using the logrank test.

The intra- and interobserver agreement for FAF detection of RPE atrophy were determined using the kappa index (κ) in a randomly selected sample of 35 drusen. The κ measures agreement between categorical observations was adjusted for chance.

Data analysis was conducted using Stata IC, version 15.1 (StataCorp, Texas, USA). A two-tailed p value <0.05 was considered statistically significant.

3. Results

One hundred and fifty-one drusen from 22 eyes in 22 patients with iAMD showed hypertransmission or nGA after a minimum follow-up of ≥18 months and were initially enrolled. Eighteen of these drusen (seven patients) were excluded: eight could not be assessed by being present in a region with dense macular pigment and ten by incomplete clinical information. Therefore, 133 drusen from 22 patients were finally included in the analysis. The mean age of these patients was 71.1 ± 6.9 years, 93.3% being female and all being Caucasian. The number of drusen included per eye ranged from 1 to 27, with a mean of 13.9 ± 8.8. The mean baseline BCVA of the studied eyes was 0.11 ± 0.13 logMAR (equivalent to approximately 20/25 in Snellen notation). Eighteen out of the 22 eyes (81.8%) were phakic at baseline, and the rest were pseudophakic. Only one phakic eye (1/18, 5,6%) became pseudophakic during the follow-up. Given the small number of pseudophakic eyes, the results were largely driven by the phakic sample and no stratified analysis could be conducted.

Incipient RPE atrophy overlying drusen was observed simultaneously on both tests in 52/133 drusen (39.1%, 95% CI 30.8% to 47.9%), while early RPE loss was detected first by FAF in 51/133 (38.40%, 30.1% to 47.2%) and first by SD-OCT in 30/133 (22.6%, 95% CI 15.8% to 30.6%), as seen in Table 1 and Figure 3. Statistically significant differences between early detection with FAF or using SD-OCT were found ($p = 0.005$), being FAF more sensitive.

Considering only cases in which atrophy detection was not simultaneous in both imaging modalities, the median time from initial detection with FAF to subsequent detection with SD-OCT was 6.6 months (95% CI, 5.5 to 8.6 months); and it was 12.6 months (95% CI, 6.0 to 23.3 months) from detection with SD-OCT to later detection with FAF. Figure 4(a) shows these differences being statistically significant (p-value = 0.0003).

Taking into account only the detection of incipient atrophy using SD-OCT, we found choroidal hypertransmission in 112/133 of the cases (84.5%, 95% CI 76.9% to 90.0%) and nGA in 21/133 (15.5%, 95% CI 10.0% to 23.1%). Therefore, the odds ratio (OR) of identifying incipient RPE atrophy overlying drusen by choroidal hypertransmission in comparison with nGA was 5.33 (95% CI 3.16 to 9.01, p value <0.0001).

Considering only cases in which atrophy detection was not simultaneous in both imaging modalities, detection through choroidal hypertransmission was made with a median of 6.5 months after the detection of incipient atrophy with FAF (95% CI, 4.9 to 8.6 months) and detection through nGA after a median of 6.7 months (95% CI, 2.5 to 27.3 months; p value = 0.09), differences not being statistically significant (Figure 4(b)).

Finally, the consistency within and between observers in grading the presence or absence of incident RPE atrophy as measured with FAF was determined by the kappa index. The intraobserver agreement, determined for just one of the evaluators (AR), was 100%, with kappa = 1.00 (95% CI, 1.00 to 1.00; p value < 0.0001). The interobserver agreement was

TABLE 1: Percentage of drusen showing incipient atrophy of the retinal pigment epithelium detected first with each imaging tool.

Imaging exam detecting first GA signs	n	Percentage* (95% CI)
Fundus autofluorescence	51/ 133	38.4 (30.1 to 47.2)
SD-OCT	30/ 133	22.6 (15.8 to 30.6)
Simultaneously on both exams	52/ 133	39.1 (30.8 to 47.9)

*Percentages do not add up to 100% due to rounding. CI: confidence interval; SD-OCT: spectral domain optical coherence tomography.

91.4%, with kappa = 0.62 (95% CI, 0.23 to 1.00; p value < 0.0001).

4. Discussion

This study compared FAF and SD-OCT in the detection of incipient RPE atrophy overlying drusen in patients with iAMD. We chose to compare FAF with SD-OCT because they are the standard diagnostic tests used in the detection, evaluation, and monitoring of GA. Atrophic AMD does not have treatment, so understanding the evolution at the early stages of the disease with current imaging techniques may be key to future advances.

The results of this study show that detection of early atrophy overlying drusen was observed simultaneously on both imaging techniques about 40% of the time (Figure 3(a)). Therefore, in 60% of the occasions, one method detected signs of incipient atrophy earlier than the other (Figures 3(b) and 3(c)). This suggests that a multimodal approach including both FAF and SD-OCT would be recommendable for early detection of atrophy overlying drusen.

When atrophy was detected just on one imaging method, FAF detected it earlier than SD-OCT (38.4% vs 22.6%, $p = 0.005$). True differences favoring FAF may be related to the advantages of using an *en face* modality to visualize changes in the retina as opposed to the cross-sectional nature of structural SD-OCT, in which protocols with wide interscan distances may miss the point of early atrophy if the B-scan is not located precisely in the location of the RPE loss. Given that even very dense protocols have a distance between adjacent B-scans in the range of tenths of microns, combined use of FAF with SD-OCT increases the likelihood of detection of early signs of GA. We also excluded the drusen located closer to the foveola due to the impossibility to differentiate the absence of autofluorescence caused by macular pigment absorption from that caused by true early atrophy, and this fact may have favored an increased sensitivity of detection using FAF.

Also, once atrophy was detected only with one imaging modality, time to detection with the other method differed markedly ($p = 0.0003$). It took approximately 6 months to detect incipient atrophy with SD-OCT after FAF detected it, while detection with FAF once it was detected with SD-OCT took approximately 12 months. These differences are not
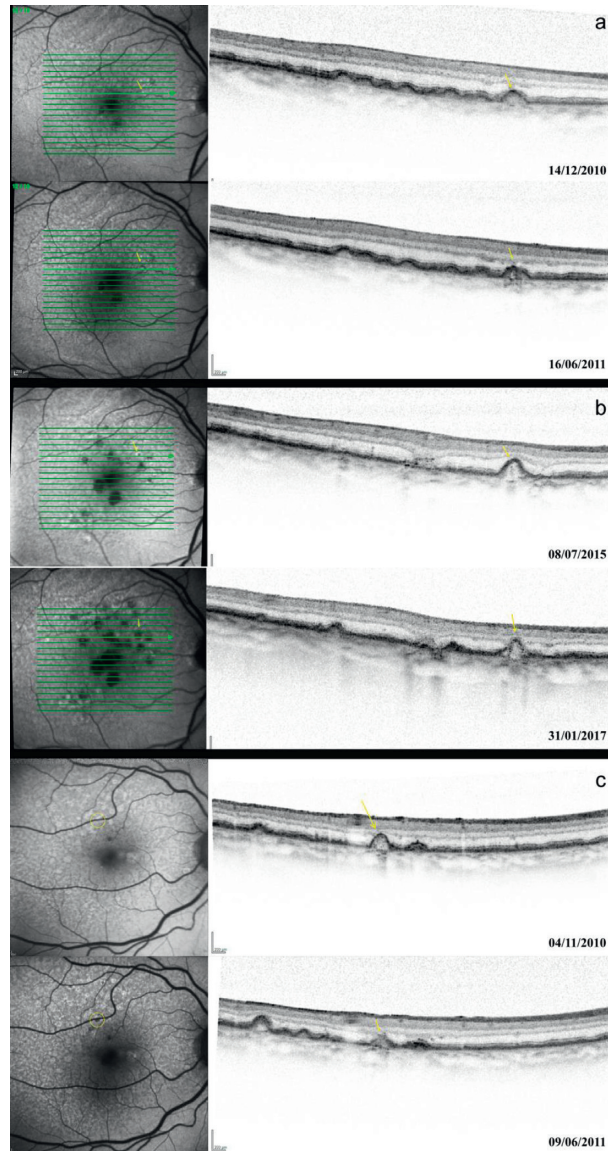
Figure 3: Examples of simultaneous detection, earlier detection with FAF, and earlier detection with SD-OCT. FAF: fundus auto-fluorescence; RPE: retinal pigment epithelium; and SD-OCT: spectral domain optical coherence tomography. (a) Simultaneous detection (the incipient RPE atrophy was observed at the same time with both exams). In the top image (14/Dec/2010), the selected druse (yellow arrow) showed normal autofluorescence on FAF and no hypertransmission on SD-OCT. In the next visit (16/Jun/2011), incipient atrophy of the RPE by both imaging techniques was observed. (b) Earlier detection with FAF (RPE atrophy overlying drusen is detected earlier on FAF than on SD-OCT). The top image (08/Jul/2015) shows that while a marked area of absence of autofluorescence appears on FAF, no signs of RPE atrophy were detected with SD-OCT. In the bottom image (31/Jan/2017), after 18 months, signs of atrophy on SD-OCT can be observed and the area of atrophy on FAF increased in size. (c) Earlier detection with SD-OCT. In the top image (04/Nov/2010) there is SD-OCT hypertransmission (yellow arrow), but normal FAF. Seven months later (09/Jun/2011), the absence of autofluorescence was noticeable (bottom image).

easily explained taking into account that, in almost half of the sample, the detection of atrophy was simultaneous with both imaging modalities. Certainly, differences between the follow-up times of each patient hinder the estimation of the precise moment in which atrophy appears on each of the individual drusen. On the other hand, we can speculate that the underlying mechanism leading to RPE loss may differ between distinct drusen, making some imaging modalities to be more readily apt to detect incipient atrophy than other. In fact, using fluorescence lifetime imaging ophthalmoscopy

(FLIO) eyes with drusen showed longer autofluorescence lifetimes than healthy controls, and different lifetime values were found in different drusen, suggesting a heterogeneous ultrastructural composition in phenotypically similar lesions [22].

In the vast majority of cases in which atrophy was detected with SD-OCT, choroidal hypertransmission was observed more frequently than nGA (84% vs. 16%, $p < 0.0001$), although the median time to detection with either phenomenon was not significantly different. This
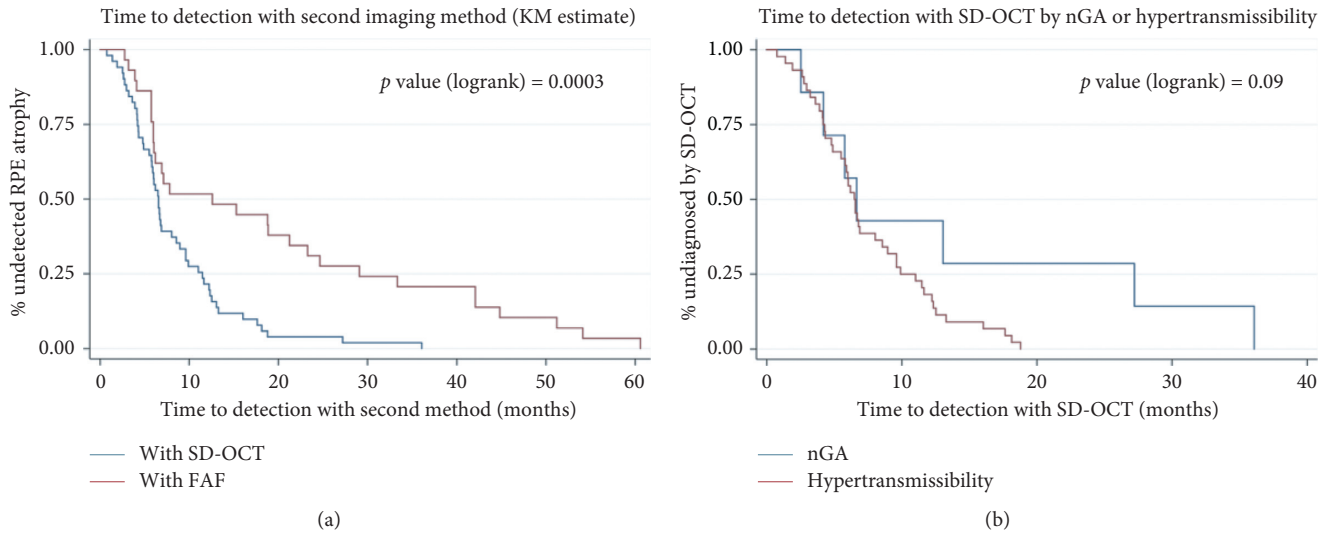
Figure 4: Comparison of time to secondary detection of incipient GA. FAF: fundus autofluorescence; nGA: nascent geographic atrophy; SD-OCT: spectral domain optical coherence tomography. (a) On the left-hand side, the Kaplan–Meyer curves of time to detection with SD-OCT when FAF detected atrophy earlier (blue) and with FAF when SD-OCT detected atrophy earlier (red) are shown. (b) On the right-hand side, the Kaplan–Meyer estimates compare if earlier detection was made by showing choroidal hypertransmission or nGA when SD-OCT detected the atrophy.

suggests that hypertransmission may be a precursor of nGA. This could be expected since hypertransmission arises as an immediate consequence of tissue loss, whereas nGA is detected after subsidence of inner retinal tissue and the appearance of the hyperreflective wedge-shaped band, which arise as a consequence (not as a primary cause) of a certain amount of tissue loss. Besides, like other authors [23], here, we demonstrate that nGA is a predictor for GA providing supportive evidence of the potential value of nGA as a surrogate endpoint in future intervention trials for the early stages of AMD.

Everyone agrees that multimodal imaging is the gold standard nowadays to study AMD. Other new techniques that should be evaluated and compared in the future with those tested here would include the optical coherence tomography angiography (OCT-A) and the *en face* OCT. OCT-A allows for three-dimensional visualization of retinal blood flow and, in recent studies, has shown choriocapillaris flow alterations particularly associated with the development of GA that exceed atrophy boundaries spatially and that are a prognostic factor for future GA progression. Besides, OCT-A may be helpful to differentiate GA from mimicking diseases [24]. Furthermore, *en face* OCT imaging could also be useful for identifying areas suspicious for nGA, in differential diagnosis, study design, and patient assessment [25, 26].

However, this study has limitations that need to be acknowledged. First, this is a retrospective study, although the fact that patients are studied backwards to the time when the retinal images were normal provides some prospective nature to the study. Second, the number of eyes was small, but our unit of analysis was the numerous individual drusen observed. Third, drusen within the foveal area were excluded to avoid interference caused by the presence of the luteal

pigment in the evaluation of the FAF, so the detection of incipient atrophy in this region may be easier with SD-OCT because its signal is not interfered as much by the luteal pigment as it is with FAF. Also, detection with SD-OCT could have been improved by the use of more dense volume protocols (decreased distance between B-scans that may have had an increased chance of crossing a focal area of RPE loss), but anyway, this is always a limitation with a cross-sectional device. It remains to be determined if the use of *en face* strategies at different heights could have improved the SD-OCT detection rate. Pseudofaquia influence could not be checked because of the small number of pseudophakic eyes. Finally, the patients were visited at irregular intervals, and therefore, estimates of time to appearance of RPE atrophy may be overestimated.

In any case, FAF imaging allows greater accuracy of border identification, revealing patterns predictive of growth rates once the GA is stated in advanced AMD [27], but here, we demonstrate that it is also the best tool to detect it early. Our study suggests that FAF is more sensitive that SD-OCT as a biomarker that could help to predict individual disease progression from early to advanced AMD. These finding could be useful to plan artificial intelligence diagnostic tools and to test new treatments for atrophic AMD.

5. Conclusions

In summary, 40% of the drusen in the iAMD showed signs of incipient RPE cell loss over them simultaneously in the FAF and SD-OCT. Incipient GA was initially detected only in one of the two imaging methods in 60%. In the latter case, the FAF detected signs of atrophy earlier than SD-OCT showing the absence of autofluorescence. While SD-OCT can detect signs of atrophy indistinctly through the observation of both,

choroidal hypertransmission or nGA, we should learn to recognize these patterns. Therefore, multimodal imaging in the iAMD including both examination tools is recommended to detect signs of incipient GA as soon as possible.

Data Availability

The data used to support the findings of this study are available from the corresponding author upon reasonable request.

Conflicts of Interest

The authors declare no conflicts of interest.

Authors' Contributions

All authors contributed to the study conception and design. Material preparation, data collection, and analysis were performed by Anabel Rodríguez, Marc Biarnés, and Anna Sala-Puigdollers. The first draft of the manuscript was written by Anabel Rodríguez, and all authors commented on previous versions of the manuscript. Rosa M Coco-Martin and Jordi Mones revised the final draft. All authors read and approved the final manuscript.

References

[1] J. S. Steinberg, J. Auge, G. J. Jaffe, M. Fleckenstein, F. G. Holz, and S. Schmitz-Valckenberg, "Longitudinal analysis of reticular drusen associated with geographic atrophy in age-related macular degeneration," *Investigative Opthalmology & Visual Science*, vol. 54, no. 6, pp. 4054–4060, 2013.

[2] T. L. Van der Schaft, C. M. Mooy, W. C. de Bruijn, F. G. Oron, P. G. H. Mulder, and P. T. V. M. de Jong, "Histologic features of the early stages of age-related macular degeneration," *Ophthalmology*, vol. 99, no. 2, pp. 278–286, 1992.

[3] H. R. Coleman, C.-C. Chan, F. L. Ferris, and E. Y. Chew, "Age-related macular degeneration," *The Lancet*, vol. 372, no. 9652, pp. 1835–1845, 2008.

[4] J. P. Sarks, S. H. Sarks, and M. C. Killingsworth, "Evolution of soft drusen in age-related macular degeneration," *Eye*, vol. 8, no. 3, pp. 269–283, 1994.

[5] A. Bindewald, A. C. Bird, S. S. Dandekar et al., "Classification of fundus autofluorescence patterns in early age-related macular disease," *Investigative Opthalmology & Visual Science*, vol. 46, no. 9, pp. 3309–3314, 2005.

[6] Y. Xuan, P. Zhao, and Q. Peng, "Fundus autofluorescence patterns of drusen in age-related macular degeneration," *Chinese Journal of Ophthalmology*, vol. 46, no. 8, pp. 708–713, 2010.

[7] F. Batoǧlu, S. Demirel, E. Özmert, Y. G. Oguz, and P. Özyol, "Autofluorescence patterns as a predictive factor for neovascularization," *Optometry and Vision Science*, vol. 91, no. 8, pp. 950–955, 2014.

[8] A. Ly, L. Nivison-Smith, N. Assaad, and M. Kalloniatis, "Fundus autofluorescence in age-related macular degeneration," *Optometry and Vision Science*, vol. 94, no. 2, pp. 246–259, 2017.

[9] U. Kellner, S. Kellner, and S. Weinitz, "Fundus autofluorescence (488 Nm) and near-infrared autofluorescence (787 Nm) visualize different retinal pigment epithelium

[10] S. Bearelly, A. A. Khanifar, D. E. Lederer et al., "Use of fundus autofluorescence images to predict geographic atrophy progression," *Retina*, vol. 31, no. 1, pp. 81–86, 2011.

[11] A. A. Khanifar, D. E. Lederer, J. H. Ghodasra et al., "Comparison of Color Fundus Photographs and fundus autofluorescence images in measuring geographic atrophy area," *Retina*, vol. 32, no. 9, pp. 1884–1891, 2012.

[12] M. M. Mauschitz, S. Fonseca, P. Chang et al., "Topography of geographic atrophy in age-related macular degeneration," *Investigative Opthalmology & Visual Science*, vol. 53, no. 8, pp. 4932–4939, 2012.

[13] L. Xu, A. M. Blonska, N. M. Pumariega et al., "Reticular macular disease is associated with multilobular geographic atrophy in age-related macular degeneration," *Retina*, vol. 33, no. 9, 2013.

[14] C. Balaratnasingam, J. D. Messinger, K. R. Sloan, L. A. Yannuzzi, K. B. Freund, and C. A. Curcio, "Histologic and optical coherence tomographic correlates in drusenoid pigment epithelium detachment in age-related macular degeneration," *Ophthalmology*, vol. 124, no. 5, pp. 644–656, 2017.

[15] M. Fleckenstein, S. Schmitz-Valckenberg, C. Martens et al., "Fundus autofluorescence and spectral-domain optical coherence tomography characteristics in a rapidly progressing form of geographic atrophy," *Investigative Opthalmology & Visual Science*, vol. 52, no. 6, pp. 3761–3766, 2011.

[16] M. Fleckenstein, S. Schmitz-Valckenberg, C. Adrion et al., "Tracking progression with spectral-domain optical coherence tomography in geographic atrophy caused by age-related macular degeneration," *Investigative Opthalmology & Visual Science*, vol. 51, no. 8, pp. 3846–3852, 2010.

[17] S. Bearelly, F. Y. Chau, A. Koreishi, S. S. Stinnett, J. A. Izatt, and C. A. Toth, "Spectral domain optical coherence tomography imaging of geographic atrophy margins," *Ophthalmology*, vol. 116, no. 9, pp. 1762–1769, 2009.

[18] J. Monés, M. Garcia, M. Biarnés, A. Lakkaraju, and L. Ferraro, "Drusen ooze: a novel hypothesis in geographic atrophy," *Ophthalmology Retina*, vol. 1, no. 6, pp. 461–473, 2017.

[19] Z. Wu, C. D. Luu, L. N. Ayton et al., "Fundus autofluorescence characteristics of nascent geographic atrophy in age-related macular degeneration," *Investigative Opthalmology & Visual Science*, vol. 56, no. 3, pp. 1546–1552, 2015.

[20] Z. Wu, C. D. Luu, L. N. Ayton et al., "Optical coherence tomography-defined changes preceding the development of drusen-associated atrophy in age-related macular degeneration," *Ophthalmology*, vol. 121, no. 12, pp. 2415–2422, 2014.

[21] C. Cukras, E. Agrón, M. L. Klein et al., "Natural history of drusenoid pigment epithelial detachment in age-related macular degeneration: age-related eye disease study report No. 28," *Ophthalmology*, vol. 117, no. 3, pp. 489–499, 2010.

[22] C. Dysli, R. Fink, S. Wolf, and M. S. Zinkernagel, "Fluorescence lifetimes of drusen in age-related macular degeneration," *Investigative Opthalmology & Visual Science*, vol. 58, no. 11, pp. 4856–4862, 2017.

[23] Z. Wu, C. D. Luu, L. A. B. Hodgson et al., "Prospective longitudinal evaluation of nascent geographic atrophy in age-related macular degeneration," *Ophthalmology Retina*, vol. 4, no. 6, pp. 568–575, 2020.

[24] P. L. Müller, M. Pfau, S. Schmitz-Valckenberg, M. Fleckenstein, and F. G. Holz, "OCT-angiography in geographic atrophy," *Ophthalmologica*, vol. 4, 2020.

[25] K. B. Schaal, G. Gregory, and P. J. Rosenfeld, "En face optical coherence tomography imaging for the detection of nascent

geographic atrophy," *Ophthalmologica*, vol. 174, pp. 145–154, 2017.

[26] A. Giocanti-Auregan, R. Tadayoni, F. Fajnkuchen, P. Dourmad, S. Magazzeni, and S. Y. Cohen, "Predictive value of outer retina en face OCT imaging for geographic atrophy progression," *Investigative Opthalmology & Visual Science*, vol. 56, no. 13, pp. 8325–8330, 2015.

[27] R. Guymer and Z. Wu, "Age-related macular degeneration (AMD): more than meets the eye. The role of multimodal imaging in today's management of AMD," *Investigative Opthalmology & Visual Science*, vol. 56, 2020.